UNCLASSIFIED

AD NUMBER
AD870292

LIMITATION CHANGES

TO:

Approved for public release; distribution is unlimited.

FROM:

Distribution authorized to U.S. Gov't. agencies and their contractors; Critical Technology; MAY 1970. Other requests shall be referred to Air Force Materials Laboratory, Wright-Patterson AFB, OH 45433. This document contains export-controlled technical data.

AUTHORITY

afml ltr, 7 dec 1972

THIS PAGE IS UNCLASSIFIED

AFML-TR-70-50

STRUCTURAL AND PHYSICAL PROPERTIES OF GRAPHITE-ZIRCONIUM DIBORIDE-SILICON CARBIDE COMPOSITES

AD870292

UNION CARBIDE CORPORATION
CARBON PRODUCTS DIVISION

TECHNICAL REPORT AFML-TR-70-50

MAY 1970

AD No. _____
DDC FILE COPY

DDC
JUN 17 1970

AIR FORCE MATERIALS LABORATORY
AIR FORCE SYSTEMS COMMAND
WRIGHT-PATTERSON AIR FORCE BASE, OHIO

79

NOTICE

When Government drawings, specifications, or other data are used for any purpose other than in connection with a definitely related Government procurement operation, the United States Government thereby incurs no responsibility nor any obligation whatsoever, and the fact that the Government may have formulated, furnished, or in any way supplied the said drawings, specifications, or other data, is not to be regarded by implication or otherwise and in any manner licensing the holder or any other person or corporation, or conveying any rights or permission to manufacture, use, or sell any patented invention that may in any way be related thereto.

This document is subject to special export controls and each transmittal to foreign Governments or foreign Nationals may be made only with prior approval of the Nonmetallic Materials Division, MAN, Air Force Materials Laboratory, Wright-Patterson Air Force Base, Ohio 45433.

Copies of this report should not be returned unless return is required by security considerations, contractual obligations, or notice on a specific document.

STRUCTURAL AND PHYSICAL PROPERTIES OF
GRAPHITE-ZIRCONIUM DIBORIDE-SILICON CARBIDE
COMPOSITES

Union Carbide Corporation
Carbon Products Division

FOREWORD

The work reported herein was performed under the sponsorship of the Advanced Research Projects Agency, Department of Defense, through a contract with the Air Force Materials Laboratory, MAN, AFSC Wright-Patterson Air Force Base, Ohio, Contract No. AF 33(615)-3110, ARPA Order No. 719, Program Code 6D10. Mr. H. S. Schwartz, MAN is the Air Force Program Manager.

The Contractor is Union Carbide Corporation, Carbon Products Division, Parma Technical Center, P.O. Box 6116, Cleveland, Ohio 44101. The Program Supervisor is Dr. Herbert F. Volk. Major contributors to the work reported herein were Dr. George B. Spence, Dr. Tu-Lung Weng, Mr. Owen L. Blakslee, Mr. Robert G. Fenish, and Mr. Charles W. Nezbeda.

The work reported herein was conducted during the period from May 1965 to June 1967, and the report was submitted for publication in May 1970.

This technical report has been reviewed and is approved.
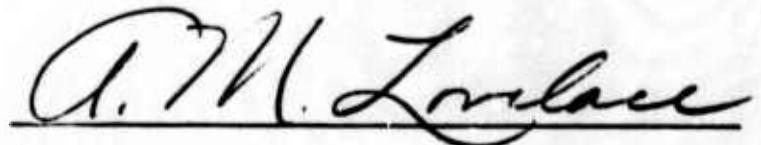
A. M. Lovelace
Director
Air Force Materials Laboratory

ABSTRACT

Three series of graphite based, refractory composites compositionally related to commercial Grade JTA, but containing 30, 50, and 70 weight percent additives (ZrB_2 and Si), were prepared. Within each series, the porosity was varied from approximately 2 to 17 percent. Property measurements were carried out as a function of composition and porosity and along the two principal symmetry axes, i.e., normal and parallel to the molding direction. Property measurements carried out at room temperature consisted of tension, compression, flexural, torsion, ultrasonic, and resonant bar tests. The specific heat, thermal conductivity, coefficient of thermal expansion, and effect of high temperature annealing were also determined. Stress-strain relations and fracture strength under multiaxial stress were determined for the material with 50 percent additive. A generalized stress-strain relation for a transversely isotropic, nonlinear material has been obtained without assuming volume constancy. Various theories of fracture for anisotropic materials were compared with the fracture strength of JT materials. The comprehensive property data compilations in this report should provide designers with sufficient information for structural applications of JT materials.

TABLE OF CONTENTS

TABLE OF CONTENTS (Cont'd.)

LIST OF ILLUSTRATIONS

LIST OF ILLUSTRATIONS (Cont'd.)

LIST OF ILLUSTRATIONS (Cont'd.)

LIST OF TABLES

SECTION I

INTRODUCTION

The information presented in this report was generated as part of a much larger program, "Integrated Research on Carbon Composite Materials," which is designed to fulfill three different, but clearly interdependent needs of the Department of Defense: a material need, a structural design capability need, and a need for more scientists and engineers trained in applied materials problems and advanced design methods. The Carbon Products Division of Union Carbide Corporation, Case Western Reserve University, and Bell Aerospace Company have formed an Association through which a joint effort is made to meet these needs. The Association has formulated a broad program which includes the development of new materials, generation of advanced analyses and design methods, and education of graduate students. The graphite based refractory compostes (designated by Union Carbide as JT series) which are the subject of this report are excellent candidates to satisfy the needs of weapons and aerospace systems for structural materials exhibiting high temperature oxidation resistance, good thermal shock resistance, refractoriness, and good machinability. These composites, upon exposure to oxygen at elevated temperatures, enclose themselves with a protective oxide coating. In this fashion, they represent an improvement over coated systems by providing oxidation protection in depth. Should processes such as erosion, chemical reaction, or vaporization result in local or general loss of the protective layer. Based on this mode of behavior, this class of composites is a candidate material for use above 3000°F in an oxidizing environment. Previous Air Force Materials Laboratory reports containing information on the JT series composites are listed as Reference 1-5 inclusive. Commericial Grade JTA is but one example of this series of composites; the properties of these materials can be varied over a wide range through appropriate changes in composition and/or porosity. The objective of this work was to provide designers and structural engineers with sufficient characterization of the JT-series composites to permit proper materials selection and structural optimization.

The results obtained under the Association's program have been reported in four Annual[6-11] Reports. However, the overall program is primarily concerned with graphite fiber reinforced composites; the results on particulate composites are scattered throughout a number of these reports and are, therefore, not conveniently accessible. Moreover, some property measurements[1] on the JT-series composites have been superseded by more accurate later work and/or by data obtained on billets fabricated by a more optimized process. Some of these newer data were reported only in Quarterly Progress Reports which are not as readily available

as the Annual Reports. For these reasons, it was decided to pub-
lish the present Topical Report, which in a convenient format pro-
vides the designer with sufficient details for the structural
application of these materials.

SECTION II

SUMMARY

The fabrication procedures and properties of a series of graphite-based, particulate refractory composites containing ZrB_2 and SiC were investigated. The hot-pressing parameters (particularly temperature and pressure conditions) required to produce dense cylindrical billets up to 3-inch diameter by 3-1/2-inch high were determined. A float mold technique was found to produce the most uniform billets, and this method was used to produce twenty-seven 3 x 3.5-inch specimens for the property evaluation work.

The elements Zr, B, and Si (the "metallic additives") were always maintained in the same proportion as in the commercial composite Grade JTA*, i.e., 42.4 parts of ZrB_2 to 9.5 parts of Si. Three series of composites containing 30, 50, and 70 weight percent metallic additives were prepared; within each series, the porosities of the billets were intentionally varied from approximately 2 to 17 percent. Thus, the physical properties were determined as a function of composition and of porosity.

Since the JT-series materials have the symmetry characteristics of transverse isotropy (the symmetry axis is parallel to the direction of molding pressure), it was necessary to measure all physical properties in two directions: parallel and normal to the symmetry axis. Mechanical properties were determined at room temperature by both static and sonic techniques. The static measurements included tension, compression, flexural, and torsion tests; the sonic tests consisted of ultrasonic and resonant bar tests. In addition to the ambient temperature measurements, the thermal properties of the JT-series materials were also determined, again as a function of both composition and of porosity. The specific heat, thermal diffusivity, thermal conductivity, and coefficient of thermal expansion were determined. The effects of annealing JT-materials at various temperatures were also studied. The uniaxial stress-strain relations for JT-materials are nonlinear and nonconservative, and brittle fracture is preceded by plastic flow. Strengths and moduli increase with increasing metallic additive content and decreasing porosity. The physical property data, both mechanical and thermal, provide sufficient information to optimize the material and geometry of a structural component for specific applications.

---

*A product of Union Carbide Corporation, Carbon Products Division.

-3-

Stress-strain relations and fracture strength of JT-50 (50 percent metallic additive) for all four biaxial stress quadrants were determined on thin-walled cylindrical specimens subjected to combinations of internal pressure, external pressure, and axial load. The stress-strain relations of this material under combined stresses are also nonlinear and nonconservative. A generalized stress-strain relation for a transversely isotropic, nonlinear material has been obtained without assuming volume constancy. The correlation between effective stress and effective strain for the uniaxial and biaxial stress tests is satisfactory for engineering applications.

Various theories of fracture for anisotropic materials were compared with the fracture strength data of JT-50 materials. An empirical fracture criterion has been formulated from the fracture strength data, and the fracture envelopes for JT-50 series materials as function of composition and porosity have been calculated with these fracture criteria. Significant influences of anisotropy and stress state on the modes of fracture were observed for JT-50 material. Catastrophic fracture resulted when the specimen was subjected to a large compressive stress, regardless of whether the other stress was tensile or compressive.

SECTION III

FABRICATION OF JT-SERIES MATERIALS

1. Description of JT-Series Materials

The JT-series materials are graphite-base refractory composites similar to the commercial material having the grade designation JTA produced by the Carbon Products Division of Union Carbide Corporation (JTA is one member of the series). On a weight basis, Grade JTA is composed of 48.1 percent C, 42.4 percent ZrB_2, and 9.5 percent Si. The minimum density limit for Grade JTA is 3.0 g/cm^3. During manufacture, silicon combines with part of the carbon to form silicon carbide.

In this work, the elements Zr, B, and Si are called the metallic additives; these elements are always present in the same proportions as in JTA: 42.4 parts of ZrB_2 to 9.5 parts of Si. Let

c = mass fraction of metallic additive in the fabricated product, and

ρ = density;

Grade JTA may, then, be specified by composition c = 51.9 percent and density $\rho > 3.0$ g/cm^3.

The JT-series materials are a class of materials produced by varying the amount of metallic additives and the density. In order to vary the density at a fixed composition, variations had to be made in processing temperatures or pressures; otherwise, the manufacturing conditions are kept as close as possible to those for grade JTA.[1] Therefore, to a good approximation, each member of the JT series can be uniquely identified by two values: the compositional variable, c, and a value that is equivalent to a processing variable, the density, ρ. To the same approximation, the physical properties of the JT-series materials may be considered to be functions of only two material variables, c and ρ.

2. Material Symmetry, Coordinate Orientation, and Billet Notation

All of the JT-series materials were molded in cylindrical billets. This process yields material with the symmetry characteristic of transverse isotropy, i.e., all physical properties are invariant with respect to arbitrary rotations about the symmetry axis, which is parallel to the direction of molding and perpendicular to the molding ram face.

Throughout this study, physical properties of the JT-series materials are specified with respect to a Cartesian coordinate system oriented with the x_1 and x_2 axes in the plane of transverse isotropy and the x_3 axis parallel to the axis of rotational symmetry. These symmetry oriented coordinates should not be confused with other types and orientations of coordinate systems used in the stress analysis problems. In JT material, as in other molded material, the elongated graphite particles or grains tend to be aligned with their two larger dimensions parallel to the plane of transverse isotropy, a situation which has led to properties (Young's modulus, coefficient of thermal expansion, etc.) in directions parallel to the plane of isotropy being called "with-grain" properties and properties in the direction parallel to the symmetry axis being called "against-grain" or "across-grain" properties.

The billets of JT material fabricated especially for this program are identified by the letters JT, followed by the nominal composition, and, finally, the sequential fabrication number. Thus, JT30-4 designates that the billet is the fourth fabricated and that the composition is approximately 30 percent metallic additive.

Commercial JTA billets from the standard production material which were also used in this program are identified by the letters JTA followed by the sequential order number. Thus, JTA-9 designates the ninth piece of commercial JTA used for this program.

3. Calculation of Theoretical Maximum Density
   and Porosity

Because the density varies with the composition as well as with porosity in the material, the composition c and porosity p were chosen as the material variables, rather than composition and density. Part of the porosity is in closed pores, the volume of which is not easily measured. Therefore, the porosity was calculated from the measured bulk density ρ and the calculated theoretical maximum density ρ_m:

$$p = 1 - \rho/\rho_m \qquad (1)$$

The theoretical maximum density can be calculated from the mass fraction and X-ray density of each phase in the composite material. Based on the following assumptions:

   mass ratio of ZrB_2 to Si is 42.4/9.5,
   all Si is in the form of α- and β-SiC, and
   X-ray density of pure C is 2.267 g/cm^3, of
   ZrB_2 is 6.10 g/cm^3, and of SiC is 3.216 g/cm^3,

-6-

the calculated theoretical maximum density is given by

$$\rho_m = \frac{2.267}{1 - 0.5905\ c} \tag{2}$$

where c ($0 < c < 1$) is, as above, the mass fraction of Zr,B, and Si in the fabricated composite. In practice, there are uncertainties of perhaps one percent in the mass fraction c and ZrB_2/Si ratio and in the density of ZrB_2. At low porosity levels of less than five percent, the corresponding uncertainty in the calculated porosity is several tens of percent. The possible error in the calculated porosity will not affect the stress analysis and structural synthesis work provided that Equations (1) and (2) are used consistently in calculating the porosity.

4. Fabrication of Initial Billets

The initial series of billets to be fabricated was selected to provide the initial trend of property data with composition at a fixed porosity and the trend with porosity at a fixed composition. Billets three inches in diameter by 3-1/2 inches in length were pressed on production-size equipment at a maximum observed outside-surface mold temperature of 2130°C and at pressures ranging between 3,300 and 5,500 lb/in.^{2}. Two attempts to fabricate composites with ten percent additive were unsuccessful due to mold failures. Two other billets were of smaller size. Table I gives the composition, average density and porosity of the good billets and of a commercial JTA billet. All of these billets were cut into specimens for physical property testing. The test results are given in Section IV.

TABLE I

COMPOSITION, DENSITY, AND POROSITY OF
INITIAL JT-SERIES BILLETS

Billet Number	Composition Percent Metallic Additive	Average Density g/cm^3	Average Porosity Percent
JT-30-5	31.5	2.31	17.2
JT-30-6	31.5	2.38	14.7
JT-30-4	31.5	2.58	7.4
JT-40-9	41.7	2.81	6.7
JTA-9	51.9	3.05	6.7
JT-70-3	71.4	3.66	6.7
JT-70-6	71.4	3.66	6.7

-7-

5. Process Studies on 1- and 1.5-Inch Diameter Billets

A basic premise of the entire JT-series program was that the physical properties of the materials depend on only two material variables, composition and density, and not on, say, the individual values of processing temperature and pressure used to attain a certain density. When it was found that the physical properties of commercial JTA did not fit smoothly with those of the initial experimental billets, a limited study of processing conditions was initiated to determine conditions which would yield material more comparable with commercial JTA on laboratory size equipment.

a. Method of Fabrication. Experimental billets 1.0 and 1.5 inches in diameter with the same composition as JTA were hot-pressed by a floating mold technique. The mold was heated in a 4-inch diameter tube furnace. Resistance heating, rather than the induction heating normally employed for manufacturing JTA, was used to obtain closer temperature uniformity. During hot pressing, an initial pressure of 2500 lb/in.^{2} was applied and maintained until the mold temperature reached 1800°C; at that time, the selected maximum pressure was applied. All samples were held for one hour at the hot-pressing temperature. They were then cooled under maximum pressure to a temperature of 1700°C, at which time the pressure was released. These experimental billets are designated by the letter E followed by a sequential fabrication number.

b. Temperature Series. Effects of pressing temperature on the density and microstructure were examined on samples hot pressed at temperatures ranging from 2210° to 2280°C at a pressure of 2900 lb/in.^{2}. The solidus temperature for JT composites was determined to be 2260° ±10°C by incipient melting experiments. Examination of the run-out material by metallography and X-ray diffraction disclosed a eutectic between ZrB_2 and SiC. Processing and density data are given in Table II.

Figure 1 illustrates the effect of pressing temperature on density and microstructure. Density increases with increasing pressing temperature to an extrapolated temperature of 2258°C and then decreases at higher temperatures. This decrease in density is caused by some run-out of the ZrB_2, SiC liquid eutectic. The 250 X magnification photomicrographs adjacent to the data points on Figure 1 show the representative structure of the material at different pressing temperatures. As the temperature is raised from 2210° to 2250°C, the porosity of the material decreases; the general physical structure and distribution of the ZrB_2-SiC-C phases remain essentially unchanged. As the temperature is raised above 2260°C (the solidus temperature), some of the dense metallic phases are pressed out, causing a change in composition of the

billet. Both the porosity and the density of the billet decrease, and the structure shows the presence of an increased amount of a well-dispersed metallic phase.

TABLE II

PROCESSING CONDITIONS AND DENSITY OF
EXPERIMENTAL JT-SERIES BILLETS

Specimen Number	Processing Temperature T±10°C	Processing Pressure lb/in.^{2}	Density g/cm^3	Diameter in.
E-2*	2210	2900	2.84	1.5
E-3*	2230	2900	2.98	1.5
E-4*	2250	2900	3.11	1.5
E-5*	2270	2900	3.11	1.5
E-6*	2280	2900	3.06	1.5
E-17	2240	2900	2.86	1.5
E-18	2260	2900	3.00	1.5
E-20	2265	2900·	3.03	1.5
E-16	2290	2900	2.97	1.5
E-13	2150	3500	2.78	1.0
E-14	2150	4500	2.89	1.0
E-12	2150	5500	2.97	1.0
E-10	2210	5500	3.11	1.0
E-9	2230	4500	3.09	1.0
E-8	2230	5000	3.11	1.0
E-7	2230	5500	3.13	1.0
E-19	2260	5500	3.15	1.0

*Specimens E-2 through E-6 were inadvertently made
with 53.7 instead of 51.9 percent metallic additive

An X-ray analysis was made on the liquid run-out from a specimen taken to 2400°C, well above the solidus temperature; the analysis showed only the presence of ZrB_2, SiC, and graphite.

    c. <u>Pressure Series</u>. The effect of molding pressure on density was examined on samples molded at pressures ranging from 3500 to 5500 lb/in.^{2} at temperatures of 2150° ±10 and 2230° ±10°C.
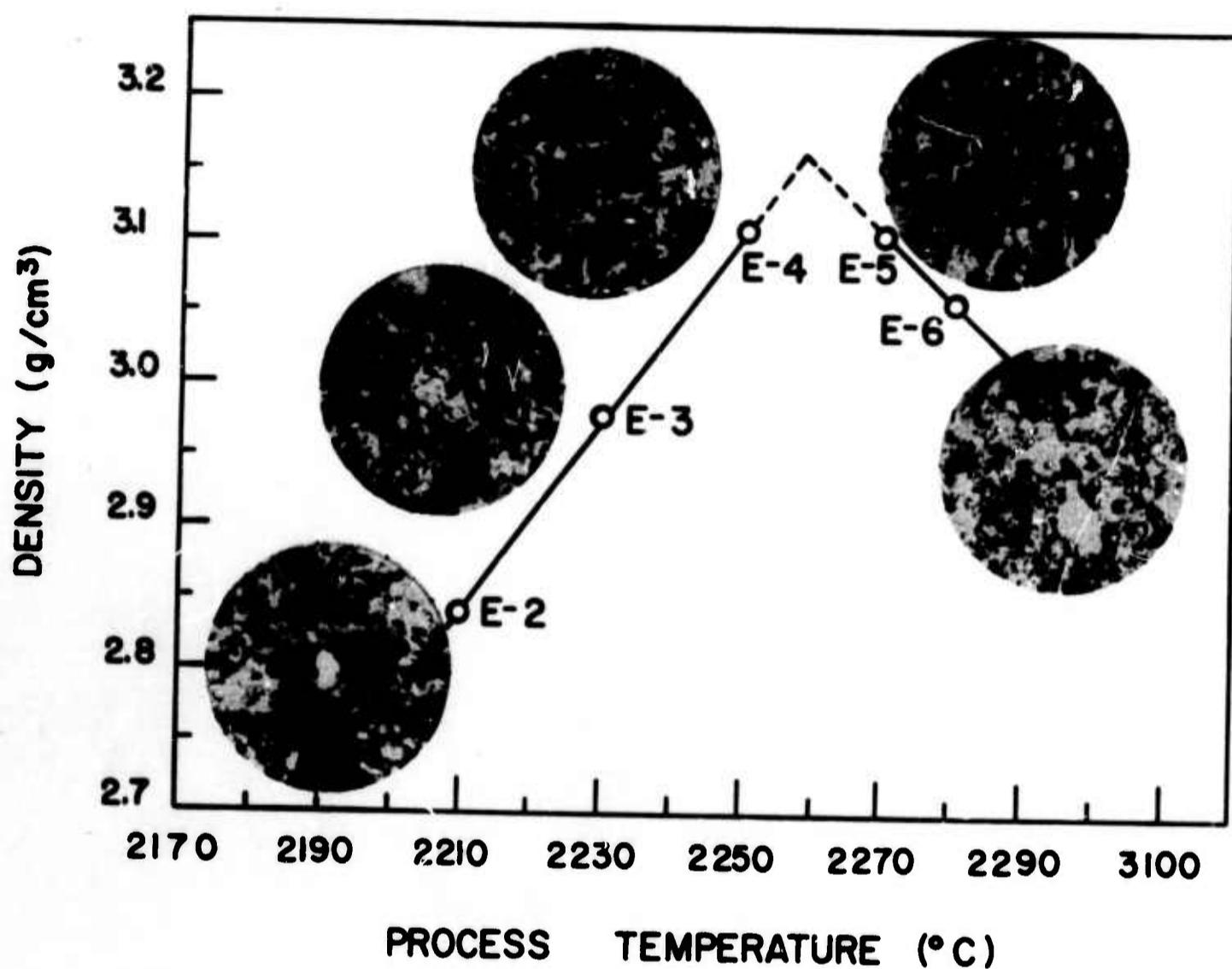
Figure 1. Effect of Processing Temperature on Density and
Microstructure of JT Material of 53.7 Percent Composition.
White Phase is ZrB_2, Light Gray Phase is SiC, and Dark
Gray and Black Phases are Graphite and Porosity.

N-9556

Figure 2 shows the dependence of density on molding pressure; the
figure also shows the density change with temperature for four
samples pressed at 5500 lb/in.^{2}. These data indicate that, to achieve
densities of 95 or higher percent of theoretical maximum density
(.95 x 3.27 = 3.11 g/cm^3), temperatures in excess of 2200°C and
pressures in excess of 5000 lb/in.^{2} are necessary.

d. <u>Ultrasonic Elastic Stiffness Constants</u>. The elastic
stiffness constants c_{ij} have been determined for the experimental
billets from measurements of the velocity of ultrasonic pulses at

-10-

one megacycle per second frequency. Figure 3 shows the stiffness
constants c_{11}, c_{33}, and c_{44} and the density for a series of billets
processed at successively higher temperatures. At a given density,
the value of each constant is 15 to 20 percent higher if the pro-
cessing temperature is above rather than below the solidus tempera-
ture. The consistently high values of the elastic constants of
the initial billets (fabricated as described in Section III-4)
are probably due to the maximum billet temperatures having been
higher than the solidus temperature, even though the outside mold
temperature was only 2130°C.
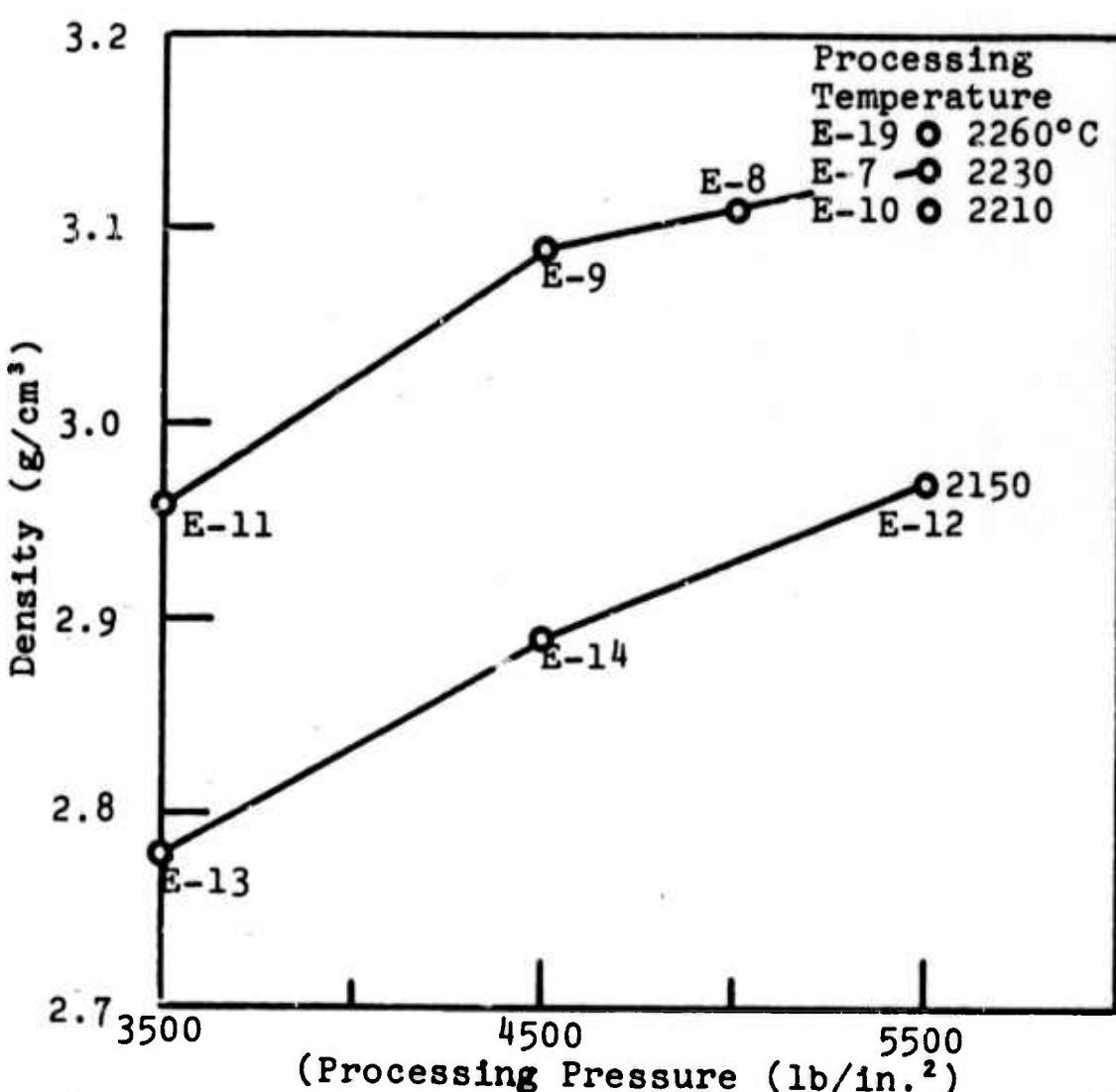
N-9481

Figure 2. Effect of Processing Pressure and Temperature on
Density of JT Material of 51.9 Percent Composition.

Figure 4 shows the stiffness constants c_{33} and c_{44} versus
density for all the 51.9 percent composition billets fabricated
at various pressures and various temperatures less than the soli-
dus temperature (see Table II for the processing conditions). It

appears that, within the reproducibility of the experiments, the elastic constants at fixed composition depend only on the density and not on the individual processing temperatures and pressures used to achieve that density, provided that the temperature is less than the solidus temperature. This result strengthens the original premise that the JT-materials program can be based entirely on composition and density as material variables.
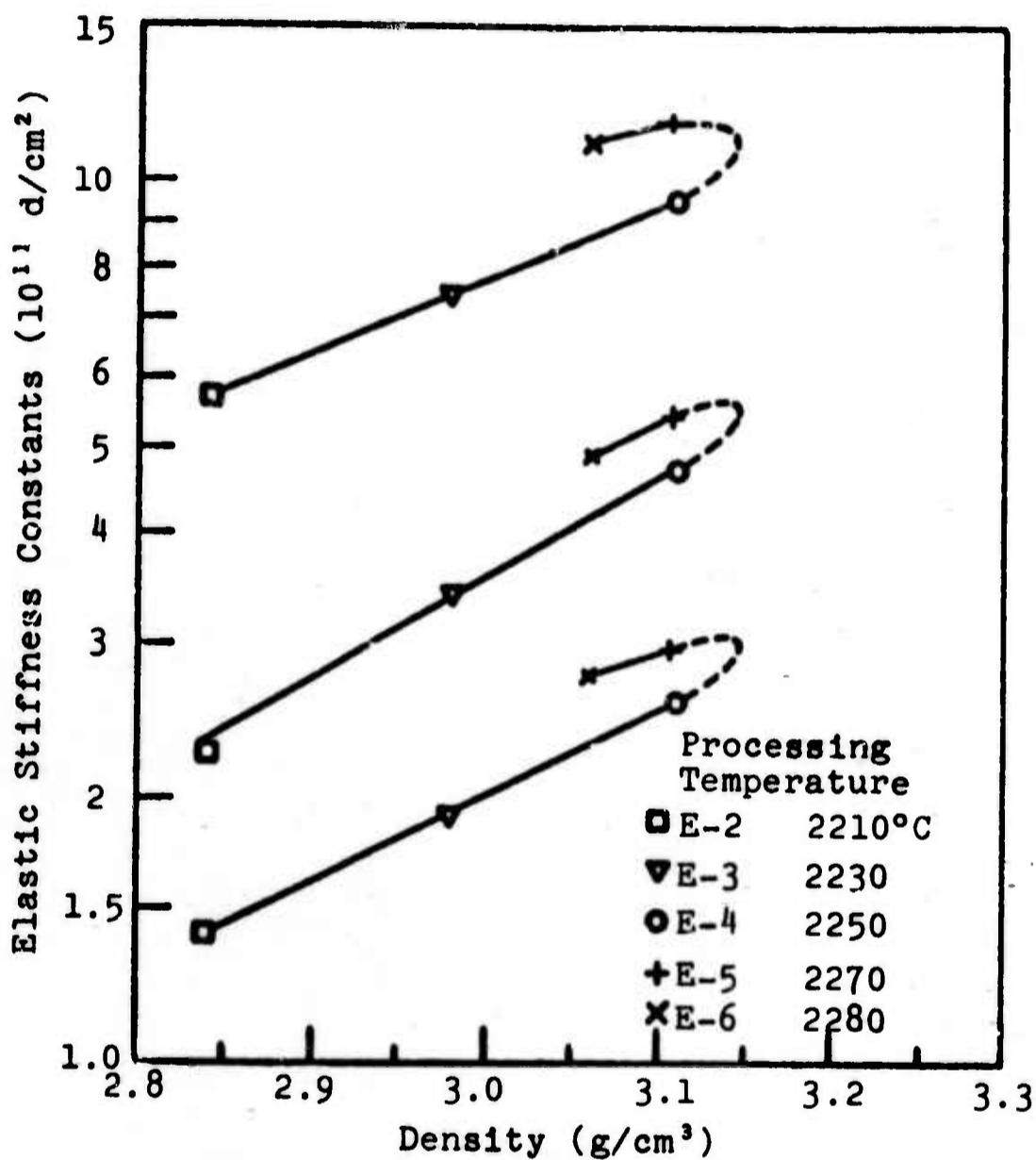
Figure 3. Effect of Processing Temperature on Density and Ultrasonic Elastic Stiffness Constants of JT Material of 53.7 Percent Composition.

N-9479

6. Process Studies on 3-Inch Diameter Billets

A 40-ton press with an induction furnace capable of attaining temperatures higher than 3000°C was employed for the process studies. Figure 5 shows an overall view of the press, including the induction coil and furnace assembly.
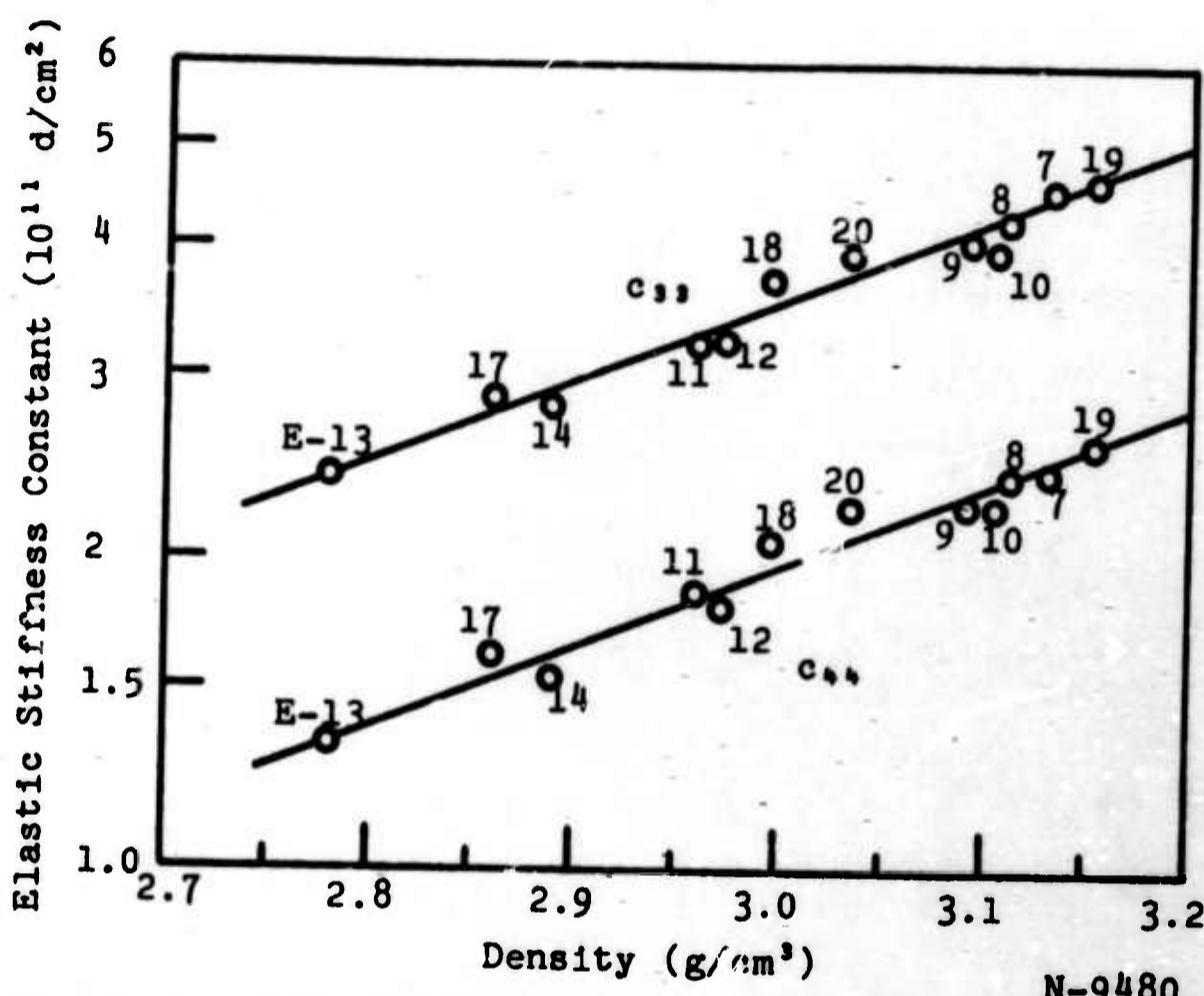
Figure 4. Ultrasonic Elastic Stiffness Constants Versus
Density for JT Materials of 51.9 Percent Composition

In induction heating at high heating rates, there is
a difference between the temperature of the outside surface of
the mold (which acts as the susceptor) and the temperature of the
billet. During normal fabrication, only the outside mold tempera-
ture is measured. Therefore, it was necessary to correlate the
surface temperature of the mold to the interior temperature of
the billet. This correlation was established by simultaneous
temperature measurements on the mold surface and at the center
of a specially prepared, prepressed billet of 51.9 percent compo-
sition. The maximum temperature difference was 140°C.

A three-inch diameter billet of JT material of 51.9
percent composition was hot pressed to 92.5 percent of theoretical
density by single ram pressing. The billet was sectioned, and a
density profile consisting of 15 specimens (1/2 x 1/2 x 1/2 inch)
was obtained. The density variation within the billet was 3.0 per-
cent; densities ranged from 3.01 to 3.10 g/cm^3. A three-inch dia-
meter billet of 31.5 percent composition was hot pressed by float
molding. The density profile of the sectioned billet resulted in
a 1.2 percent density variation; densities varied from 2.47 to
2.50 g/cm^3. Thus, float molding reduced the density variation in
a three-inch diameter billet from three percent to one percent.

-13-
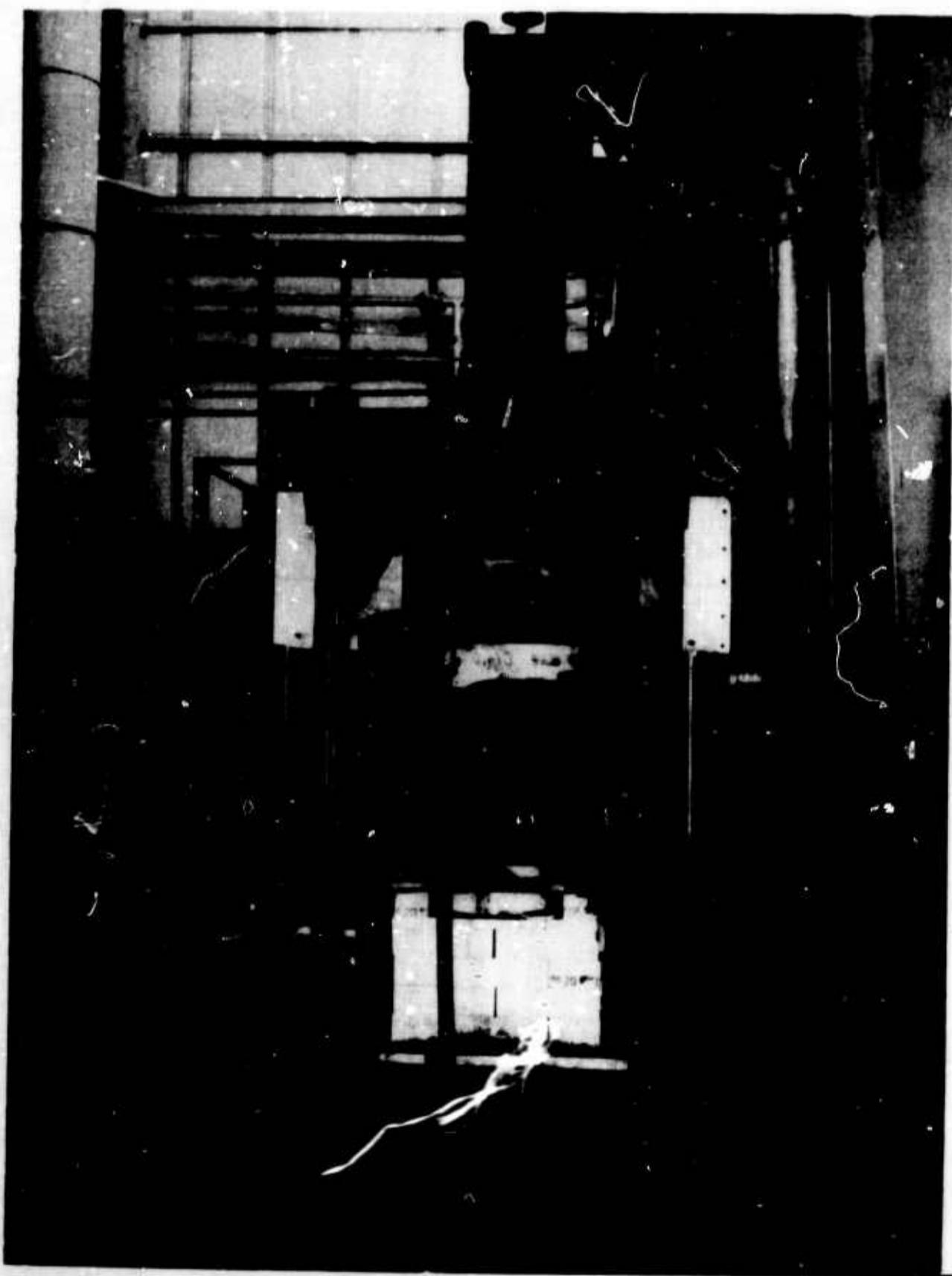
Figure 5. Forty-Ton Press and Induction Furnace Used for the Fabrication of the JT-Series Materials.

N-9557

Based on these results, additional billets of JT material were fabricated employing the float molding technique.

7. Fabrication of JT-Series Billets for Physical
    Property Evaluation

    A series of JT materials was fabricated for mechanical and thermal properties evaluation. The float mold technique and carefully controlled processing conditions were employed to hot press billets three inches in diameter and approximately 3.5 inches in length. Nominal compositions of 30, 50, and 70 percent metallic additive were used; at each composition the porosity was varied from a low of two-to-six percent to a high of 17 percent. Table III lists the composition, density, and porosity of the 27 billets fabricated.

TABLE III

COMPOSITION, DENSITY, AND POROSITY OF JT-BILLETS
USED FOR PROPERTY EVALUATION

Billet Number	Composition Percent Additive	Density g/cm^3	Porosity Percent
JT-30-16	31.5	2.61	6.2
JT-30-48	31.5	2.57	7.9
JT-30-40	31.5	2.54	8.8
JT-30-38	31.5	2.48	11.1
JT-30-32	31.5	2.45	11.9
JT-30-35	31.5	2.32	16.8
JT-30-31	31.5	2.30	17.6
JT-50-46	51.9	3.14	4.0
JT-50-22	51.9	3.11	4.9
JT-50-23	51.9	3.08	5.7
JT-50-43	51.9	3.08	5.7
JT-50-21	51.9	3.07	6.1
JT-50-44	51.9	3.05	6.7
JT-50-45	51.9	3.04	7.0
JT-50-28	51.9	3.02	7.7
JT-50-42	51.9	2.95	9.8
JT-50-27	51.9	2.94	10.1
JT-50-29	51.9	2.82	13.9
JT-50-26	51.9	2.71	17.3
JT-70-19	71.4	3.86	1.6
JT-70-47	71.4	3.84	2.0
JT-70-20	71.4	3.83	2.2
JT-70-18	71.4	3.82	2.6
JT-70-33	71.4	3.57	8.9
JT-70-34	71.4	3.45	11.9
JT-70-37	71.4	3.42	12.9
JT-70-17	71.4	3.26	16.9

SECTION IV

PHYSICAL PROPERTIES OF JT-SERIES MATERIALS

The objective of this work was to obtain physical property data which may be used as input information to stress analysis and structural synthesis calculations and for engineering applications of JT-series materials. The physical properties of interest are the elastic moduli, Poisson's ratios, stress-strain relations, fracture strengths, thermal conductivities, specific heats, and coefficients of thermal expansion.

1. Methods of Measurement

a. Ultrasonic. Elastic constants were determined from the velocities of propagation of longitudinal and transverse ultrasonic pulses at one megacycle per second frequency. Due to the high attenuation of the JT-series material, a through-transmission method was used with a path length of approximately 1.25 inches and with directions of propagation parallel, perpendicular, and at 45 degrees to the symmetry axis of the material.

b. Resonant Bar. Elastic constants were determined from the frequencies of longitudinal, flexural, and torsional vibrations of bars of dimensions 1/4 x 1/4 x 3 inches. In addition, measurements were made on the static tension and flexural specimens to detect defects and unusual characteristics of the specimens prior to static testing and to provide a check of the moduli determined from the initial slope of the stress-strain curves.

c. Tension and Compression Tests. Both longitudinal and transverse strains were measured with pairs of strain gages mounted on dog bones in tension and on rectangular prisms in compression. The dog-bone blank dimensions were 1/4 x 5/8 x 2-3/4 inches, and the gauge-section dimensions were 1/4 x 1/4 x 1-1/2 inches. The size of the compression sample was 1/4 x 1/4 x 1 inch.

d. Flexural Tests. Four-point loading on 1/4 x 1/4 x 3 inch bars was used for flexural testing. Transverse and longitudinal tensile and compressive strains were measured at the top and bottom surfaces with strain gages. Because the load versus strain relations are nonlinear and slightly different in tension and compression, the data obtained from flexural tests were converted to uniaxial stress-strain relations by means of Naidai's graphical method.[12] The effect of frictional forces at the loading and supporting edges was taken into account in the calculation of the true stresses.

e.   Thermal Diffusivity. Thermal diffusivities were measured from ambient to approximately 600°C by a flash method.[13] The sample size was 5/8 x 5/8 x 0.04 inch.

f.   Specific Heat. Specific heats were calculated by multiplying the weight percent of each constituent phase by the specific heat per unit mass of that phase [carbon,[14] zirconium diboride,[15] and silicon carbide,[16] assuming complete conversion of Si into SiC]. The calculations were made at 100-degree intervals from room temperature to 700°C. These calculations have been checked from room temperature to 400°C by measurements made with a Perkin-Elmer Differential Scanning Calorimeter.

g.   Coefficients of Thermal Expansion. The coefficients of thermal expansion from room temperature to 700°C were measured by the Newton's rings method on 1/2-inch cubes. Measurements in the temperature range from 20° to 2000°C have been made on bars 2-1/2 inches in length heated in a tube furnace. Telescopes equipped with micrometer eyepieces were used to measure the elongation.

2.   Mechanical Properties

Room temperature mechanical property measurements on the billets listed in Table III were made by using ultrasonic and sonic resonant bar tests and by static tensile, flexural, and compressive tests. For each material composition and for each property, a graph of the property versus density and porosity was prepared on which the data points from the various test methods were plotted. Representative examples of these graphs for JT-50 material are shown in Figures 6, 7, and 8. A curve was drawn through the points, and property values were obtained from the curve at porosities of 5, 10, and 15 percent. These values are listed in Table IV.

a.   Moduli. In most cases, static values of the Young's moduli are approximately 10 percent less than the sonic values. This discrepancy is due to the uncertainty in determining the initial slopes of the static stress-strain curves and, possibly, to other systematic errors. The sonic modulus results are considered to be more accurate and should be used at near-zero stress levels; the static stress-strain curves must, of course, be used at higher stress levels.

Typical longitudinal stress-strain curves for tension and compression of samples of JT-30, JT-50, and JT-70 material in the with-grain and against-grain directions are shown in Figures 9 and 10. Each curve is a composite of tension and compression data and represents the results of measurements on six samples (three tension and three compression). The range marks on each curve indicate both high and low stress values for the samples, and the

-17-
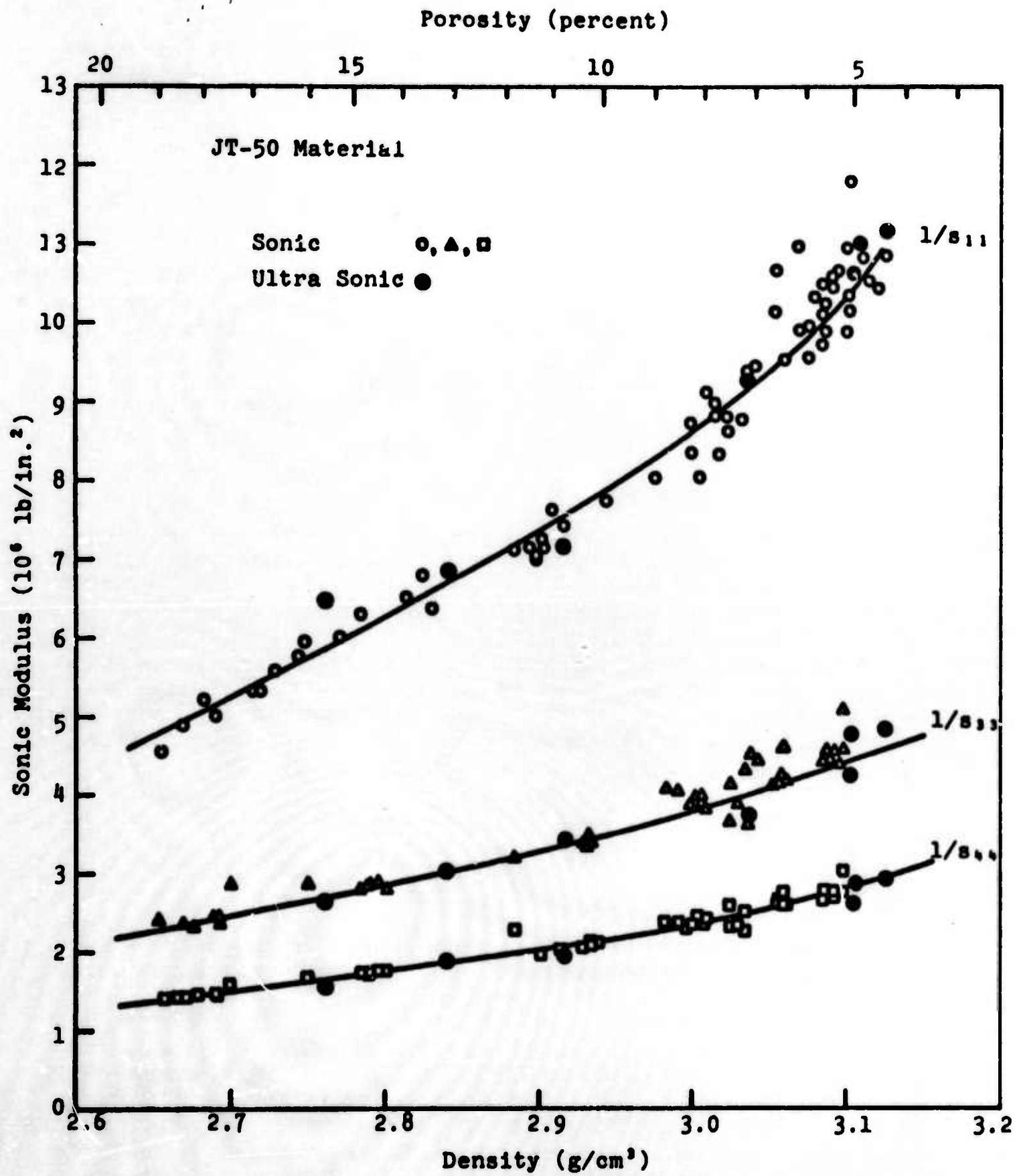
Figure 6. Variation of Sonic Moduli with Density and Porosity
JT-50 Material.

N-22146

-18-
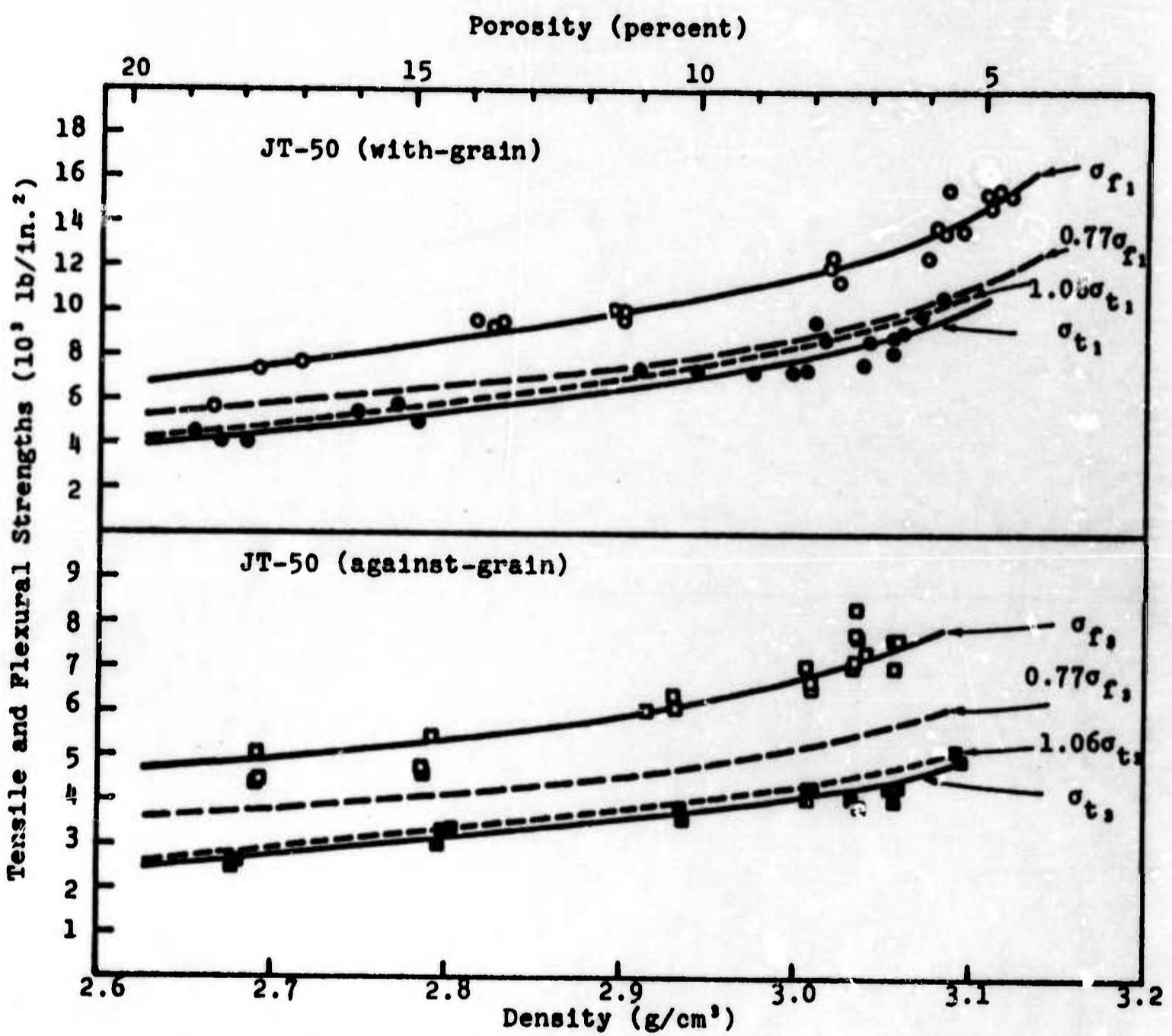
Figure 7. Variation in Tensile and Flexural Strengths with Density and Porosity for JT-50 Materials.

N-22145

-19-
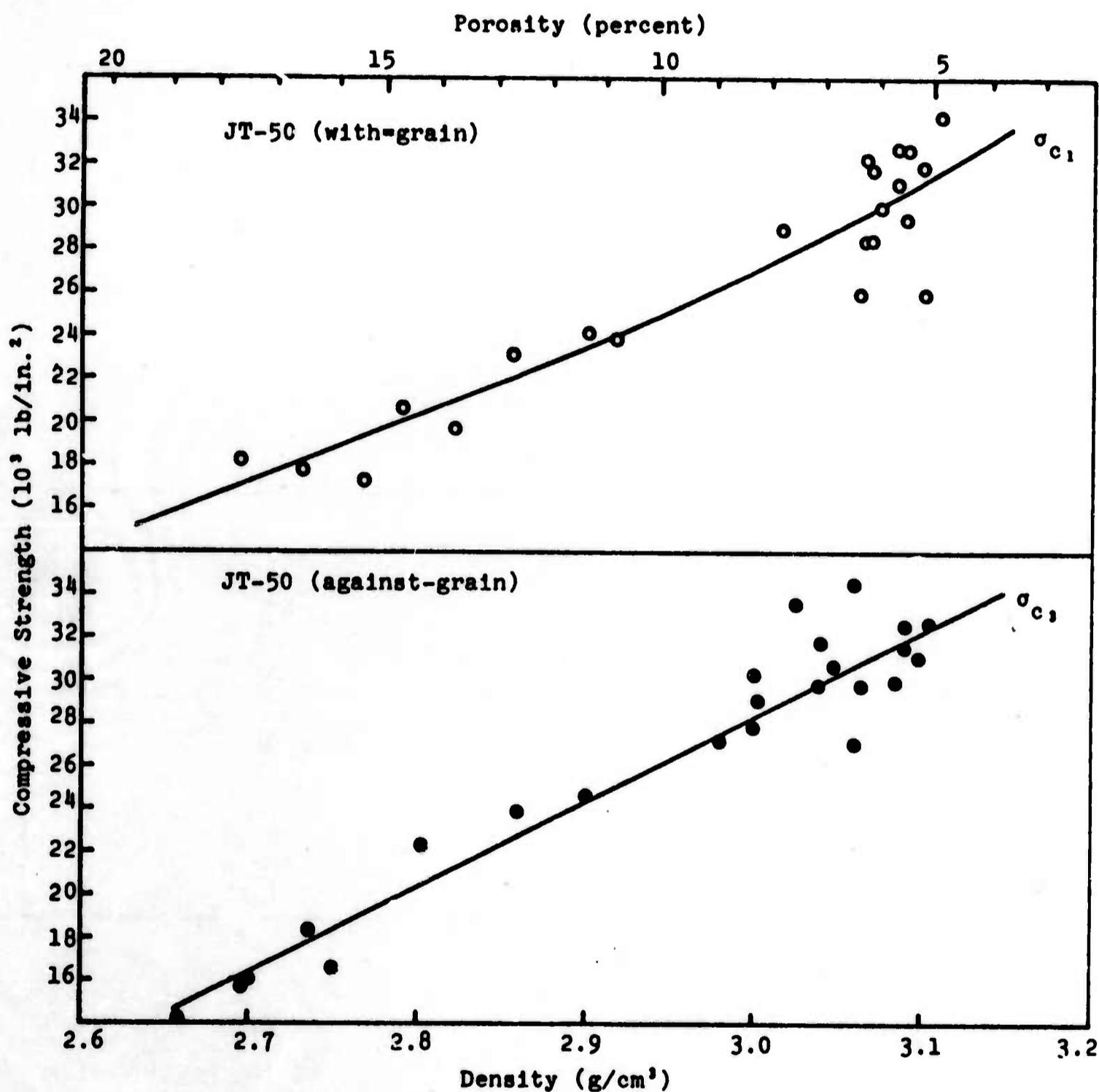
Figure 8. Variation in Compressive Strength with Density and Porosity for JT-50 Material.

N-22147

TABLE IV

SUMMARY OF MECHANICAL PROPERTY DATA FOR JT-SERIES COMPOSITES

Composition (%)		30			50			70	
Porosities (%)	5	10	15	5	10	15	5	10	15
Densities (g/cm³)	2.65	2.51	2.37	3.11	2.94	2.78	3.73	3.53	3.33
Young's Modulus $1/s_{11}$, sonic	5.67	4.46	3.34	10.41	7.87	6.10	22.00	16.80	14.00
$1/s_{11}$, static	5.28	4.38	3.55	9.50	7.21	5.93	21.90	16.60	13.75
$1/s_{33}$, sonic	2.26	1.86	1.51	4.42	3.50	2.77	11.90	9.04	7.33
$1/s_{33}$, static	2.04	1.70	1.40	3.81	3.17	2.53	11.70	8.93	7.11
Shear Modulus $1/s_{44}$, sonic	1.42	1.15	0.91	2.84	2.13	1.69	6.86	5.28	4.32
Poisson's Ratio $-s_{12}/s_{11}$	.095	.089	.085	.110	.104	.099	.136	.136	.136
$-s_{13}/s_{33}$	.145	.133	.123	.143	.133	.122	.136	.129	.122
Tensile Strength σ_{t_1}	6.31	5.33	4.51	11.13	7.58	5.67	13.50	9.15	7.00
σ_{t_3}	3.53	2.96	2.46	5.32	4.01	3.28	8.05	5.60	3.98
Compressive Strength σ_{c_1}	17.6	15.0	12.5	31.5	25.1	19.7	70.0	56.0	41.6
σ_{c_3}	23.0	19.2	15.5	32.5	26.1	19.6	56.5	45.5	34.2
Flexural Strength σ_{f_1}	8.22	6.46	4.85	11.40	8.20	6.51	16.17	10.70	5.47
σ_{f_3}	4.01	3.37	2.80	6.29	4.79	4.07	9.01	6.08	3.57

Units = Moduli - 10^6 psi; strength - 10^3 psi

curves were drawn through their midpoints. The general shapes of
the curves in tension and compression are similar with compressive
strengths and compressive strains being consistently higher in
each of the two orientations. The tensile and compressive strengths
are in each case an increasing function of the amount of metallic
additive.
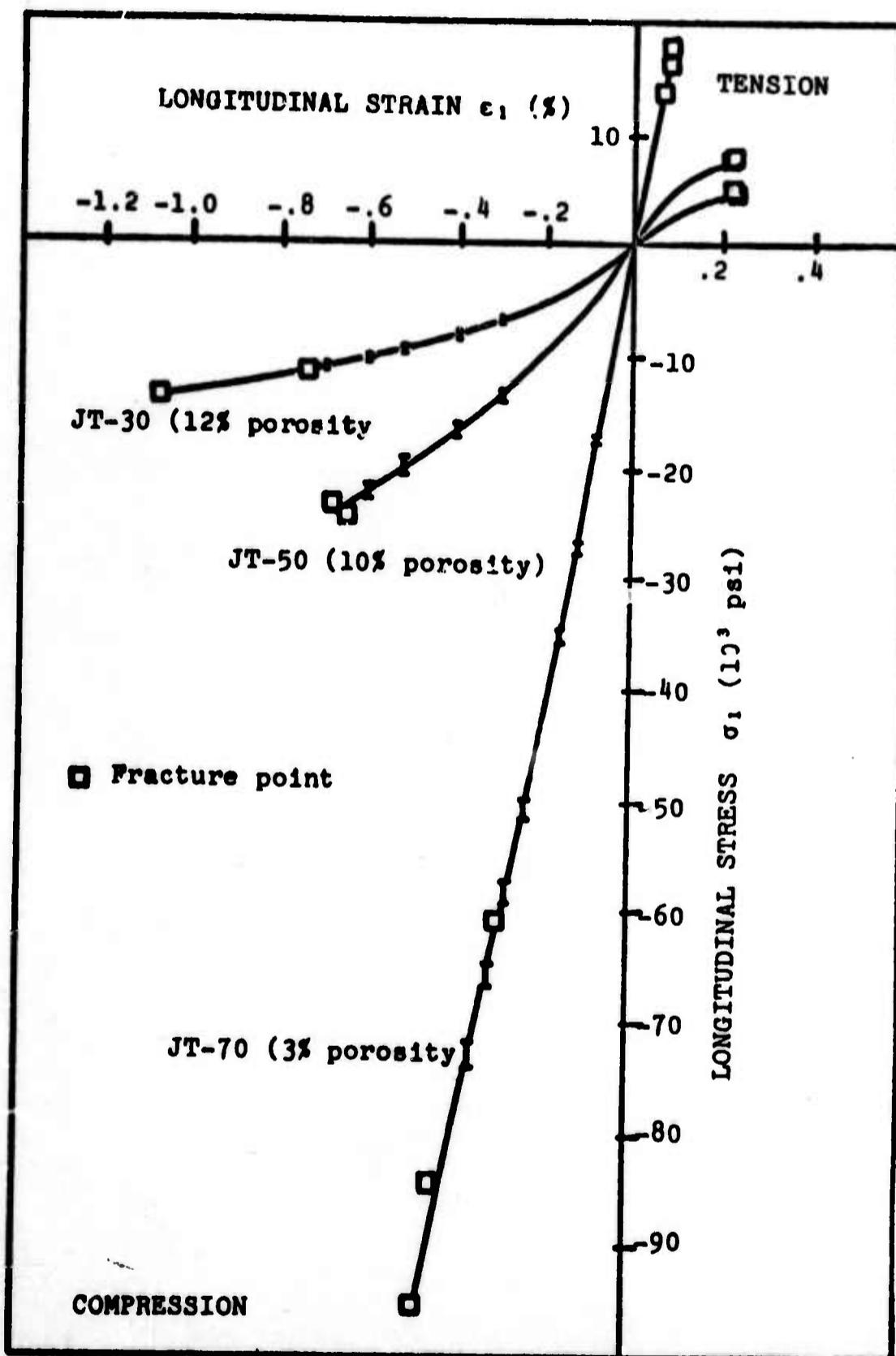
Figure 9. Stress-Strain Curves for With-Grain Samples of JT-30,
JT-50, and JT-70 Material in Tension and Compression.

-22-

N-22100
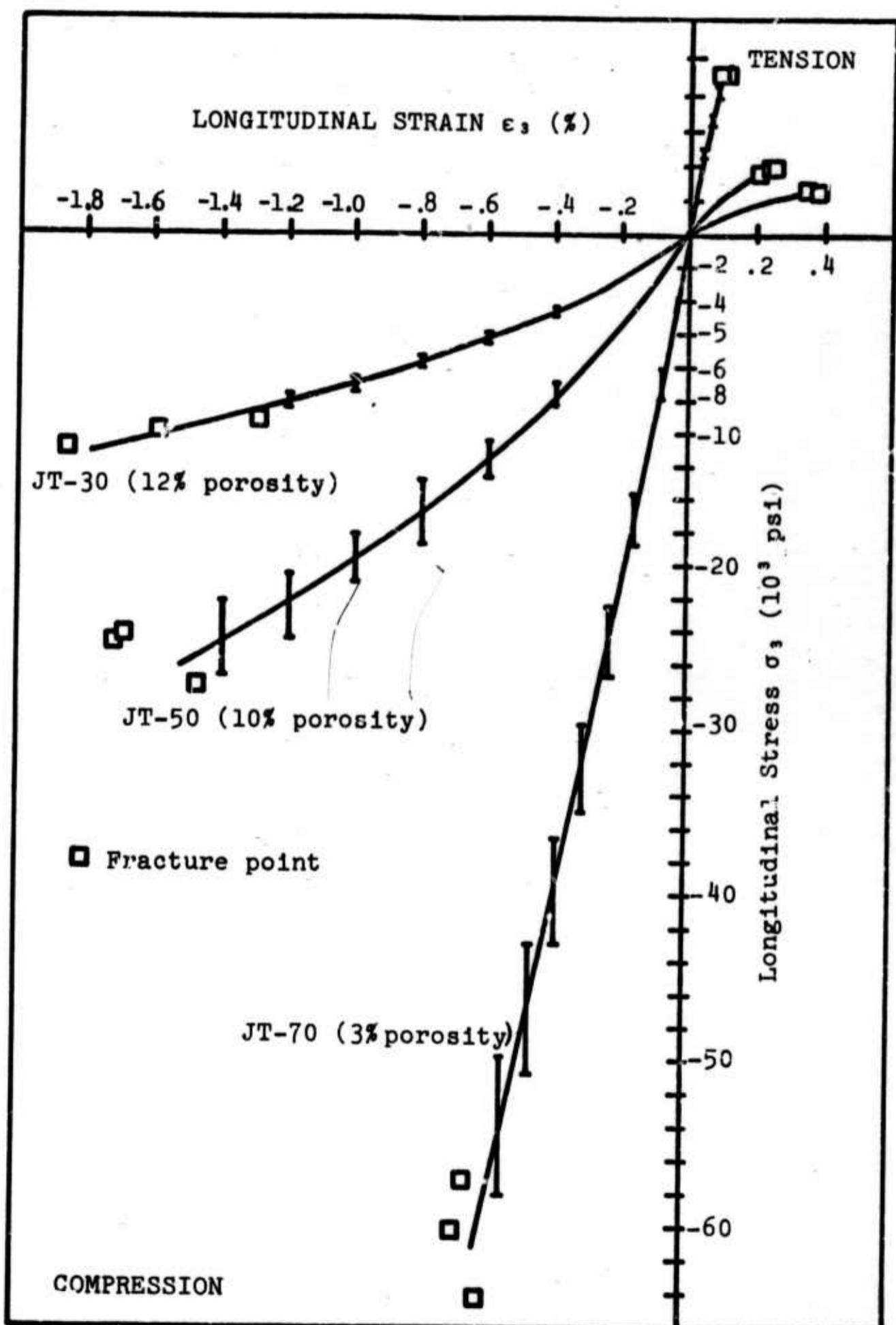
Figure 10. Stress-Strain Curves for Against-Grain Samples of JT-30, JT-50, and JT-70 Material in Tension and Compression.

N-22150

-23-

Typical longitudinal and transverse stress-strain curves for tension and compression on samples of JT-50 material in the with-grain and against-grain directions are shown in Figures 11 and 12. The stresses are longitudinal in every case. The transverse curves have slightly different shapes not only in tension and compression, but also with orientation. In the tension curves, the transverse strains are negative indicating that when a longitudinal tensile stress is applied a contraction takes place in the transverse direction. In the compression curves the transverse strains are positive indicating that when a longitudinal compressive stress is applied an expansion takes place in the transverse direction. The transverse strains for the with-grain orientation are considerably larger than the transverse strains for the against-grain orientation in both tension and compression. The transverse strain curves are all nonlinear, and, with the exception of one curve, have curvatures opposite to that of the longitudinal curves.

The variation of the with-grain and across-grain Young's moduli, with composition and porosity, determined by the sonic resonant bar test is shown in Figure 13. The moduli increase with increasing metallic additive composition and decreasing porosity. The variation of Poisson's ratios with composition is negligible, and the Poisson's ratios decrease slightly with increasing porosity. The range of Poisson's ratios are: $-s_{12}/s_{11} = 0.08$ to 0.11, and $-s_{13}/s_{33} = 0.12$ to 0.15, and $-s_{13}/s_{11} = 0.28$ to 0.37.

The shear moduli follow the same general variation with composition and porosity as do the Young's moduli; i.e., the shear moduli increase with increasing composition and decreasing porosity. This variation of the shear moduli, determined by the sonic resonant bar test, is illustrated in Figure 14.

b. Strengths. The flexural test data (see results for JT 50 material, Figure 7) have been corrected by a factor of 0.77 for nonlinearity in the shear-strain curves and for friction between the specimens and the fixture. The tensile strengths, computed from load divided by cross-sectional area, have been increased by a factor of 1.06 (see results for JT 50 material, Figure 7) to allow for stray bending moments in the gauge section. Even after these corrections are made, the tensile strength is consistently less than the flexural strength by approximately 10 to 20 percent. Two possible causes of this difference are a statistical dependence of strength on test volume and stress concentrations at the fillet of the dog-bone shaped tensile specimen. The variations of flexural, tensile, and compressive strengths with composition and porosity are shown in Figures 15, 16, and 17 for both the with-grain and across-grain properties. The strengths increase with increasing composition and decreasing porosity; the variation in the compressive strength is particularly large.

-24-
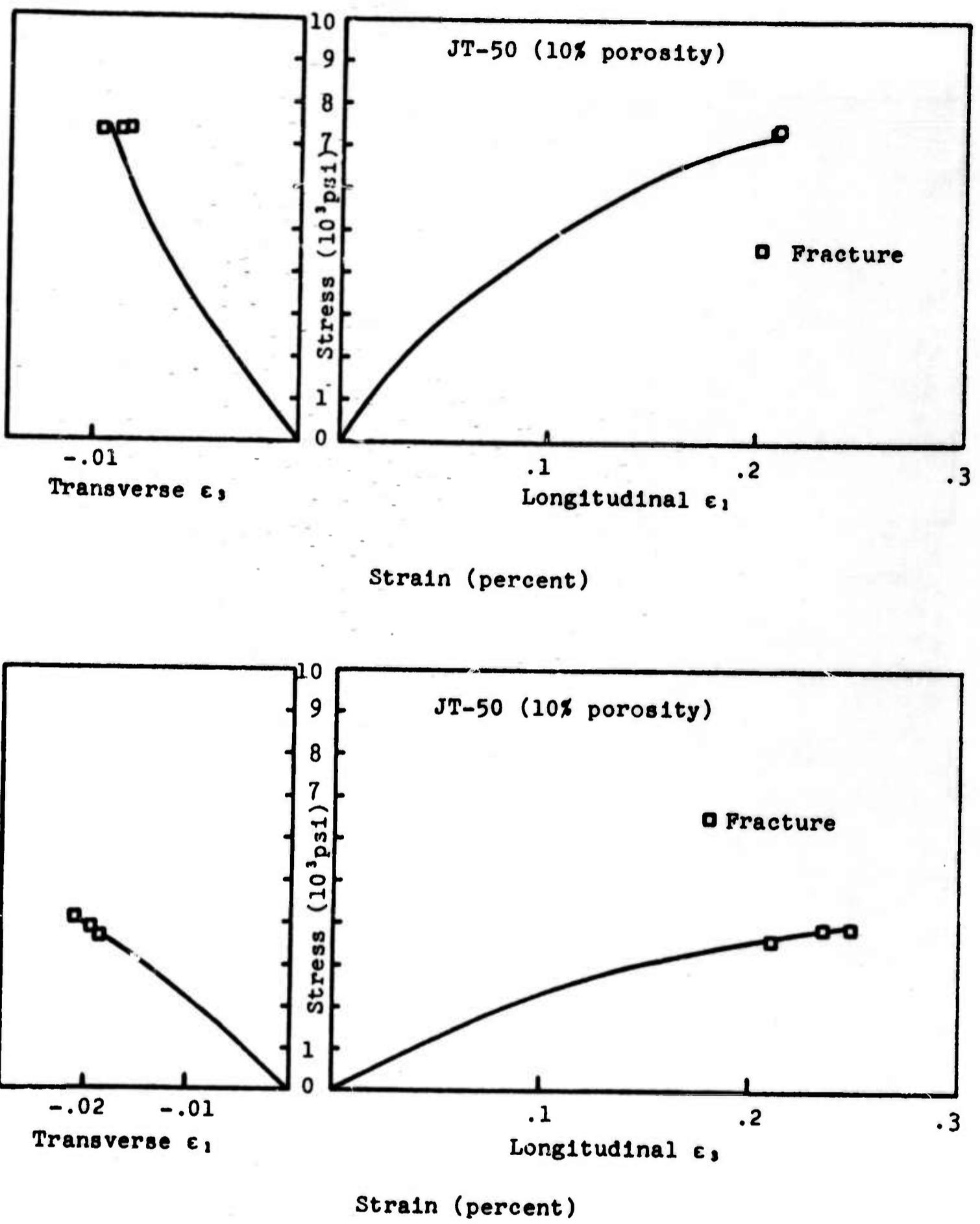
Figure 11. Stress-Strain Curves for With- and Against-Grain Samples of JT-50 Material in Tension Showing Longitudinal and Transverse Strains.

-25-

N-22149
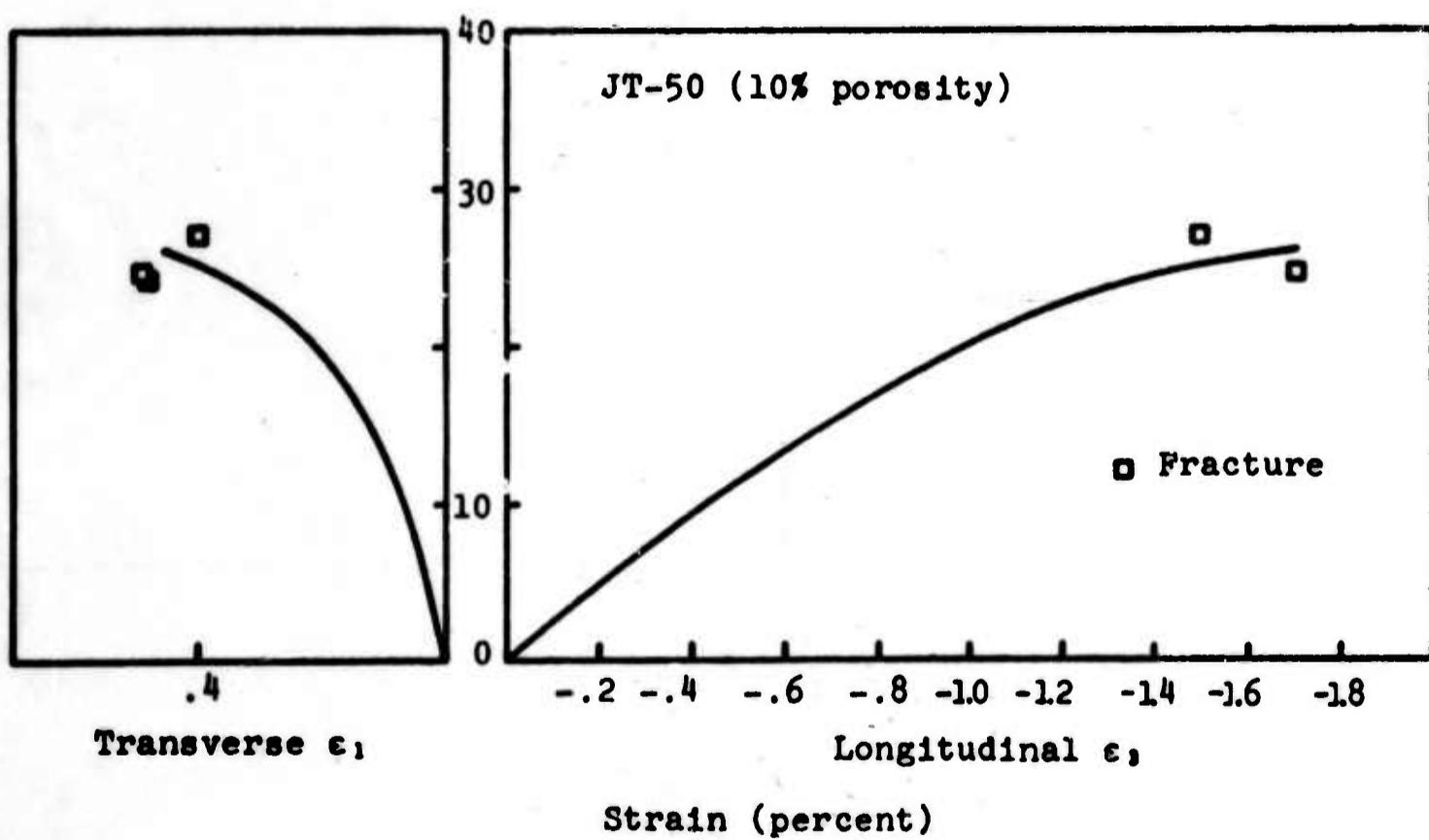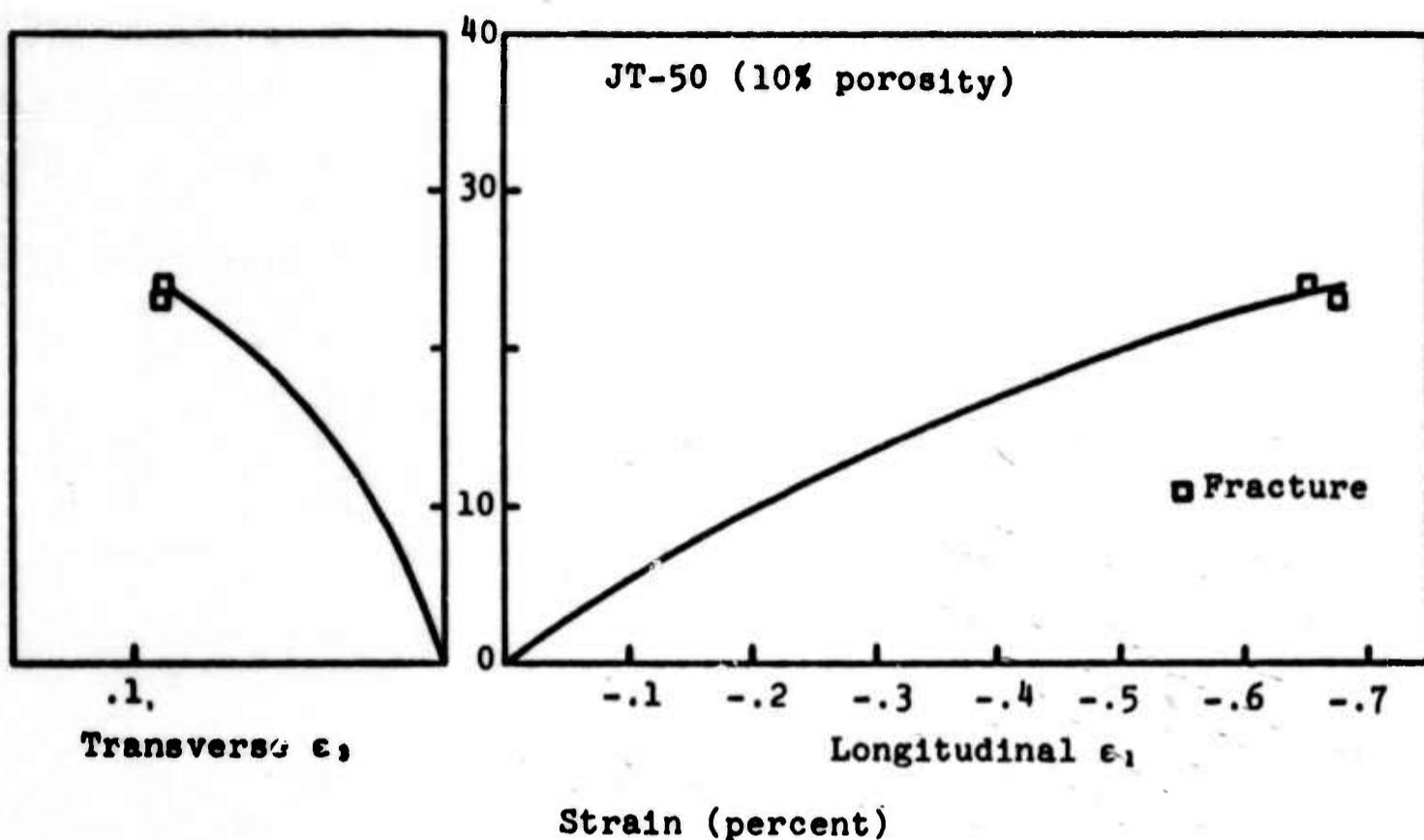
Figure 12. Stress-Strain Curves for With- and Against-Grain Samples of JT-50 Material in Compression Showing Longitudinal and Transverse Strains.

N-22148

Figure 14. Variation of Shear Moduli versus Composition and Porosity.   N-17224
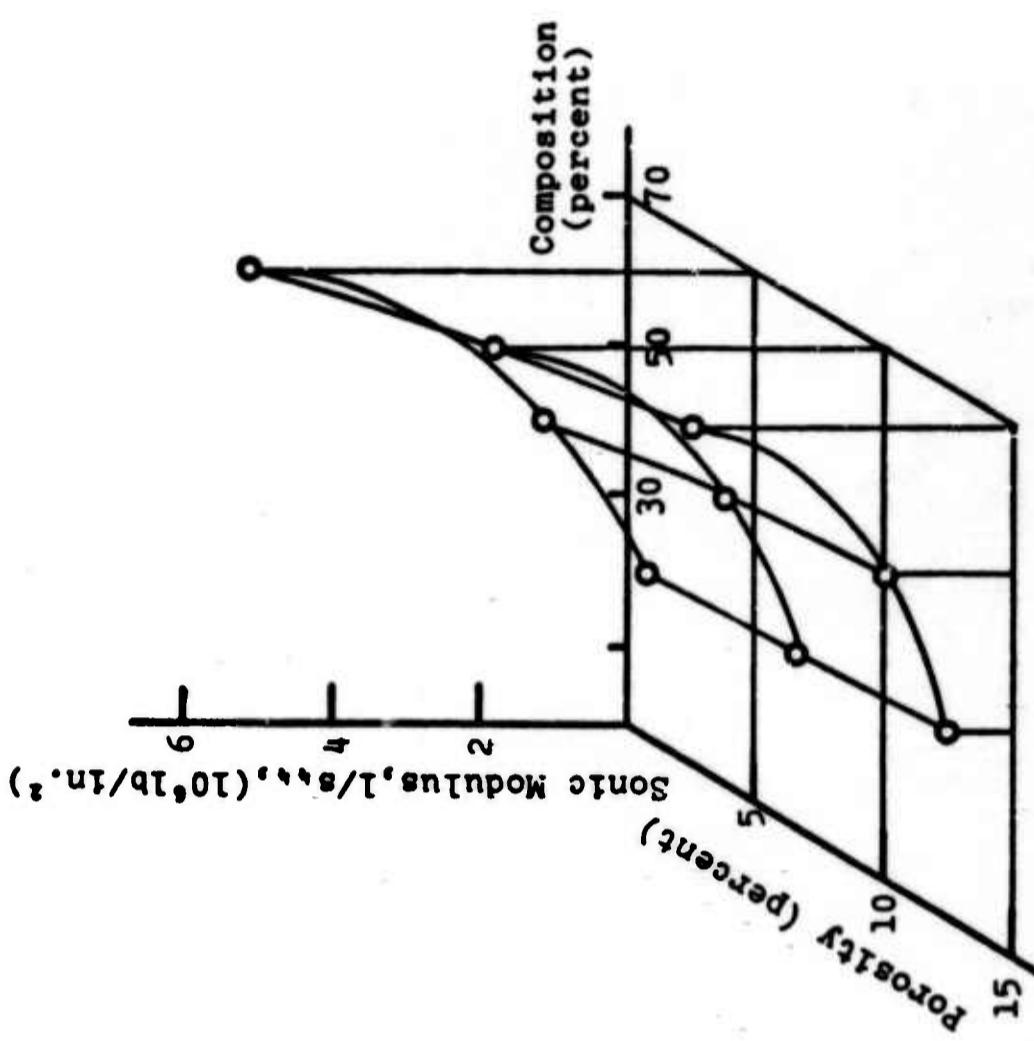
Figure 13. Variation of Young's Moduli versus Composition and Porosity.   N-10155

-27-

Figure 16. Variation of With-Grain and Across-Grain Tensile Strengths versus Composition and Porosity. N-17331
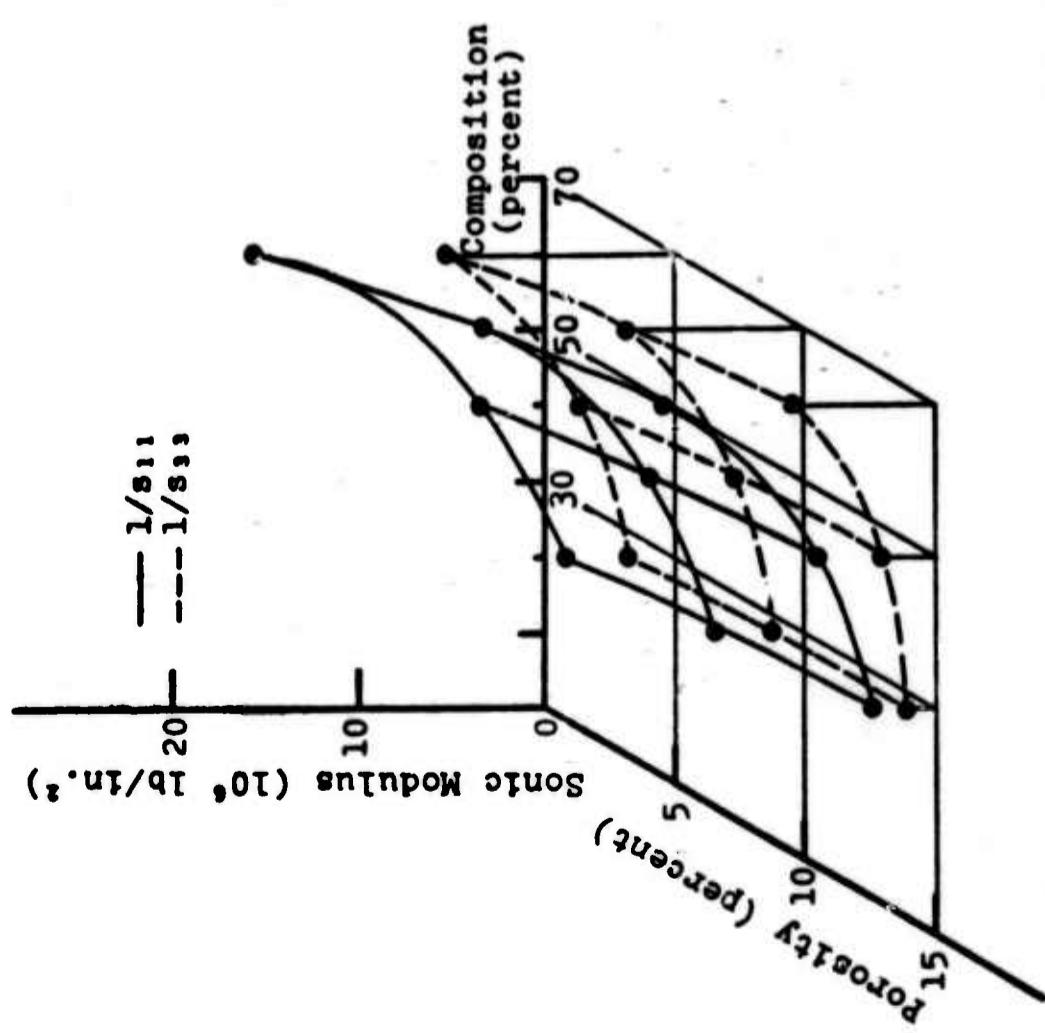
Figure 15. Variation of Flexural With-Grain and Across-Grain Strengths versus Composition and Porosity. N-17225

Composition (percent)

Tensile Strength (10^3 lb/in.^{2})

Porosity (percent)

Composition

Flexural Strength (10^3 lb/in.^{2})

Porosity (percent)
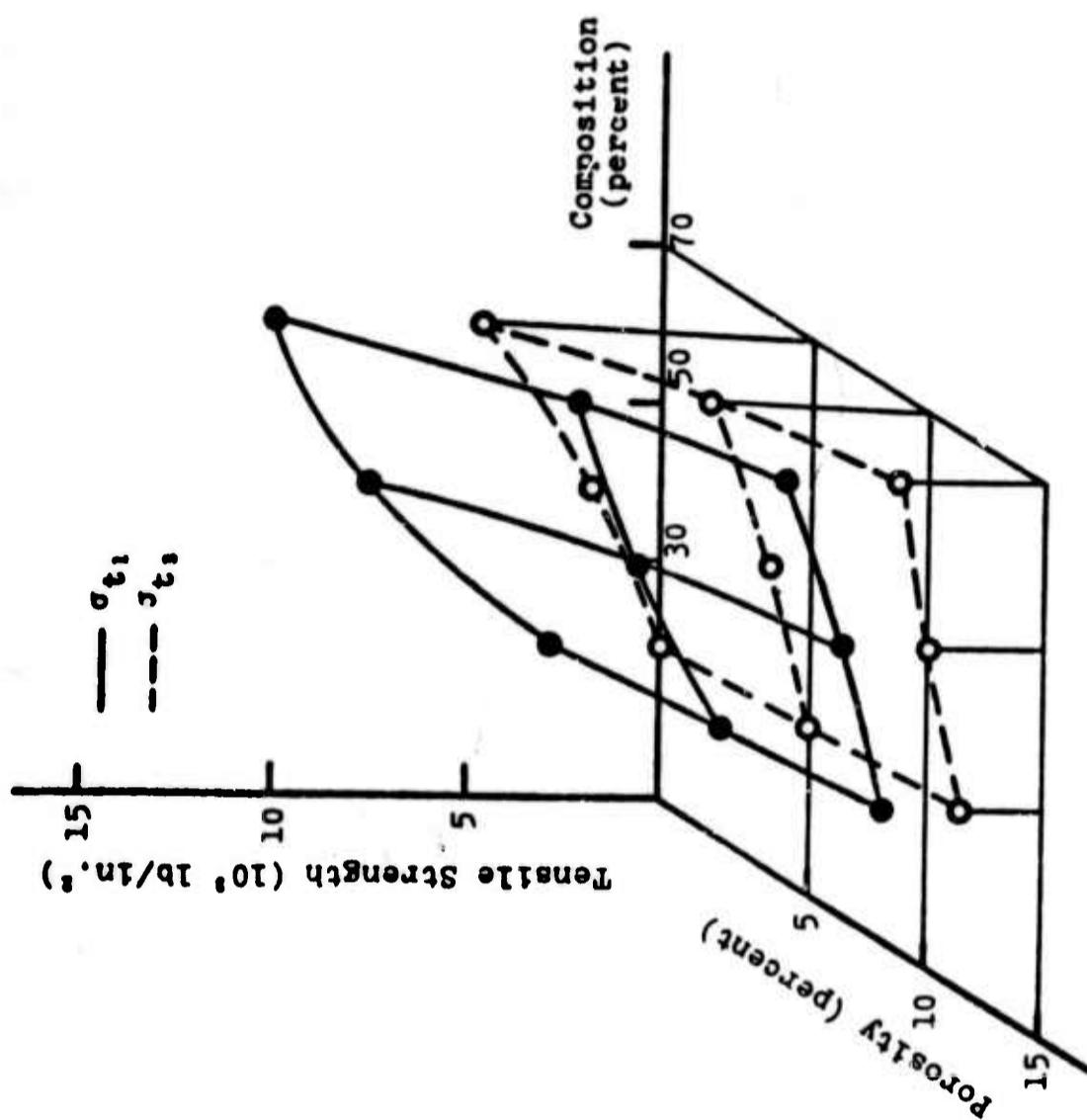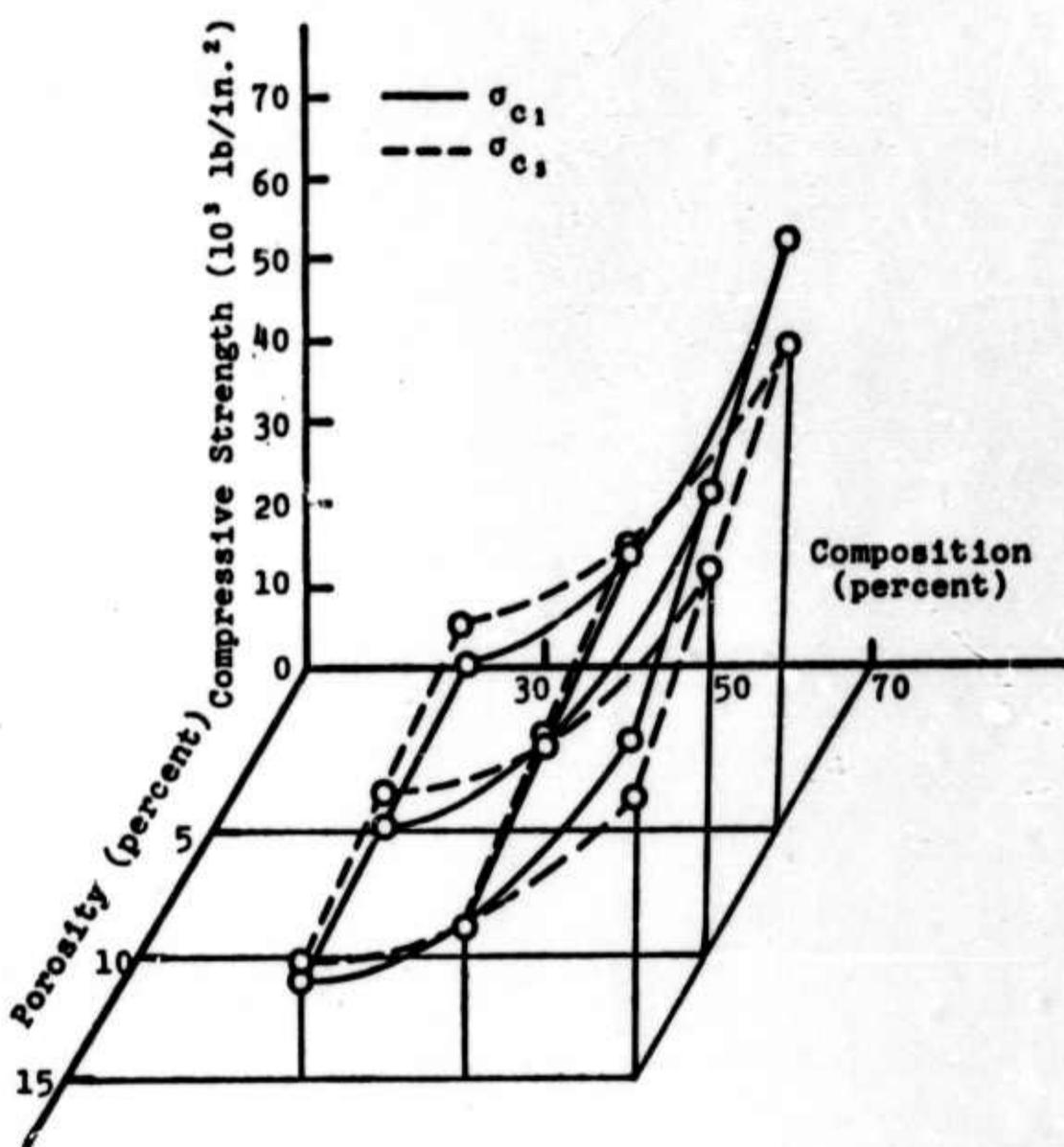
Figure 17. Variation of With-Grain and Across-Grain Compressive
Strengths versus Composition and Porosity.

N-17327

c. Hoop Tensile Tests. A fixture, similar to one
originally designed by the Stanford Research Institute, [17] was
constructed for hoop tensile stress testing by pressurizing a
short, open-end, thin-walled, hollow cylinder. The test fixture,
containing a test specimen and a Neoprene bag for pressurization,
is shown in Figure 18. By means of the hydraulic press, the upper
and lower plates of the test fixture are pressed against the spacers
which slide freely over the guiding pins. Because the length
of the specimen is slightly shorter than the length of the spacers,
there is a small clearance between the upper plate and the specimen;
thus, the specimen is free from end loads. When the Neoprene
bag is pressurized, the specimen is under pure hoop tensile stress.
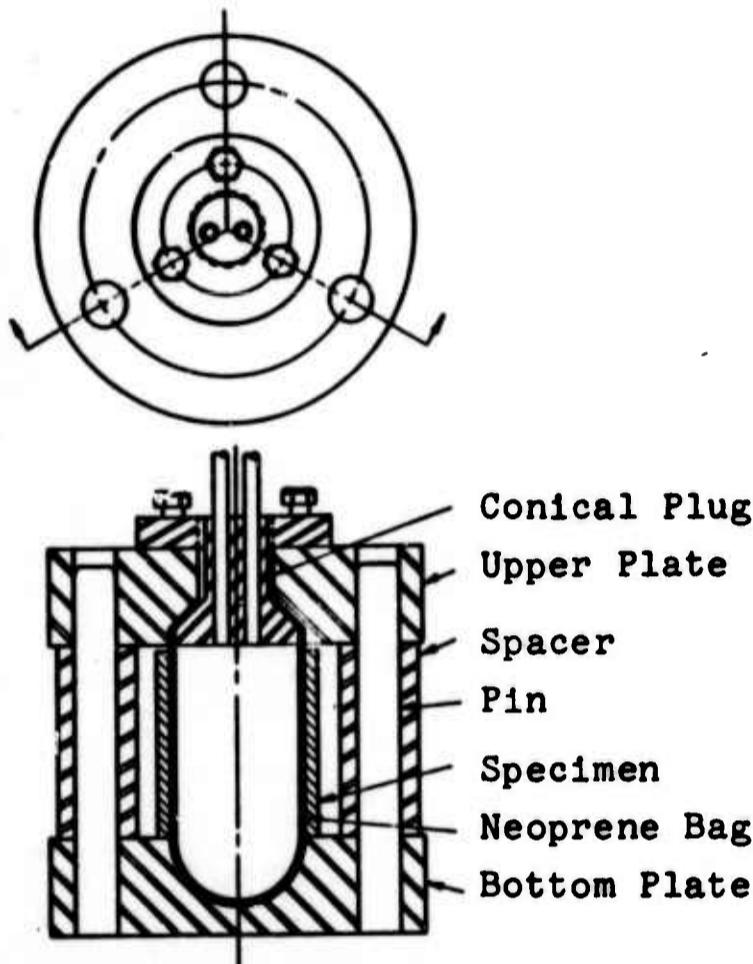
Figure 18.   Specimen and Test Fixture for Hoop
Tensile Stress Testing.

N-9469

Talc was applied between the specimen and the Neoprene bag to
minimize friction.   The inside and outside diameters of the test
cylinders are, respectively, 0.885 and 0.985 inch; the length
can be 0.5, 1.0, or 2.0 inches.

In order to check the test fixture, an epoxy cylinder
two inches long and aluminum cylinders having lengths of one and
two inches were tested to examine the effect of the specimen length
and pressure loading on uniformity of strain distribution.

The strain distribution in the epoxy cylinder was inves-
tigated with a reflection polariscope, and the variation of fringe
pattern was estimated to be less than 0.1 fringe.   This small
variation is believed to be due to variations in the properties
of the epoxy cylinder itself, rather than to variations in loading
stresses.   Strain distributions in the 1.0 and 2.0 inch aluminum
cylinders were investigated with strain gages and were also found
to be uniform; the experimental and theoretical values of the
strains are in good agreement.

Grade ATJ graphite cylinders with lengths of one and two inches were tested. The variation of the hoop strains measured with strain gages at four locations on the two-inch long ATJ graphite cylinder was two percent. Tensile strengths and strains obtained from these ATJ graphite cylinders are in good agreement with those obtained by the uniaxial tensile test. The tensile fracture strength and strain for a JTA-9 cylinder were 7500 lb/in.^{2} and 1180 μin./in., respectively.

d. <u>Torsion Tests</u>. Four solid torsion specimens of JT-50 material were tested in the apparatus shown in Figure 19.
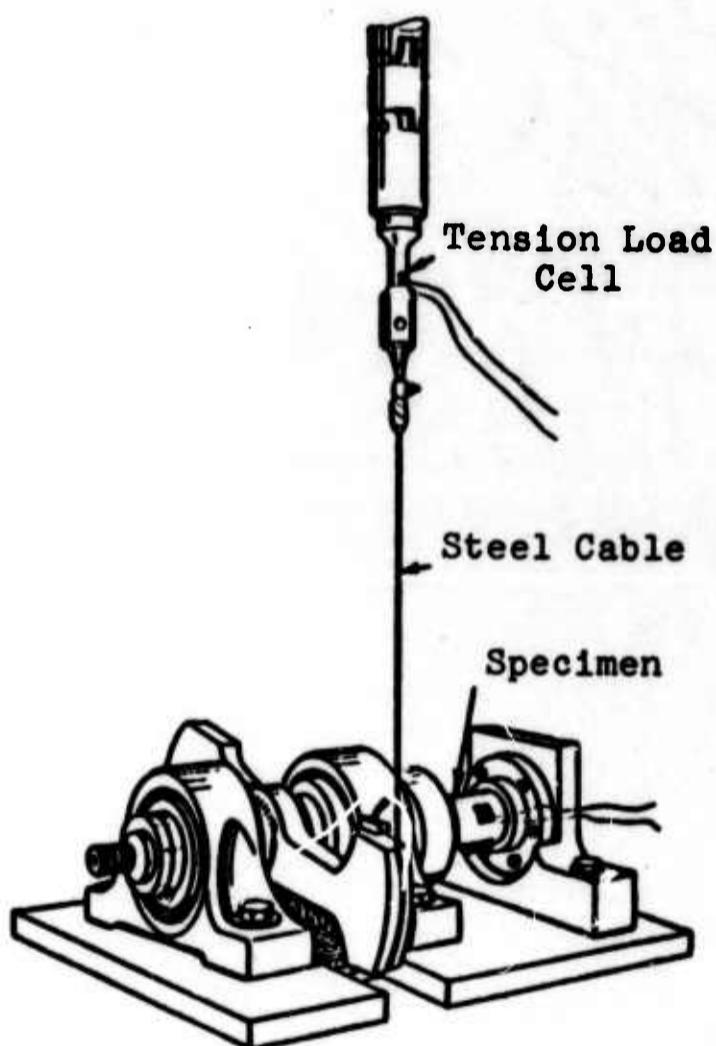
Figure 19. Torsion Testing Machine.

N-10143

The overall length of the specimens was approximately 3.5 inches; the gage section was 0.75-inch in diameter and 2.0 inches in length. The cylinder axis was oriented parallel to the symmetry axis of the material. Shear strain and longitudinal strain were measured with pairs of strain gages. The shear-stress versus shear-strain curve and the shear-stress versus longitudinal-strain curve

-31-

are shown in Figures 20 and 21, respectively, for one of the speci-
mens. The stress-strain behavior for these specimens is similar
to their uniaxial stress-strain behavior: nonlinear and nonconserva-
tive.
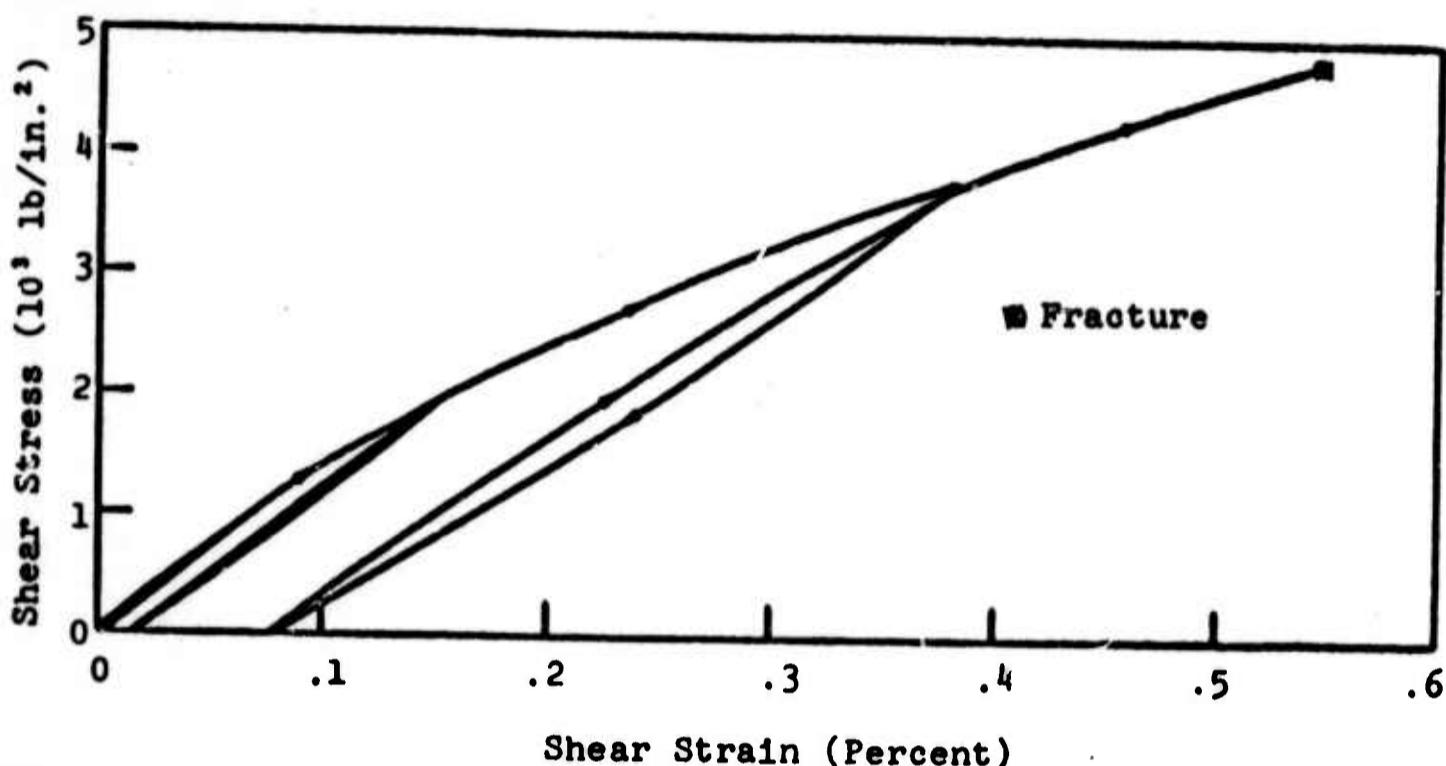
Figure 20. Shear-Stress versus Shear-Strain Curve for JT-50 Material.

Since the torque versus shear-strain curve for JT-series
composites is nonlinear and nonconservative, Naidai's graphical
method[18] was employed to obtain the shear-stress versus shear-
strain relationship from the torque versus shear-strain curve.
The shear properties for these specimens are also given in Table V.
The shear-strain for specimen 1 was not properly recorded, and,
therefore, cannot be used for construction of the shear stress as
a function of shear-strain curve. The nonlinearity correction on
shear strength is approximately nine percent.

The shear strength tends to increase and the shear strain
to decrease with increasing density. The value of the shear
strength is approximately 10 to 20 percent greater than the tensile
strength in the across-grain direction. The specimens exhibited
a small longitudinal elongation. Length changes in plastically
twisted circular metal specimens have been observed by Swift.[19]
The inherent characteristics of the torsion test and the aniso-
tropy of the materials are believed to be the source of this phe-
nomenon.[18,19,20] The theory of anisotropic plastic flow developed
by Hill[20] also supports the explanation of the length change due
to the anisotropy of the materials.
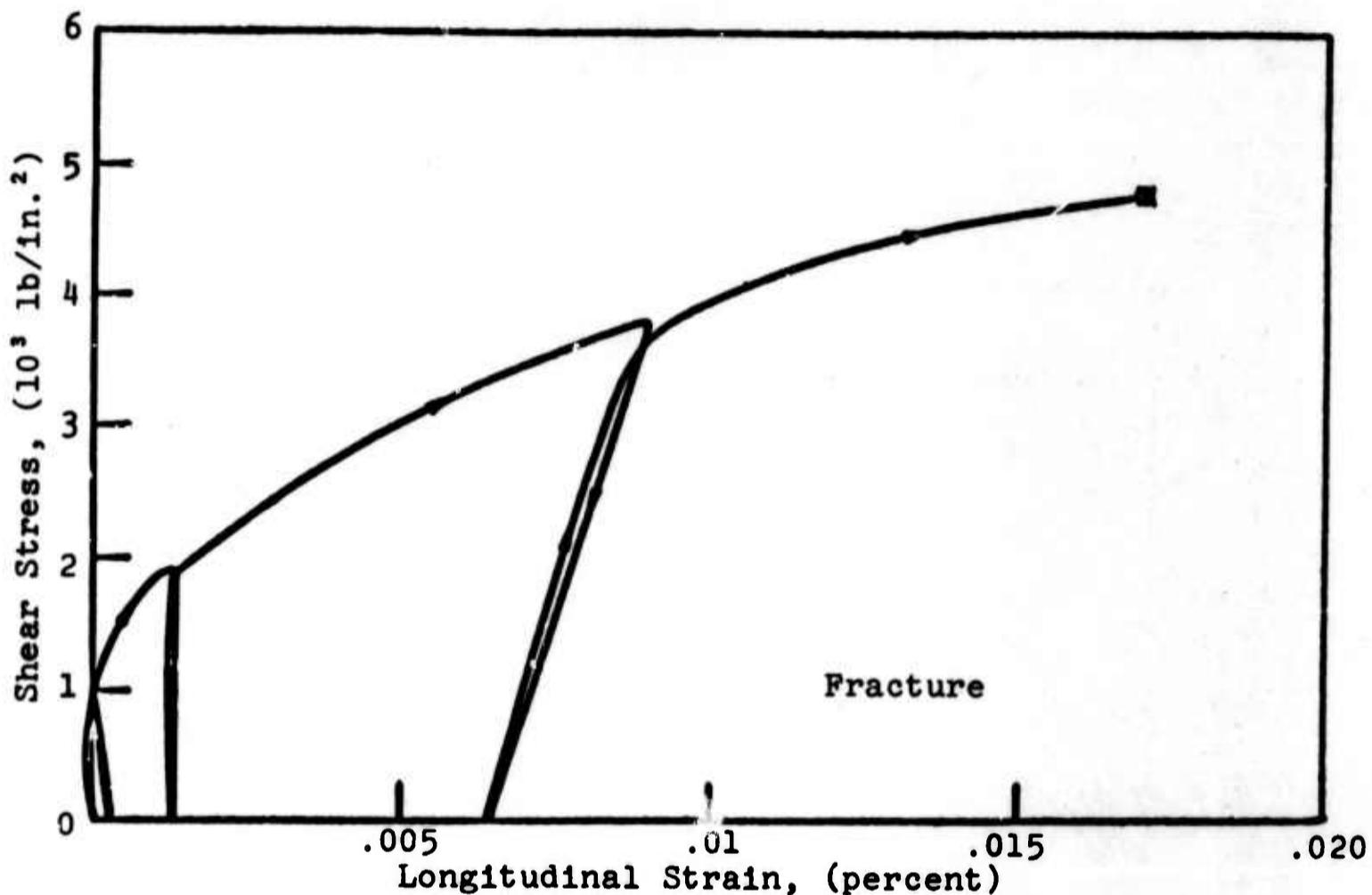
Figure 21. Shear-Stress versus Longitudinal-Strain
Curve for JT-50 Composite Material.

N-11270

TABLE V

SHEAR PROPERTIES FOR JT-50 COMPOSITE MATERIAL

Specimen	Density (g/cm³)	Shear Modulus 1/s₄₄ (10⁶ lb/in.²)		Shear Strength (lb/in.²)		Shear Strain (percent)	Long. Strain (percent)
		sonic	static	uncorrected	corrected		
1	2.934	2.11	---	5750	---	---	0.01
2	2.931	2.11	1.98	5160	4740	0.55	0.03
3	3.014	2.27	2.43	6160	5630	0.44	0.03
4	3.012	2.28	2.43	6690	6080	0.48	0.04

-33-

3. Thermal Properties

a. **Specific Heat.** The dependence of specific heat, c_p, on temperature is given in Figure 22 for the nominal compositions at 30, 50, and 70 percent. The curves were calculated from the specific heats of the constituent phases. The measured points are in very good agreement with the calculated values.
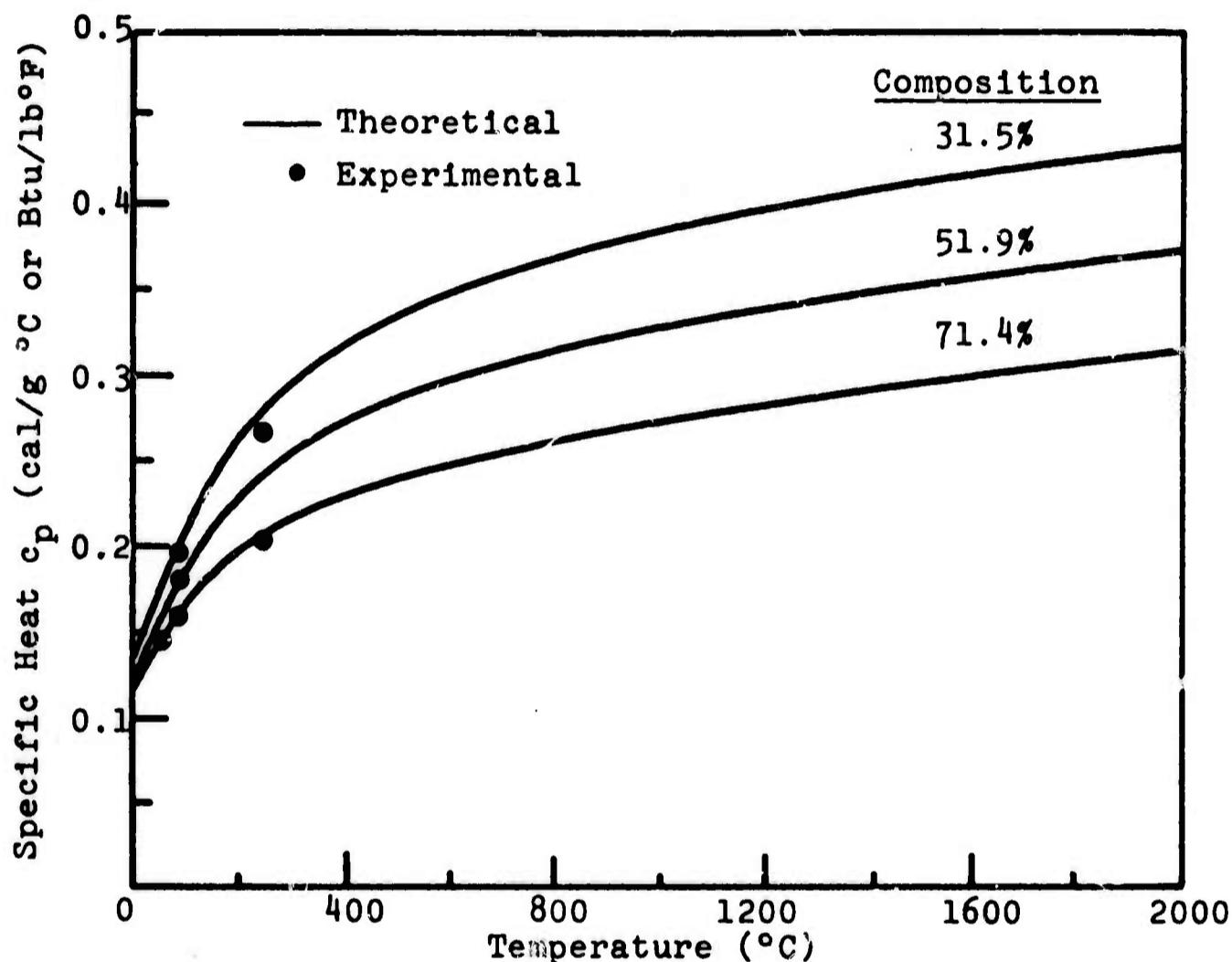
Figure 22. Specific Heat versus Temperature for JT-Material.

N-18117

b. **Thermal Diffusivity and Conductivity.** The thermal diffusivity, κ_i, has been measured from room temperature to 600°C. The thermal conductivity k_i, has been calculated from the thermal diffusivity by means of the relation

$$k_i = \rho c_p \kappa_i, \tag{3}$$

where ρ is the density. The thermal diffusivity and thermal conductivity results for the nominal 30, 50, and 70 percent composition and 5, 10, and 15 percent porosities are reported in Tables VI, VII, and VIII.

TABLE VI

THERMAL DIFFUSIVITY AND THERMAL CONDUCTIVITY OF JT-30 MATERIAL

Temperature (°C)	Thermal Diffusivity (cm²/sec)						Thermal Conductivity (cal/sec cm-deg)					
	5% Porosity		10% Porosity		15% Porosity		5% Porosity		10% Porosity		15% Porosity	
	k_1	k_3	k_1	k_3	k_1	k_3	k_1	k_3	k_1	k_3	k_1	k_3
100	.371	.186	.362	.183	.352	.179	.194	.097	.179	.091	.165	.039
200	.301	.151	.292	.148	.282	.144	.195	.098	.180	.091	.164	.084
300	.254	.127	.245	.123	.236	.119	.187	.093	.171	.086	.155	.078
400	.224	.108	.215	.104	.205	.100	.178	.086	.161	.078	.146	.071
500	.200	.094	.191	.090	.181	.087	.168	.079	.152	.072	.136	.065
600	.183	.083	.174	.079	.164	.075	.160	.073	.144	.066	.129	.059

TABLE VII

THERMAL DIFFUSIVITY AND THERMAL CONDUCTIVITY OF JT-50 MATERIAL

Temperature (°C)	Thermal Diffusivity (cm²/sec)						Thermal Conductivity (cal/sec cm-deg)					
	5% Porosity		10% Porosity		15% Porosity		5% Porosity		10% Porosity		15% Porosity	
	k_1	k_3	k_1	k_3	k_1	k_3	k_1	k_3	k_1	k_3	k_1	k_3
100	0.361	0.212	0.346	0.202	0.331	0.191	0.200	0.117	0.172	0.100	0.164	0.094
200	0.304	0.175	0.289	0.164	0.274	0.153	0.204	0.117	0.174	0.099	0.164	0.092
300	0.264	0.143	0.250	0.135	0.235	0.128	0.198	0.107	0.175	0.094	0.157	0.086
400	0.237	0.125	0.222	0.118	0.207	0.111	0.190	0.100	0.160	0.085	0.148	0.080
500	0.215	0.108	0.200	0.103	0.186	0.097	0.182	0.091	0.152	0.0??	0.140	0.073
600	0.201	0.095	0.186	0.091	0.172	0.087	0.177	0.084	0.147	0.0??	0.135	0.068

There is a large uncertainty in the last significant figure.

TABLE VIII

THERMAL DIFFUSIVITY AND THERMAL CONDUCTIVITY OF JT-70 MATERIAL

Temperature (°C)	Thermal Diffusivity (cm²/sec)						Thermal Conductivity (cal/sec cm-deg)					
	5% Porosity		10% Porosity		15% Porosity		5% Porosity		10% Porosity		15% Porosity	
	k_1	k_3	k_1	k_3	k_1	k_3	k_1	k_3	k_1	k_3	k_1	k_3
100	.324	.215	.307	.204	.292	.192	.193	.128	.174	.115	.109	.072
200	.274	.178	.257	.169	.241	.160	.192	.125	.171	.112	.106	.070
300	.238	.154	.224	.146	.211	.139	.183	.118	.163	.106	.101	.067
400	.214	.140	.200	.133	.186	.125	.175	.114	.155	.103	.095	.064
500	.196	.131	.183	.124	.170	.115	.167	.111	.147	.100	.090	.061
600	.176	.111	.166	.108	.156	.105	.155	.098	.139	.090	.086	.058

c.   Thermal Expansion. The coefficient of thermal expansion data showed somewhat greater scatter than did the other property data. This scatter masked any dependence of the thermal expansion on porosity that might exist. The thermal expansion does depend slightly on composition, but the dependence is opposite for the with-grain and across-grain directions. The coefficients of thermal expansion α_1 and α_3 are almost equal for the 70 percent composition. The trends of α_1 and α_3 with temperature up to 1500°C are shown in Figure 23 for the nominal compositions of 30, 50, and 70 percent.
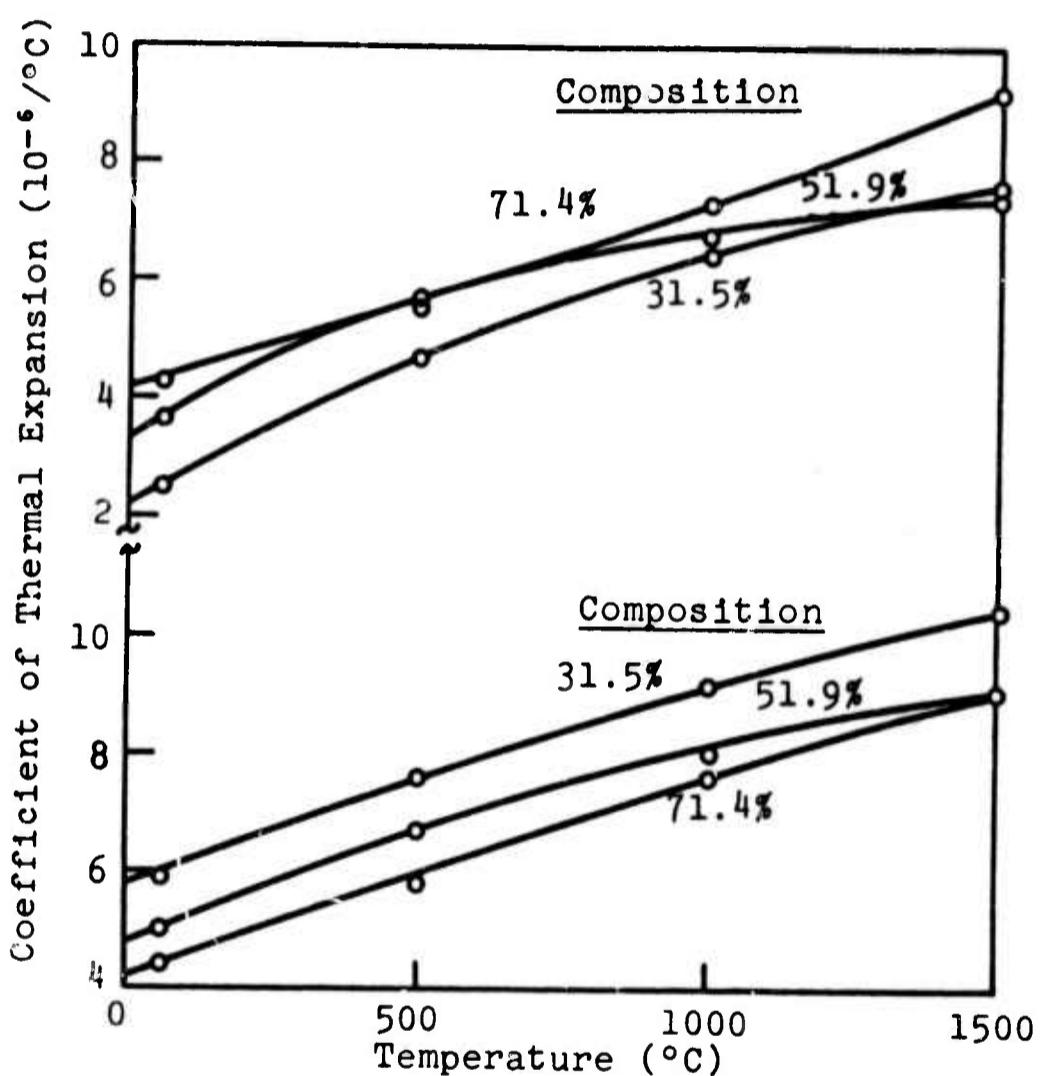
Figure 23. Coefficient of Thermal Expansion versus Temperature for JT-Material.

N-17328

4. Effects of Annealing on Thermal Expansion and Mechanical Properties

Irreversible dimensional changes occur during the initial heating of the JT-material above approximately 1600°C. In the across-grain direction, the material expands between 1600° and 2000°C by amounts of the same order as the intrinsic thermal expansion up to 1600°C. In the with-grain direction, the irreversible

dimensional changes are much smaller and are sometimes positive and sometimes negative. During the fabrication process, the JT-billets are heated to temperatures greater than 2000°C and cooled under pressure; stress relief apparently occurs when the billets are reheated. When the same specimens are cycled a second time, irreversible changes still occur on a reduced scale.

Two simple experiments have been performed to study the dimensional changes that occur during reheating. Specimens of JT-30, 50, and 70 material were machined to precise dimensions for the first experiment. These specimens were repeatedly cycled in an induction furnace (argon atmosphere) from room temperature to various higher temperatures. After each temperature cycle, the specimen dimensions were checked with a micrometer. Table IX summarizes the results of this experiment, and Figure 24 shows a representative plot of the data for one of the specimens (JT-50-26).
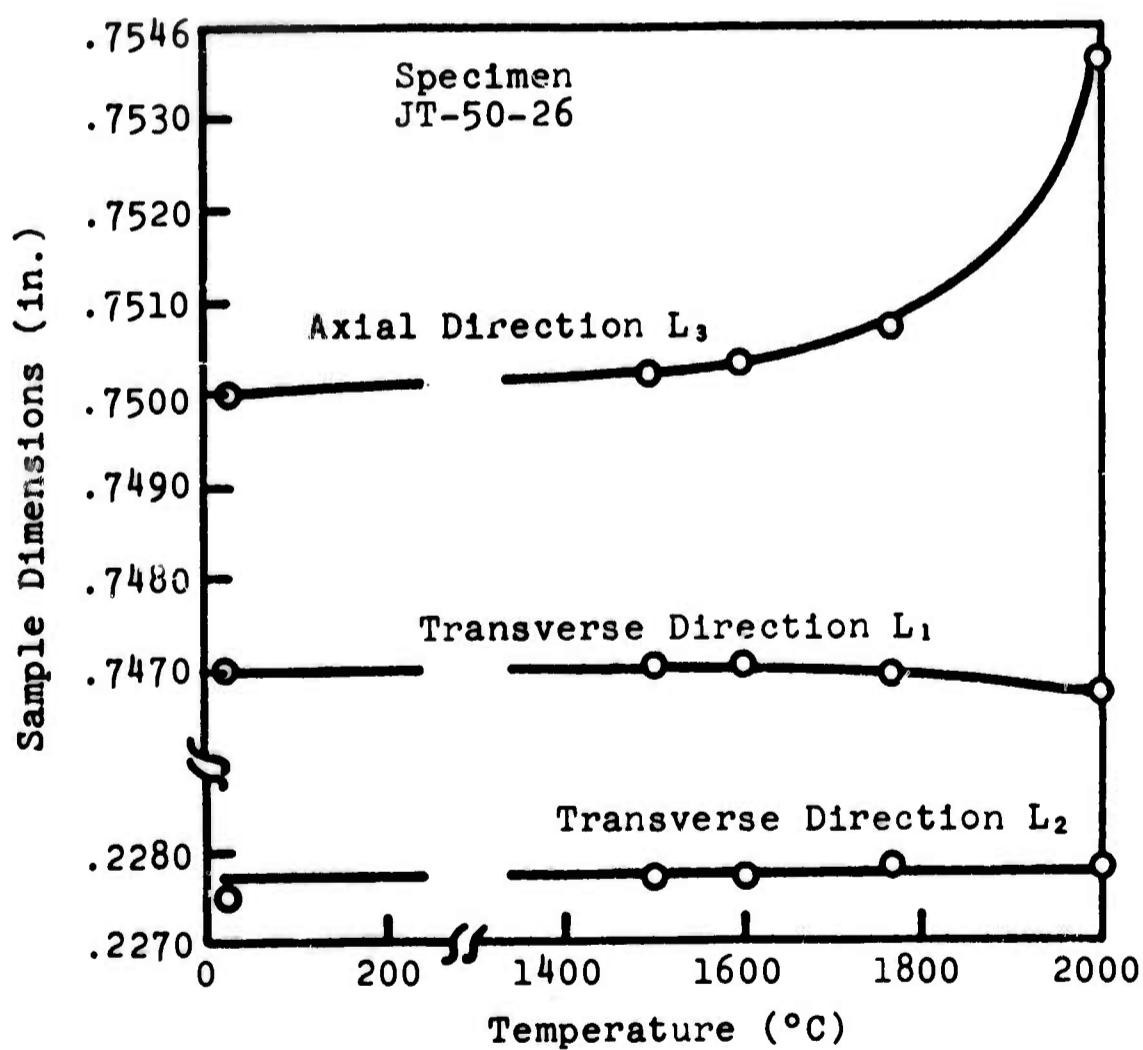
Figure 24. Room Temperature Dimensions of JT-50 Material After Repeated Anneals to Each Higher Temperature.

N-11413

-38-

In Table IX and Figure 24, L_3 is in the across-grain direction and L_1 and L_2 are in the with-grain directions. In this experiment, several minutes were required before temperature equilibrium was achieved (the hold-time was approximately 30 seconds), whereas several hours at high temperature: were required for the coefficient of thermal expansion tests. Since approximately the same amount of growth occurs in both instances, the growth is apparently independent of these heating rates.

Several additional specimens were machined for the second experiment. These specimens were repeatedly cycled between room temperature and 2000°C, and specimen dimensions were measured after each cycle. Table X summarizes the results: after two temperature cycles, no further growth occurs in either the across-grain or with-grain directions.

The specimens should be pre-annealed or cycled several times to 2000°C before measuring the coefficient of thermal expansion at temperatures greater than 1600°C to insure that no growth will occur during measurement. This procedure should insure that only the intrinsic coefficient of thermal expansion of the material is measured above 1600°C.

A third experiment was run to determine the effect that annealing may have on mechanical and thermal properties. Two-thirds of the billet JT-30-38 was annealed at 2100°C for several hours and one-third was left as received. Specimens for mechanical and thermal tests were cut from both parts.

The solid curves in Figure 25 are the best fits through all the sonic and ultrasonic moduli data taken on JT materials. The data points plotted are for samples cut from the annealed and as-received portions of billet JT-30-38. The agreement between the plotted points and the solid curves is quite good; for the JT-30 material, no appreciable change in the moduli is apparent after the material has been annealed.

Figures 26 and 27 show similar best-fit curves and points for annealed and as-received JT-30-38 material for the flexural and compressive strength data, respectively. Again, the agreement between the plotted points and solid curves is quite good. In addition, the flexural and compressive strength data for billet JT-30-38 fall well within the experimental scatter of the data points used to determine the solid curves. Therefore, no significant change in flexural or compressive strength of JT-30 material after annealing was observed.

Thermal diffusivity data and best-fit curves are shown in Figure 28 for with-grain specimens of billet JT-30-38. These data indicate that the with-grain thermal diffusivity at every temperature increases after the material has been annealed at 2100°C.

TABLE IX

DIMENSIONS OF JT-MATERIAL AFTER CYCLING TO VARIOUS TEMPERATURES*

	As Received			1st Cycle to 1500°C			2nd Cycle to 1600°C			3rd Cycle to 1765°C			4th Cycle to 2000°C		
	L_1	L_2	L_3	L_1	L_2	L_3	L_1	L_2	L_3	L_1	L_2	L_3	L_1	L_2	L_3
JT-30-16	.7500	.2275	.7535	.7505	.2278	.7535	.7505	.2277	.7534	.7504	.2277	.7538	.7502	.2277	.7581
JT-30-35	.7535	.2275	.7505	.7536	.2276	.7504	.7538	.2275	.7502	.7539	.2276	.7506	.7538	.2275	.7559
JT-50-21	.753+	.2275	.7505	.7536	.2274	.7504	.7536	.2273	.7504	.7536	.2274	.7507	.7532	.2273	.7582
JT-50-26	.7470	.2275	.750+	.7470	.2277	.7502	.7470	.2277	.7503	.7469	.2278	.7507	.7467	.2278	.753?
JT-70-18	.7480	.227+	.7505	.7477	.2274	.7503	.7478	.2273	.7502	.7478	.2273	.7503	.7476	.2272	.7516
JT-70-34	.7470	.2265	.7505	.7469	.2267	.7505	.7468	.2267	.7505	.7468	.2267	.7508	.7467	.2266	.7531

*All dimensions measured in inches at room temperature.

TABLE X

DIMENSIONS OF JT-MATERIAL AFTER CYCLING TO 2000°C*

	As Received			1st Cycle to 2000°C			2nd Cycle to 2000°C			3rd Cycle to 2000°C		
	L_1	L_2	L_3	L_1	L_2	L_3	L_1	L_2	L_4	L_1	L_2	L_3
JT-30-16	.7500	.0418	.7501	.7501	.0418	.7527	.7501	.0417	.7530	.7500	.0417	.7530
JT-50-21	.7501	.0414	.7504	.7499	.0415	.7541	.7499	.0414	.7546	.7498	.0414	.7546
JT-70-18	.7502	.0419	.7500	.7499	.0419	.7507	.7498	.0420	.7507	.7498	.0420	.7507

*All dimensions measured in inches at room temperature.
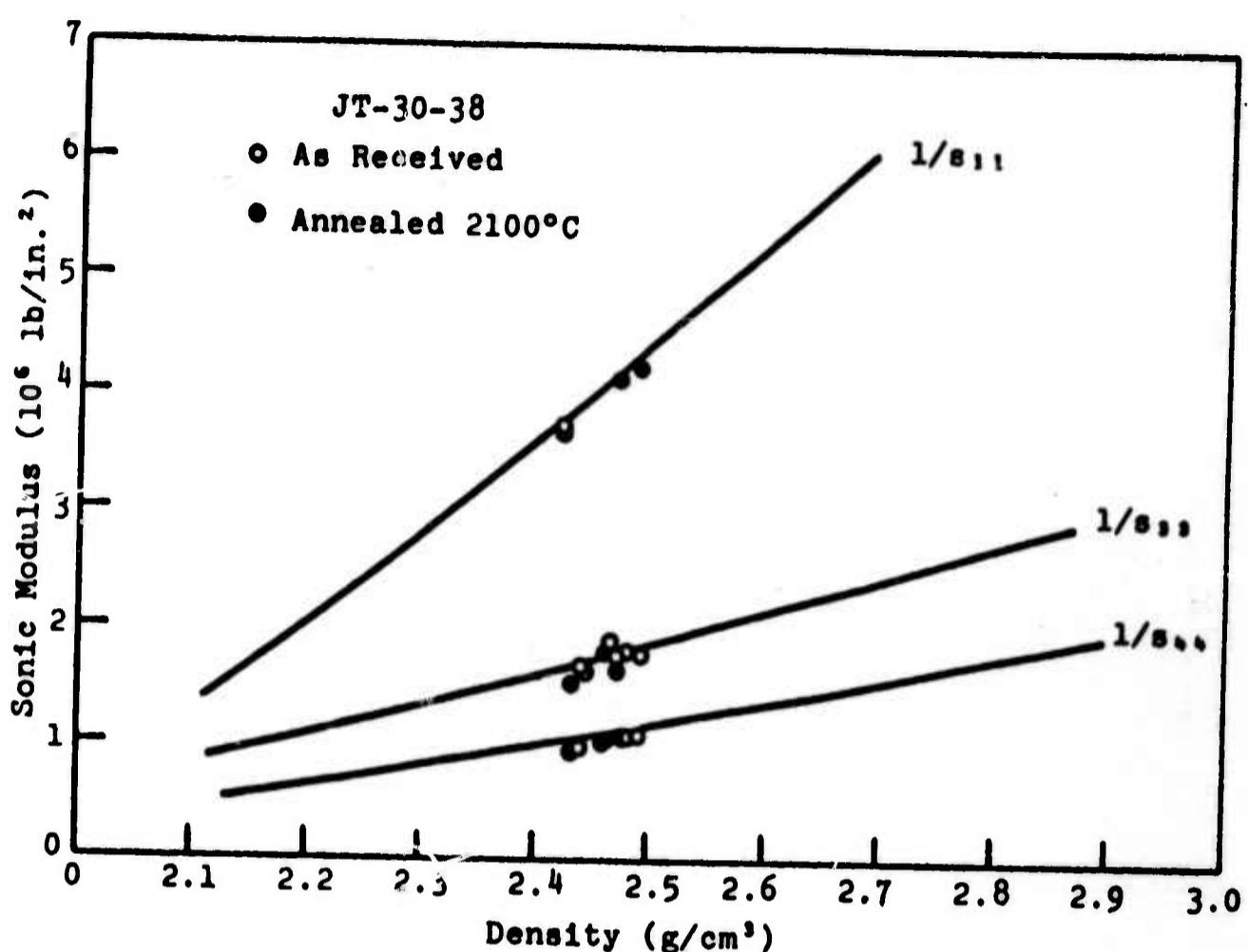
Figure 25.   Comparison of Sonic Moduli Between Samples of JT-30-38
and Best Fit Through All the JT-30 Sonic Data.

N-17907
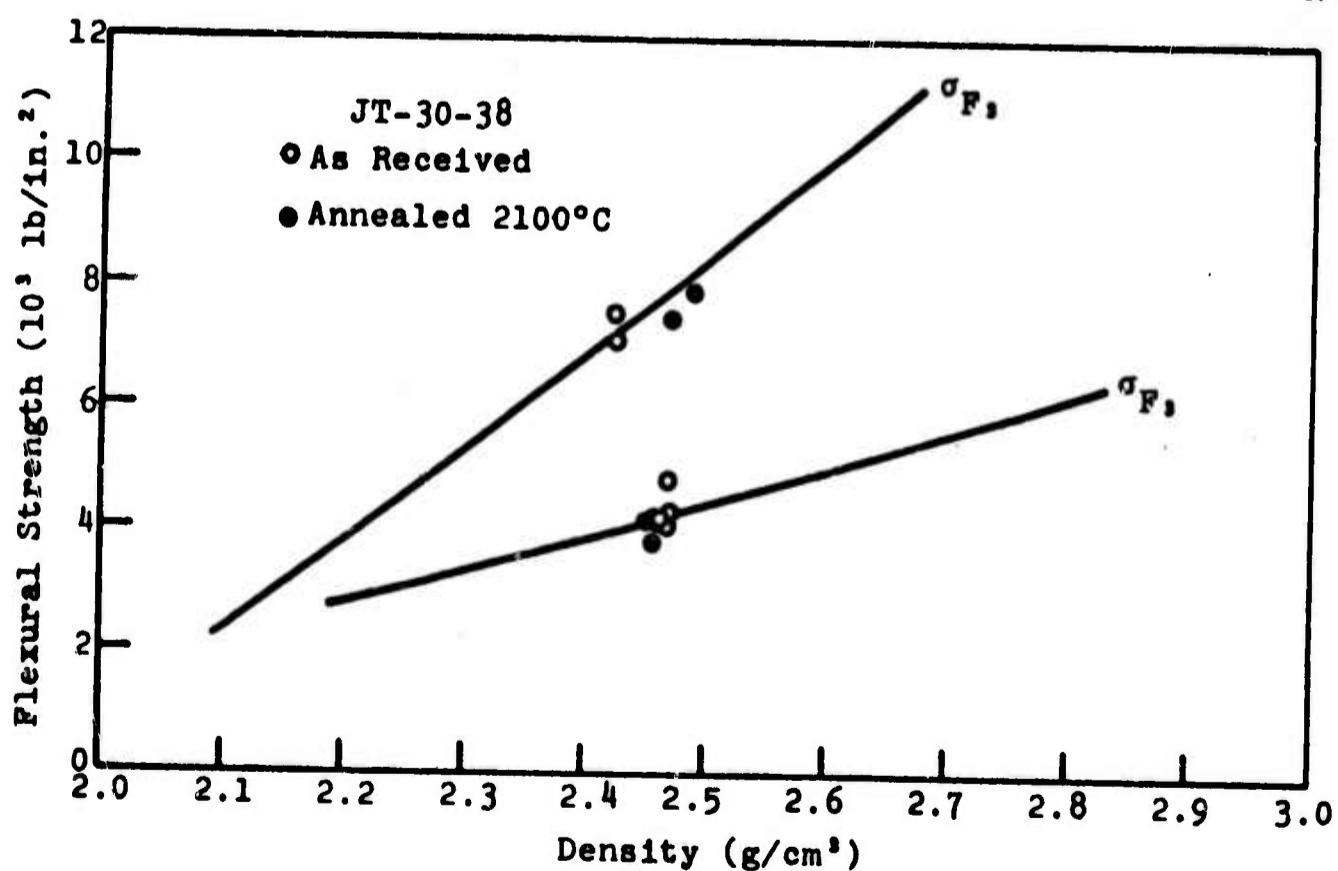
Figure 26.   Comparison of Flexural Strengths Between Samples of JT-30-38
and Best Fit Through all the JT-30 Flexural Strength Data.
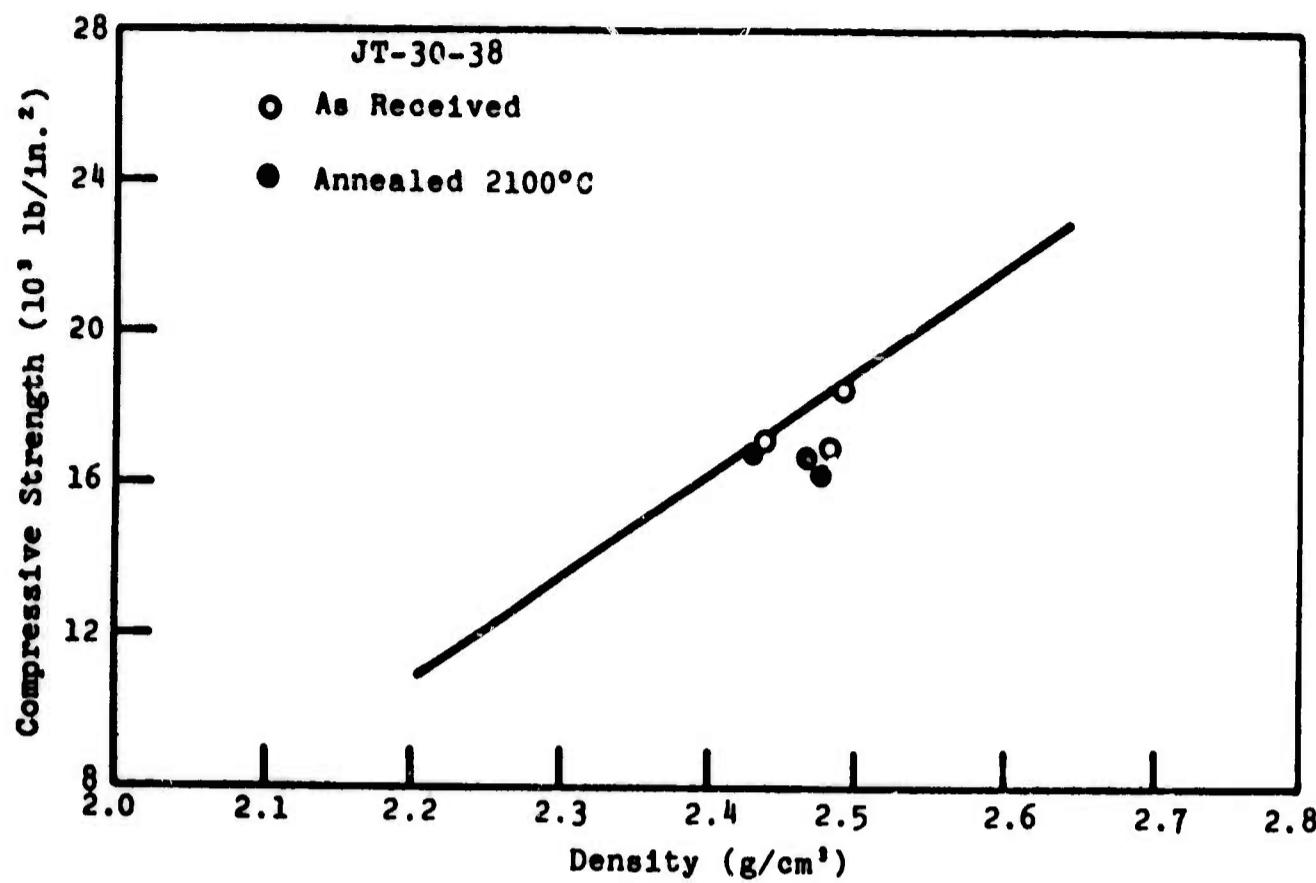
N-17903

Figure 27. Comparison of Compressive Strength Between
Samples of JT-30-38 and Best Fit Through All
the JT-30 Compressive Strength Data.

N-17904
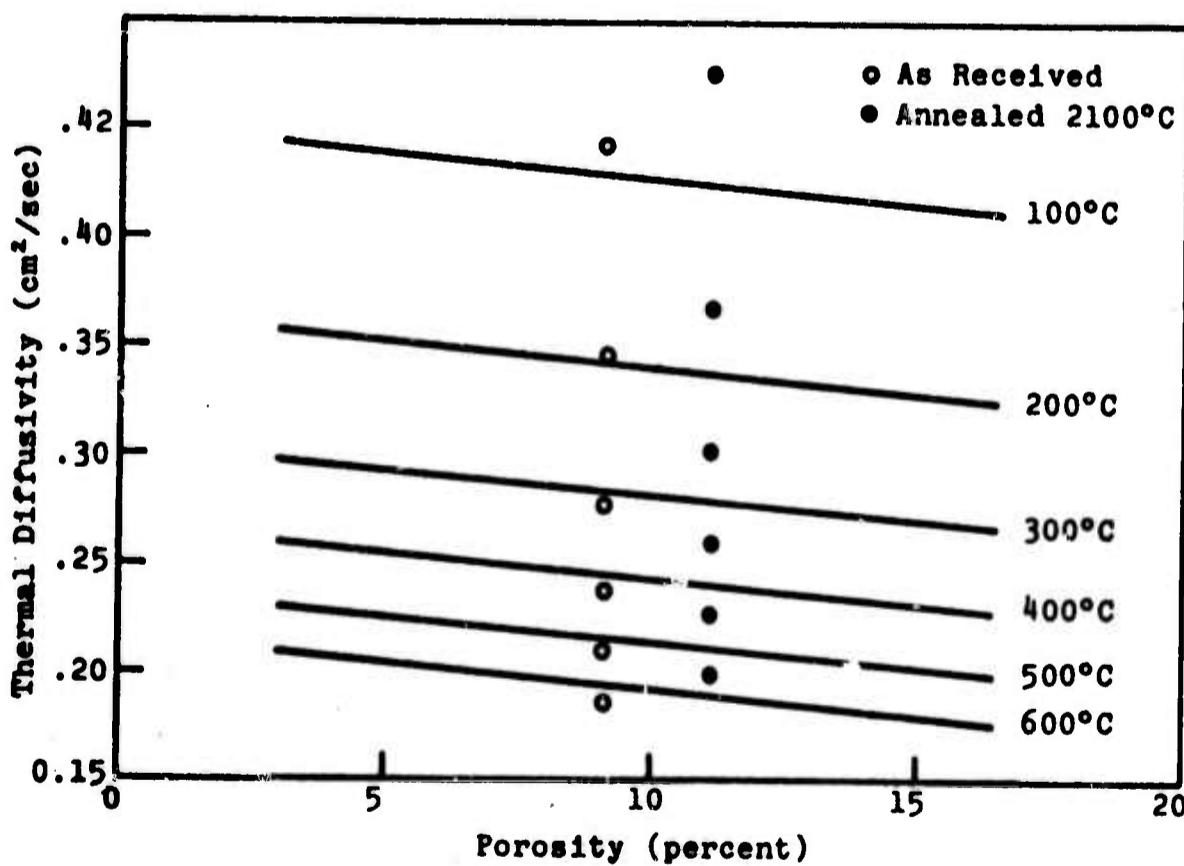
Figure 28. Comparison of With-Grain Thermal Diffusivity
Between Samples of JT-30-38 and all the JT-30
Diffusivity Data.

N-17905

-42-

The increase is approximately 11 percent at 100°C and approximately five percent at 600°C. Material was available for the annealing of only one across-grain specimen. Comparison of the thermal diffusivity of this specimen with that of the best-fit curves suggests a slight increase in diffusivity after annealing of approximately five percent. Although the effect of annealing on the thermal diffusivity and mechanical properties was studied on only 30 percent additive material, there is no reason to expect that the results would be different for other composites.

SECTION V

MULTIAXIAL STRESS TESTING AND FAILURE CRITERIA

The objective of this work was to extend and complement the physical property data presented in Section IV by determining the stress-strain relations and fracture strength under various states of combined stresses. For this work, thin-walled cylindrical specimens were subjected to combinations of internal, external, and axial pressures.

1. Multiaxial Stress Testing Apparatus

Since the JT materials are hard and abrasive, test specimens were first machined to rough dimensions from the billets by using diamond core drills and then ground to the specified dimensions with a diamond wheel. The longitudinal axis of the test specimens was oriented parallel to the symmetry axis of the material. The test specimens had the following dimensions: inside diameter, 0.885 inch; outside diameter, 0.985 inch; and length, 3.50 inches. In general, the variation of the wall-thickness throughout the test specimens was less than 0.002 inch. A thin layer of synthetic rubber coating was applied on strain gages and specimen surfaces to prevent the hydraulic oil from damaging the strain gages and penetrating pores.

The schematic diagram of the hydraulic system for the multiaxial stress test apparatus is shown in Figure 29. The basic hydraulic power unit can supply a continuous pressure to 5000 psi. The pressure from the power unit can be further increased to 7500 psi by means of a precision hydraulic cylinder and to 50,000 psi by means of a pressure intensifier. The pressure from the power unit can be increased or decreased at prescribed rates by replacing the screw for pressure adjustment in the pressure relief valve with a threaded plunger which rotates and moves axially in a linear actuator. The rate and direction of the axial motion of the threaded plunger are remotely controlled.

The pressure chamber, specially designed for combined stress tests, is shown in Figure 30. The specimen assembly, which consisted of a test specimen and two steel end-caps, is shown inside of the pressure chamber. The interior surfaces of the steel end-caps were slightly tapered, and the steel caps were attached to the test specimen with epoxy cement. Since the modulus of epoxy cement is considerably lower than that of the test specimen, the test specimen can deform without serious end-constraints. The variation of strain due to end-constraints was approximately five percent. The strain gage wires were led out from the pressure chamber by means of connectors normally used for thermocouple wires.
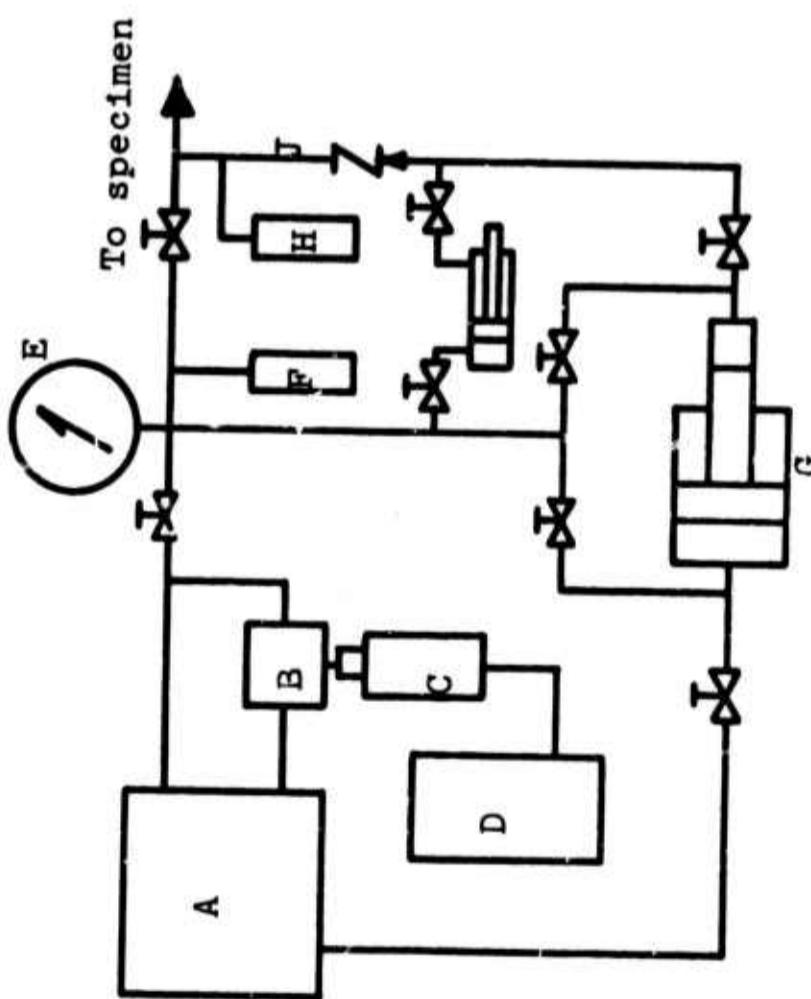
A. Hydraulic Pump (0-5,000 psi)
B. Pressure Relief Valve
C. Linear Actuator
D. Control Box for Linear Actuator
E. Pressure Gage (0-5,000 psi)

F. Pressure Transducer (0-5,000 psi)
G. Pressure Intensifier (0-50,000 psi)
H. Pressure Transducer (0-20,000 psi)
I. Hydraulic Cylinder (0-10,000 psi)
J. Pressure Check Valve

Figure 29. Schematic Diagram of Hydraulic System for Multiaxial Stress Test Apparatus.

N-16890
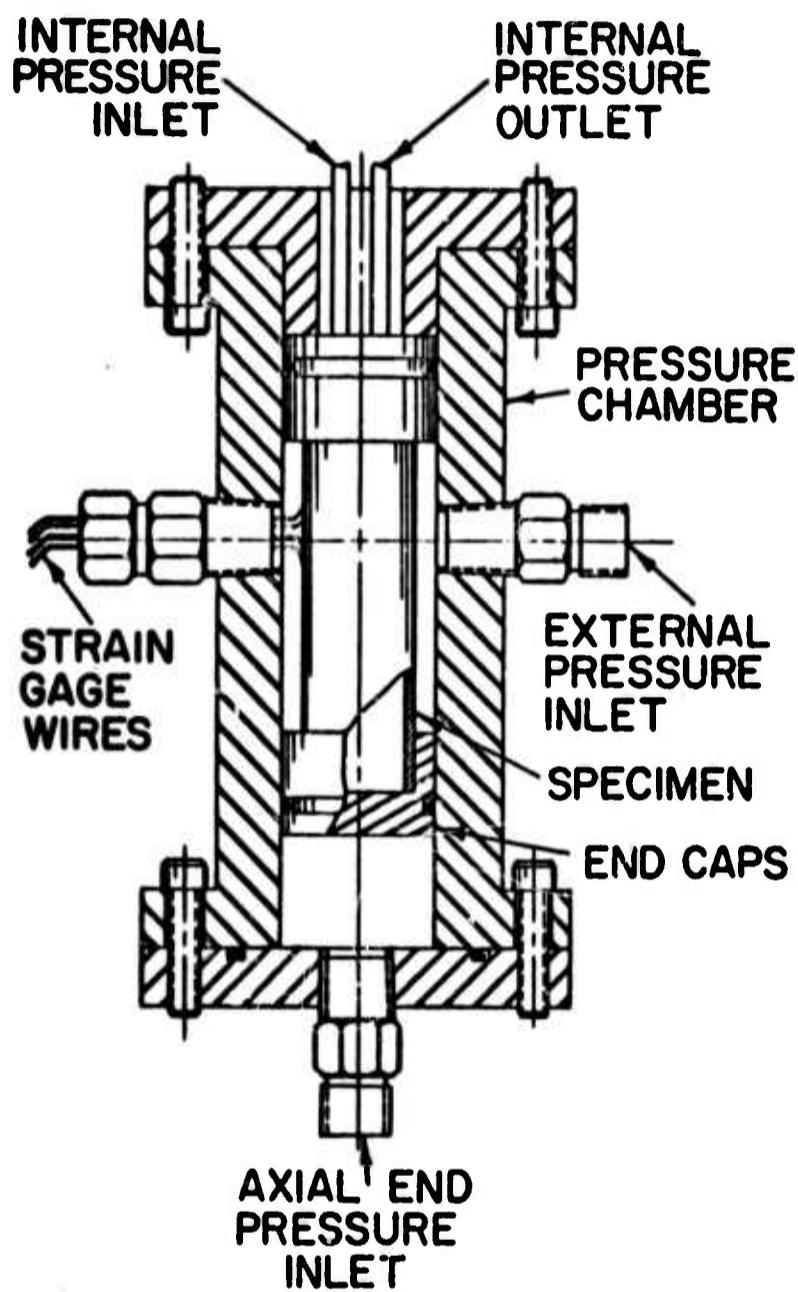
Figure 30. Pressure Chamber Assembly for Combined Stress Tests.

N-9978

Four foil strain gages, two longitudinal and two tangential, were mounted at diametrically opposite locations on the outside surfaces of most of the test specimens. The output of the longitudinal strain gages was measured individually so that any bending moment could be determined and taken into consideration in the calculation of stresses. The corrections for transverse sensitivity of the strain gages were made on the measured strains. The hydraulic power unit could supply a continuous pressure to 50,000 psi. The application of two pressures was usually necessary to obtain a

desired state of combined stresses. For most cases, the ratio of the two pressures was maintained constant to provide the so-called radial or constant stress-ratio loading condition. Pressure-strain relations and pressure-time relations were plotted by X-Y recorders.

2. Combined Stress Test Results for Nominal 50 Percent Additive JT-Series Composite Material

The tangential stress, σ_1, and radial stress, σ_2, were calculated by Lame's equations, and the longitudinal stress was calculated by the equation

$$\sigma_3 = \frac{a^2 P_1 + (d^2 - b^2) P_o - d^2 P_e}{b^2 - a^2}, \qquad (4)$$

where a is the inside radius of test specimen, b is the outside radius of test specimen, d is the inside radius of the pressure test chamber, P_1 is the internal pressure, P_o is the external pressure, and P_e is the axial end pressure. The radial stress, which is equal to the oil pressure at the surface of the test specimen, is small compared with the tangential and longitudinal stresses and could be neglected in most cases.

The longitudinal and tangential stress-strain curves, obtained by constant stress-ratio loading in various states of combined stresses, are shown in Figure 31 (a) and 31 (b). Compressive stress and strain are indicated with a negative sign. The values of stress and strain at the outside surface of the test specimen are used in Figure 31 (b). The curves designated as AT and AC in Figure 31 (a) are, respectively, uniaxial tensile and compressive stress-strain curves in the against-grain direction. The curves designated as WT and WC in Figure 31 (b) are, respectively, uniaxial tensile and compressive stress-strain curves in the with-grain direction. The material deforms considerably more in the against-grain (longitudinal) direction than in the with-grain (tangential) direction under a given compressive stress. Some scatter was present in the biaxial stress-strain data, particularly in the state of biaxial compression; this scatter was attributed to the variation of porosity of the test specimens and to errors in strain measurements. Strain measured by a strain gage depends slightly on the surface condition (size and distribution of pores) on which the strain gage is placed. The longitudinal and tangential stress-strain relations for a JT-50 composite specimen subjected to internal pressure are shown in Figure 32. The longitudinal strain and the tangential strain at a given internal pressure are approximately the same magnitude because of the highly anisotropic properties of the material. The nonconservative response under cyclic internal pressure loading is similar to that obtained for uniaxial stress loading.
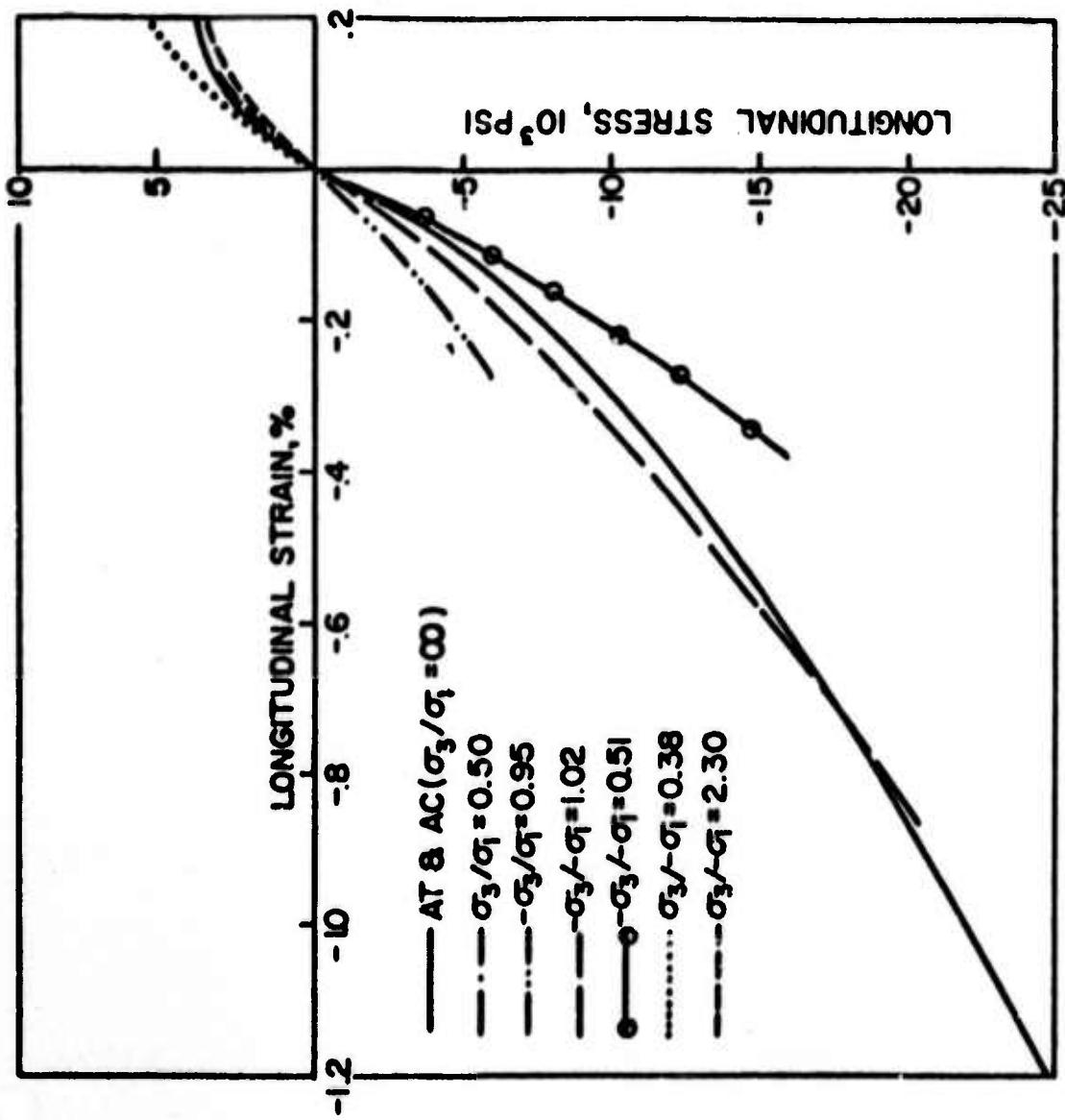
Figure 31 (a). Longitudinal Stress-Strain Curves Under Combined Stresses for the JT-50 Composite Material.

N-18224
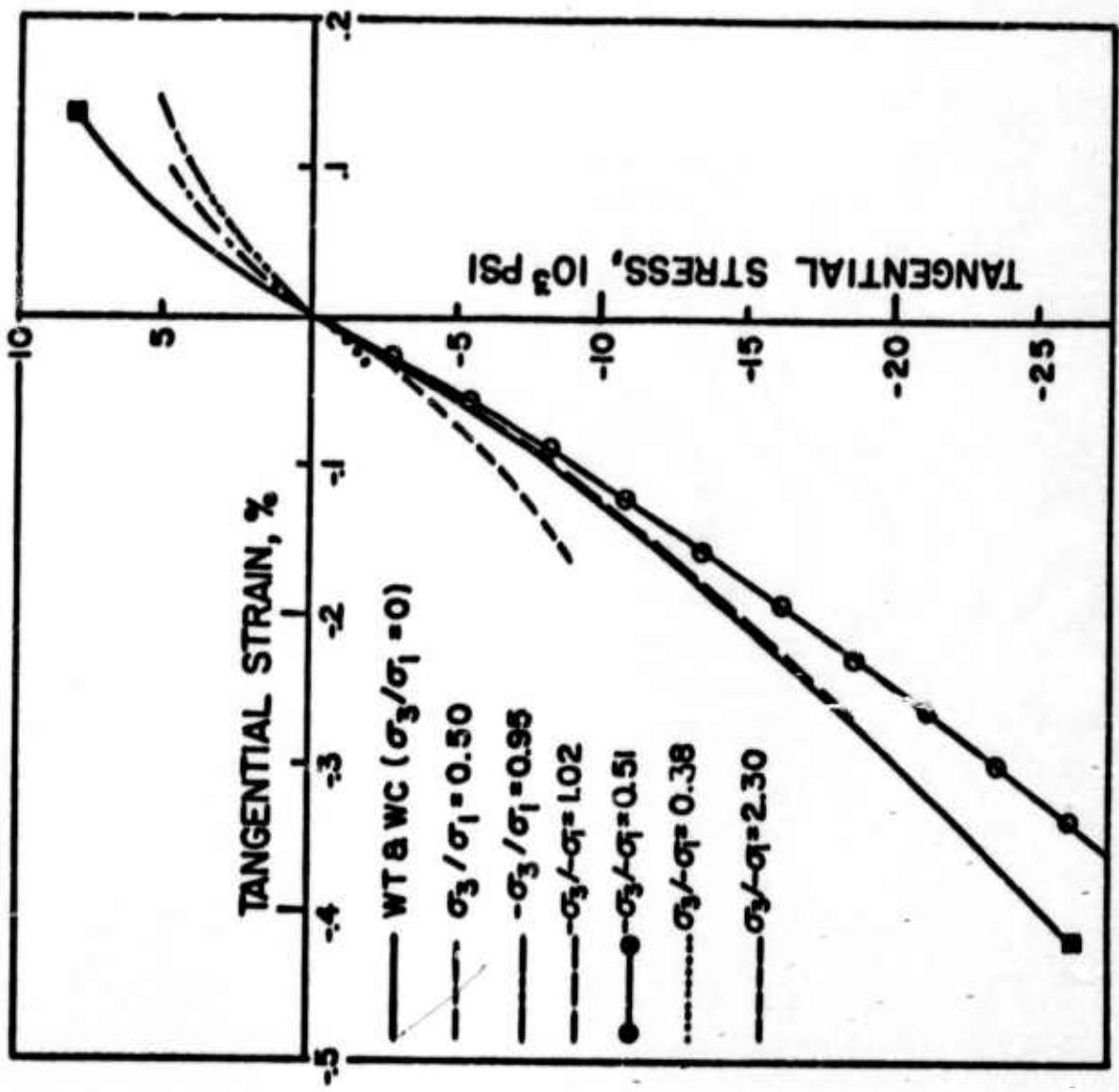
Figure 31 (b). Tangential Stress-Strain Curves Under Combined
Stresses for the JT-50 Composite Material.

N-18225
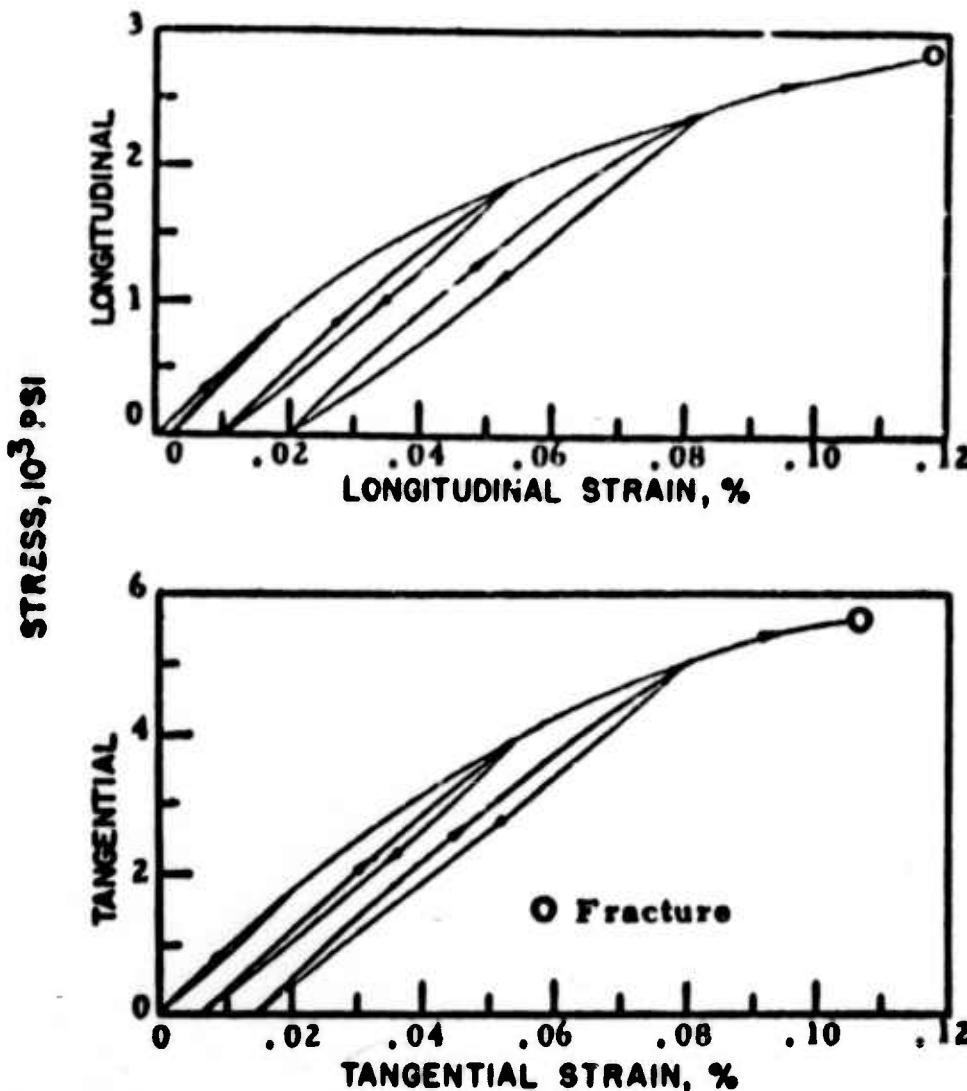
Figure 32. Longitudinal and Outside Tangential Stress-Strain
Curves for JT-50 Composite Cylinder Under Internal Pressure.

N-9607

The biaxial fracture strength of the JT-50 composite is
shown in Figure 33, which is a two-dimensional representation of
the longitudinal stress, σ_3, versus the tangential stress, σ_1, at
fracture. The radial stress, σ_2, is considered to have no effect
in Figure 33 because of its small magnitude. The scatter in the
fracture strength data in the state of biaxial compression is
believed to be due primarily to the variation of percent porosity
of the test specimen and premature failure initiated by localized
defects. An empirical fracture criterion for the JT-50 composite
is assumed to be in the form of a quadratic equation for an
ellipse, and the constants in the quadratic equation have been
determined from the fracture strength data by means of the least
squares, best fit technique. The fracture envelope predicted by
the empirical fracture criterion is shown in Figure 33, and the
empirical fracture criterion* is given as

$$(12100)^2 = \sigma_1^2 - 0.831\sigma_3^2 + 1.04\sigma_3^2 + 15515\sigma_1 + 20208\sigma_3. \qquad (5)$$

_____

*The empirical fracture criterion was obtained by Dr. C. C. Chamis
of Case Western Reserve University.

The agreement between the empirical fracture criterion and fracture strength data is not completely satisfactory, indicating that the assumption of a continuous ellipse for the fracture envelope may not be accurate.
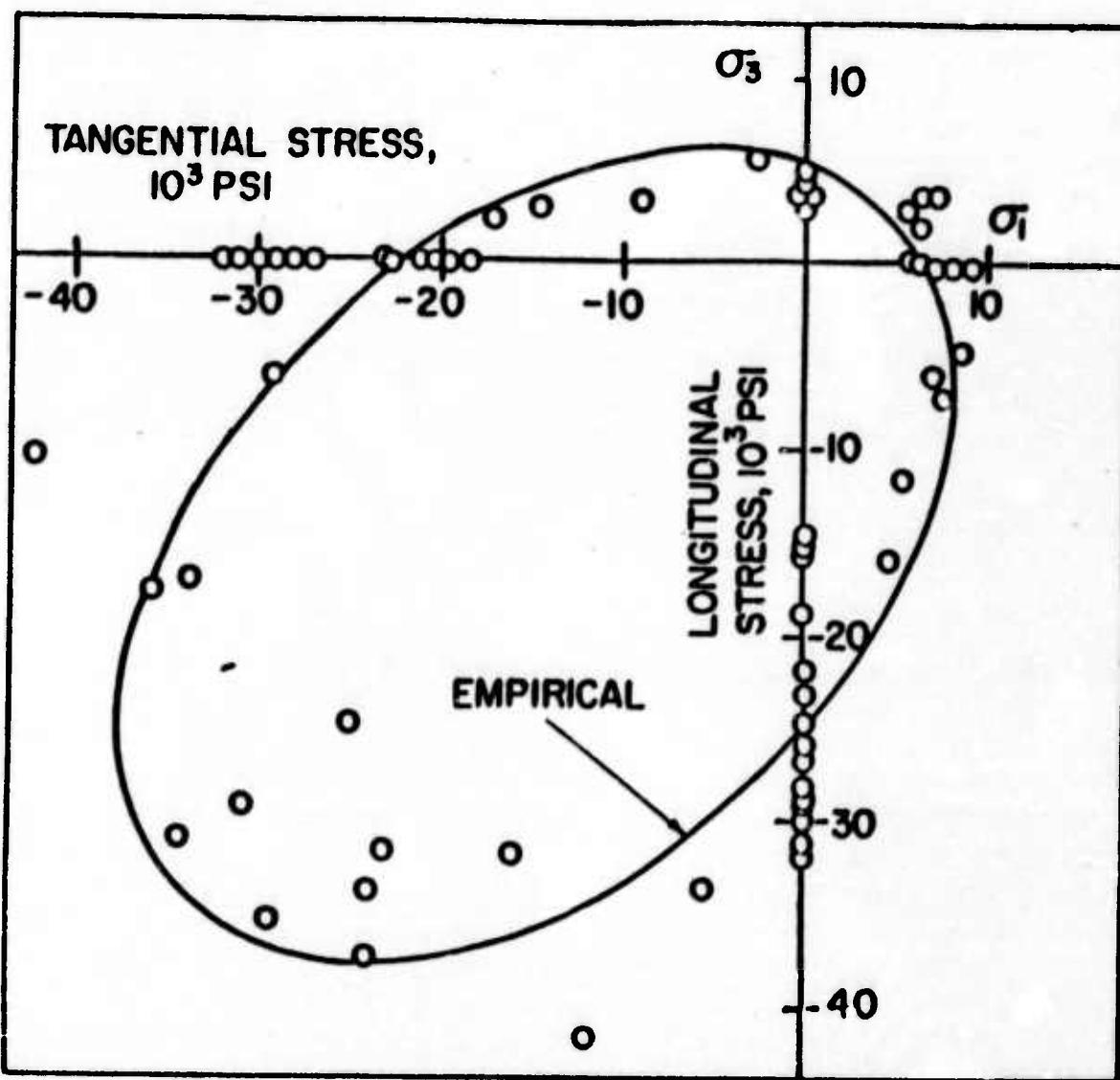
Figure 33. Biaxial Fracture Strength for the JT-50 Composite Material.

N-18505

3. Failure Criteria for Nominal 30 Percent and 70 Percent Additive JT-Series Composite Material

A limited number of JT-30 and JT-70 composite specimens were tested under biaxial stresses so that the approximate shapes of the fracture strength surfaces for these composites and the effects of the composition on biaxial fracture strength could be determined. Two specimens from each composite were tested; the results are given in Table XI. The biaxial fracture strength for the JT-30-49-2 specimen appeared to be lower than the estimated value. The strains measured on the outside surface of the specimen are also given in Table XI.

TABLE XI

BIAXIAL FRACTURE STRENGTH AND STRAIN OF
JT-30 AND JT-70 COMPOSITES

| Specimen | Density (g/cm^3) | Strength*(10^3 lb/in.^{2}) | | Strain* (percent) | |
		Inside Hoop σ_{u1}	Axial σ_{u3}	Hoop ε_{u1}	Axial ε_{u3}
JT-30-48-1	2.62	4.4	2.0	0.15	0.17
JT-30-49-2	2.54	-13.8	-11.1	-1.15	-0.24
JT-70-47-1	3.82	16.5	-16.6	0.09	-0.15
JT-70-47-2	3.82	17.2	7.7	0.06	0.06

*Negative values indicate compression.

4.   Comparison of Theories of Fracture with the
      Experimental Data

        A number of theories of fracture have been developed for
the determination of allowable design stresses for the complicated
stress conditions which occur in actual situations. By using such
theories of fracture, designers are able to predict when failure
will occur under combined stresses from the known fracture strength
data in simple tension, compression, and shear loading or from the
shape and size of cracks in the material. Maximum stress theory
and Mohr's theory are, perhaps, the earliest theories of fracture
which take into account different strengths in tension and compres-
sion. Several theories of fracture have been proposed more recent-
ly for materials having various types of anisotropy.[21-28] These
theories are generally in the form of a quadratic equation for an
ellipse in terms of stresses, and the constants in the equation
are related to uniaxial tensile and compressive strengths and
shear strength in different ways. The fracture envelopes predicted
by these theories of fracture were compared with the experimental
data for the JT-50 composite material; most theories of fracture
do not predict satisfactorily the experimental data. Among the
theories which predict a fracture envelope in the form of an ellipse,
the theories proposed by Stassi[23] and Hoffman[27] gave the best
agreement with the experimental data.

        The correlations of the experimental data with the empiri-
cal fracture criterion shown in Figure 33 and with the theories of
fracture which predict a continuous ellipse for the fracture enve-
lopes are not entirely satisfactory, since these theories do not
consider the different fracture mechanisms operative under differ-
ent states of biaxial stresses for this composite. Consequently,
the biaxial fracture envelope of this material may be taken to be

composed of four separate fracture envelopes which are consistent with the fracture mechanism operative for each state of biaxial stresses.

Norris, et al.[29]* formulated a theory of fracture for orthotropic materials based on the assumptions that the orthotropic material is composed of walls of an isotropic material surrounding voids in the shape of equal rectangular prisms and that fracture under combined stresses is governed by the distortion-energy criterion. Norris's fracture criterion can be written in the generalized form

$$\frac{\sigma_1^2}{\sigma_{i_1}^2} - \frac{\sigma_1\sigma_3}{\sigma_{i_1}\sigma_{j_3}} + \frac{\sigma_3^2}{\sigma_{j_3}^2} = 1, \qquad (6)$$

where σ_{i_1} and σ_{j_3} are the uniaxial fracture strengths in the symmetry directions. The values of σ_{i_1} and σ_{j_3} can be either tensile strengths σ_{t_1} and σ_{t_3} or compressive strengths σ_{c_1} and σ_{c_3}, depending on whether the principal stresses σ_1 and σ_3 are tensile or compressive stresses. Four fracture envelopes, each of which is applicable to only a particular stress state, are obtained when the appropriate uniaxial fracture strengths for each stress state are substituted in Equation (6). Equation (6) can be obtained in a different manner through the generalization of the distortion-energy criterion to include the different strengths in tension and compression and the transverse isotropy.

Norris's theory has been applied to the fracture data for the JT-50 composite material. Good agreement between predicted and measured strengths was obtained, except in the biaxial-tension stress state for which the predicted strength was somewhat high. The fracture envelope in biaxial tension may be best represented by the modified maximum stress theory given by

$$\frac{\sigma_1}{\sigma_{t_1}} = 1 \text{ or } \frac{\sigma_3}{\sigma_{t_3}} = 1. \qquad (7)$$

Therefore, the fracture strength of JT-series composites can be predicted satisfactorily by Equation (7) for the state of biaxial tension and by Equation (6) for the states of tension-compression and biaxial compression.

---

*A series of reports pertaining to this subject have been published by C. B. Norris and his associates at the Forest Products Laboratory.

The fracture envelopes for the JT-50 composite material at five, ten, and fifteen percent porosity have been calculated with Equations (6) and (7) and the uniaxial strength data given in Table IV and are shown in Figure 34. Most of the fracture strength data fall between the fracture envelopes of ten and five percent porosity, since the porosities of the JT-50 composite billets fabricated for this program were generally slightly smaller than eight percent. The calculated fracture envelopes for JT-30, JT-50, and JT-70 composites at ten percent porosity are shown in Figure 35.
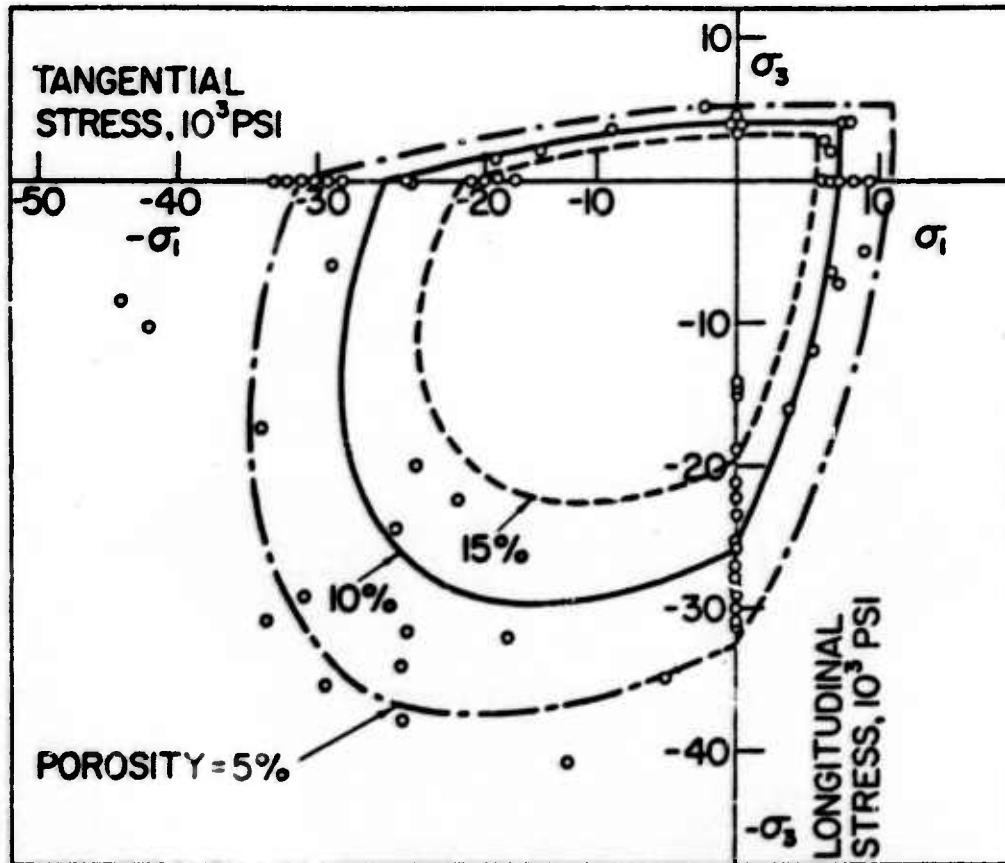
Figure 34. Biaxial Fracture Strength as a Function of Porosity, Composition = 50 Percent.

N-18228

5. Correlation of Stress and Strain Under Combined Stress

a. Effective Stress-Effective Strain Relation for the JT-50 Composites. In the designing of machine and structural components, the designers must be able to predict the plastic stress-strain relations under various states of combined stresses from the uniaxial stress-strain relations. These predictions have been made with some degree of success for ductile materials by correlating certain invariant characteristics of the states of stress and strain which are often defined as the effective stress and effective strain. The relationship between the effective stress and

effective strain is commonly called the generalized plastic stress-strain relation. If a generalized stress-strain relation can be established for the JT-series composites, the known solutions in plasticity theory may be applied to these composites.
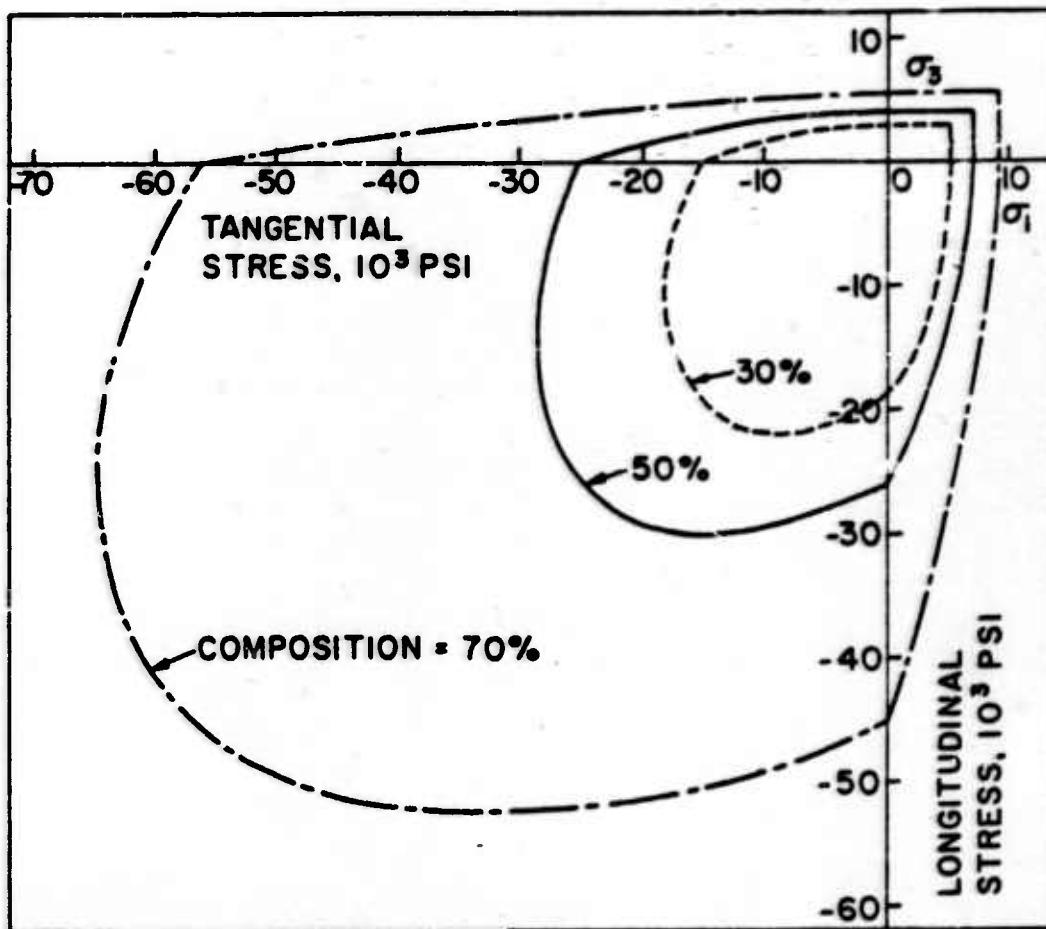
Figure 35. Biaxial Fracture Strength as a Function of
Composition, Porosity = 10 percent.

N-18229

The effective stress, $\bar{\sigma}$, and the effective strain, $\bar{\epsilon}$, defined by the deformation-type theory of plasticity for ductile isotropic material are

$$\bar{\sigma} = \frac{1}{\sqrt{2}} \left[(\sigma_1 - \sigma_2)^2 + (\sigma_2 - \sigma_3)^2 + (\sigma_3 - \sigma_1)^2 \right]^{\frac{1}{2}} \qquad (8)$$

and

$$\bar{\epsilon} = \frac{\sqrt{2}}{3} \left[(\epsilon_1 - \epsilon_2)^2 + (\epsilon_2 - \epsilon_3)^2 + (\epsilon_3 - \epsilon_1)^2 \right]^{\frac{1}{2}}, \qquad (9)$$

-55-

where σ_1, σ_2, and σ_3 are principal stresses and ϵ_1, ϵ_2, and ϵ_3 are principal strains. Hill[30] suggested a theory of plastic flow for anisotropic materials by postulating the effective stress to be given by

$$\bar{\sigma} = [F(\sigma_1 - \sigma_2)^2 + G(\sigma_2 - \sigma_3)^2 + H(\sigma_3 - \sigma_1)^2]^{\frac{1}{2}}, \quad (10)$$

where F, G, and H are parameters characteristic of the current state of anisotropy. Similar stress-strain relations for aniso-tropic materials were proposed by Jackson, Smith, and Lankford,[31] Dorn,[32] and Fisher[33]. More recently, Hsu[34] proposed a yield criterion and plastic stress-strain relations for anisotropic mate-rials exhibiting the Bauschinger effect. Hu,[35] starting with Hill's effective stress, obtained an expression for the incre-mental effective strain for materials which obey the law of con-stancy of plastic volume. The assumption of plastic volume con-stancy is approximately correct for many ductile materials and is often used in the theory of plasticity because the assumption leads to greatly simplified solutions to many problems. The assumption of volume constancy cannot be used in the study of deformation and fracture of the JT-series composites since significant volume changes under uniaxial stresses have been observed for these mate-rials. The volume changes under stresses are believed to be due largely to changes in the size of the macroscopic pores and, to a lesser extent, to volume changes in the graphite particles (the particles contain microscopic porosity).

    b.   A Generalized Stress-Strain Relation. A genera-lized form of the plastic stress-strain relation for anisotropic materials can be written as

$$\epsilon_i = \sum_j \alpha_{ij} \sigma_j \phi \qquad (i,j, = 1,2, --,6), \qquad (11)$$

where the α_{ij} are the constants of anisotropy and ϕ is the propor-tionality function defined by

$$\phi = \bar{\epsilon}/\bar{\sigma}; \qquad (12)$$

the expressions for $\bar{\epsilon}$ and $\bar{\sigma}$ are given later. The proportionality function, ϕ, is a monotonically increasing function of $\bar{\sigma}$ and des-cribes the degree of nonlinearity in the stress-strain behavior. The constants of anisotropy, α_{ij}, are assumed to be independent of deformation. The use of the total strain components is permissible if the stress-ratio is constant during deformation, the stress increases monotonically, and the material exhibits little elastic behavior. These assumptions are justified for the JT-50 composite and the present test program. There are 36 constants of anisotropy

in Equation (11). Because of the symmetric property $\alpha_{ij} = \alpha_{ji}$ and the transversely isotropic property of the material, the number of independent α_{ij} is reduced to 5, namely, α_{11}, α_{33}, α_{12}, α_{13}, and α_{44}. Since the material symmetry axes coincide with the principal axes of the test specimens, the stress distribution is axially symmetric and the shear stress components vanish; hence, α_{44} does not appear in Equation (11). Therefore, the plastic stress-strain relations of interest become

$$\epsilon_1 = (\alpha_{11}\sigma_1 + \alpha_{12}\sigma_2 + \alpha_{13}\sigma_3)\,\phi, \qquad (13a)$$

$$\epsilon_2 = (\alpha_{12}\sigma_1 + \alpha_{11}\sigma_2 + \alpha_{13}\sigma_3)\,\phi, \text{ and} \qquad (13b)$$

$$\epsilon_3 = (\alpha_{13}\sigma_1 + \alpha_{13}\sigma_2 + \alpha_{33}\sigma_3)\,\phi. \qquad (13c)$$

The stress components, in terms of the strain components, can be obtained for Equations (13) and are given by

$$\sigma_1 = (k_{11}\epsilon_1 + k_{12}\epsilon_2 + k_{13}\epsilon_3)/\,\phi, \qquad (14a)$$

$$\sigma_2 = (k_{12}\epsilon_1 + k_{11}\epsilon_2 + k_{13}\epsilon_3)/\,\phi, \text{ and} \qquad (14b)$$

$$\sigma_3 = (k_{13}\epsilon_1 + k_{13}\epsilon_2 + k_{33}\epsilon_3)/\,\phi, \qquad (14c)$$

where

$$k_{11} = (\alpha_{11}\alpha_{33} - \alpha_{13}^2)/\,\Delta,$$

$$k_{12} = (\alpha_{13}^2 - \alpha_{12}\alpha_{33})/\,\Delta,$$

$$k_{13} = (\alpha_{12} - \alpha_{11})\,\alpha_{13}/\Delta, \qquad (15)$$

$$k_{33} = (\alpha_{11}^2 - \alpha_{12}^2)/\,\Delta, \text{ and}$$

$$\Delta = (\alpha_{11}^2 - \alpha_{12}^2)\,\alpha_{33} + 2\,(\alpha_{12} - \alpha_{11})\,\alpha_{13}^2.$$

For a deformed body, the total work per unit volume is

$$w = \bar{\sigma}\bar{\epsilon} = \sigma_1\epsilon_1 + \sigma_2\epsilon_2 + \sigma_3\epsilon_3. \qquad (16)$$

The expression for the effective stress for the present case can be obtained by the substitution of Equations (12) and (13) into Equation (16):

$$\bar{\sigma} = [\alpha_{11}\,(\sigma_1^2 + \sigma_2^2) + \alpha_{33}\sigma_3^2 + 2\,\alpha_{12}\sigma_1\sigma_2 + 2\,\alpha_{13}(\sigma_2\sigma_3 + \sigma_3\sigma_1)]^{\frac{1}{2}}$$

$$(17)$$

The corresponding expression for the effective strain can be derived from Equations (12), (14), and (16):

$$\bar{\varepsilon} = [k_{11}(\varepsilon_1{}^2 + \varepsilon_2{}^2) + k_{33}\varepsilon_3{}^2 + 2k_{12}\varepsilon_1\varepsilon_2 + 2k_{13}(\varepsilon_2\varepsilon_3 + \varepsilon_3\varepsilon_1)]^{\frac{1}{2}}$$

(18)

   c. <u>Numerical Calculation</u>. In order for Equations (13) to represent the stress-strain curves at the origin (Hooke's Law for transverse isotropy), the proportionality function ϕ is defined to have the value 10^{-6} in.^{2}/lb in the limit of zero stress and each anisotropy constant α_{ij} is chosen to be a dimensionless quantity having the numerical value of 10^6 times the value of the corresponding elastic compliance constant s_{ij}; the values of the s_{ij} can be calculated from the data given in Table IV. The value of ϕ for a given value of $\bar{\sigma}$ can be computed from the average effective stress-effective strain curve which was determined from the uniaxial tensile and compressive stress tests. For the biaxial tests, the values of $\bar{\sigma}$ can be calculated with Equation (17) and the values of $\bar{\varepsilon}$ can be computed with Equation (18) by using the experimental values of ε_1 and ε_3 and the values of ε_2 calculated with Equation (13b).

   Figure 36 shows the effective stress-effective strain relations calculated for a number of test specimens, including those represented in Figures 31(a) and 31(b). The average effective stress-effective strain curve for the uniaxial stress tests is also plotted in Figure 36 (the dashed line). Some scatter exists in the correlation between the effective stress and the effective strain, but the correlation is satisfactory for engineering applications. An increase of scatter in the correlation with increasing compressive stresses is probably due to statistical variation and to difficulties in determining the values of strain under such unstable stress states. The scatter in the correlation for the combined stress test specimens is not any greater than that for the uniaxial stress test specimens. In fact, the effective stress-effective strain relations for the combined stress test specimens generally fall within a band formed by the effective stress-effective strain relations for uniaxial stress test specimens. Thus, the stress-strain relations under combined stresses can be predicted for the JT-50 composite material with the same degree of accuracy which is obtainable in the measurements of uniaxial stress-strain relations.

6. <u>Microscopic Observation</u>

   a. <u>Modes of Fracture</u>. The influence of the high degree of anisotropy and the state of combined stresses on the modes of fracture can be observed from the photographs of the fractured specimens of the JT-50 composite material shown in Figure 37.
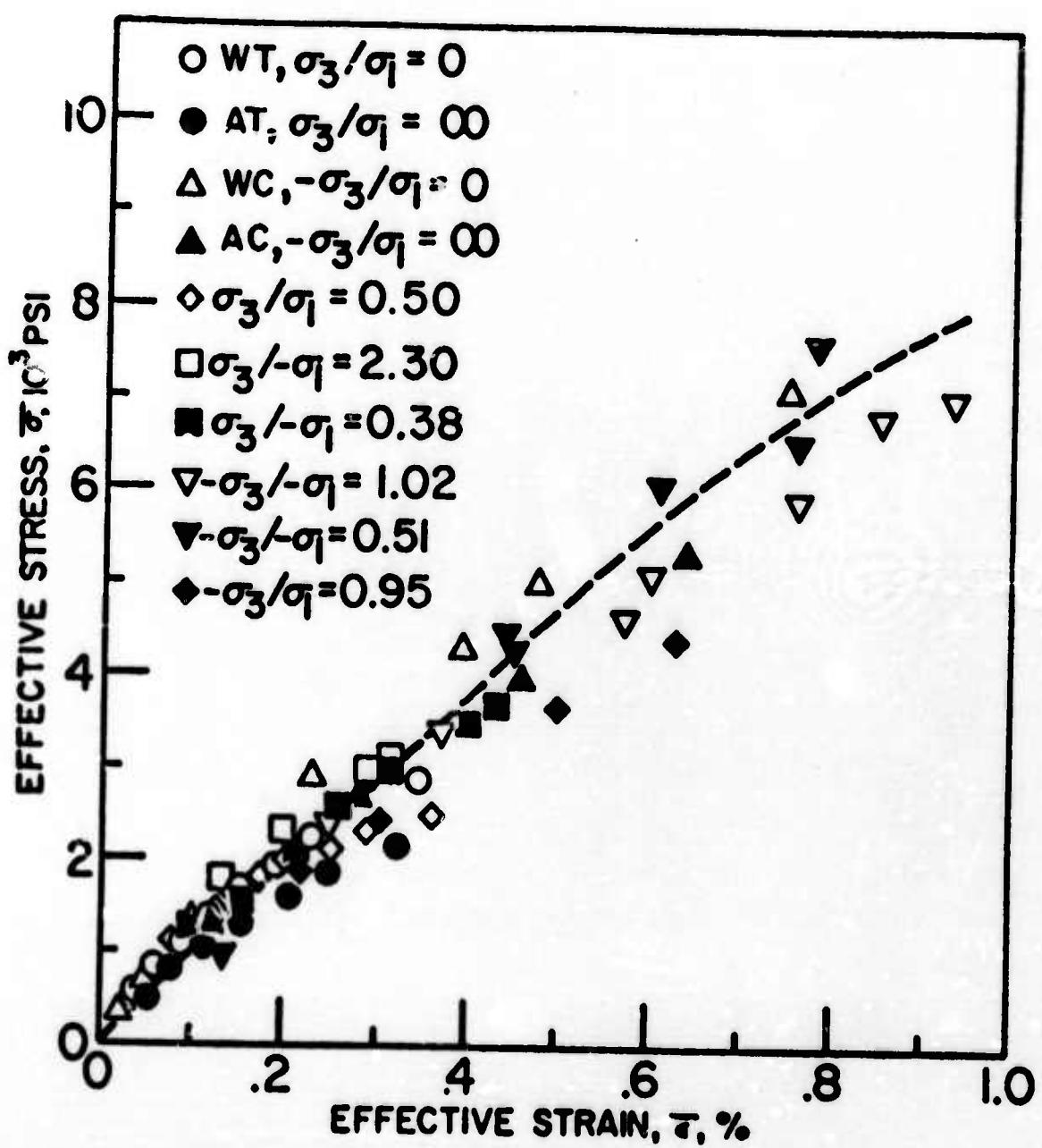
Figure 36. Effective Stress-Effective Strain Relation for the JT-50 Composite Material.

N-18397

Specimen (a) was fractured by an internal pressure, but it does not have the longitudinal crack which occurs normal to the direction of the largest tensile stress in an isotropic cylinder. The irregular fractured surface may be due to the fact that the longitudinal and tangential stresses, just prior to fracture, were approaching simultaneously the values of the uniaxial tensile strengths in the against-grain and with-grain directions of the composite, since the stress-ratio and the uniaxial tensile strength-ratio are both approximately 0.5.

The effect of a state of combined stresses on the mode of fracture is clearly illustrated by specimens (b) and (c). These specimens were fractured under an internal pressure and an axial

compressive load. The axial compressive load applied to specimen
(c) was approximately twice that applied to specimen (b). The
fracture of specimen (b) resulted from a barely visible longitudinal
cleavage crack caused by the tangential tensile stress. The frac-
ture of specimen (c) occurred as a result of catastrophic, random
cracks. Catastrophic cracks such as those shown by specimen (c)
have been observed in specimens subjected to a large compressive
stress, regardless of whether the other stress was tensile or
compressive.

$$\frac{\sigma_3}{\sigma_1}=0.5 \qquad \frac{-\sigma_3}{\sigma_1}=2.24 \qquad \frac{-\sigma_3}{\sigma_1}=4.31$$

(a)   (b)   (c)
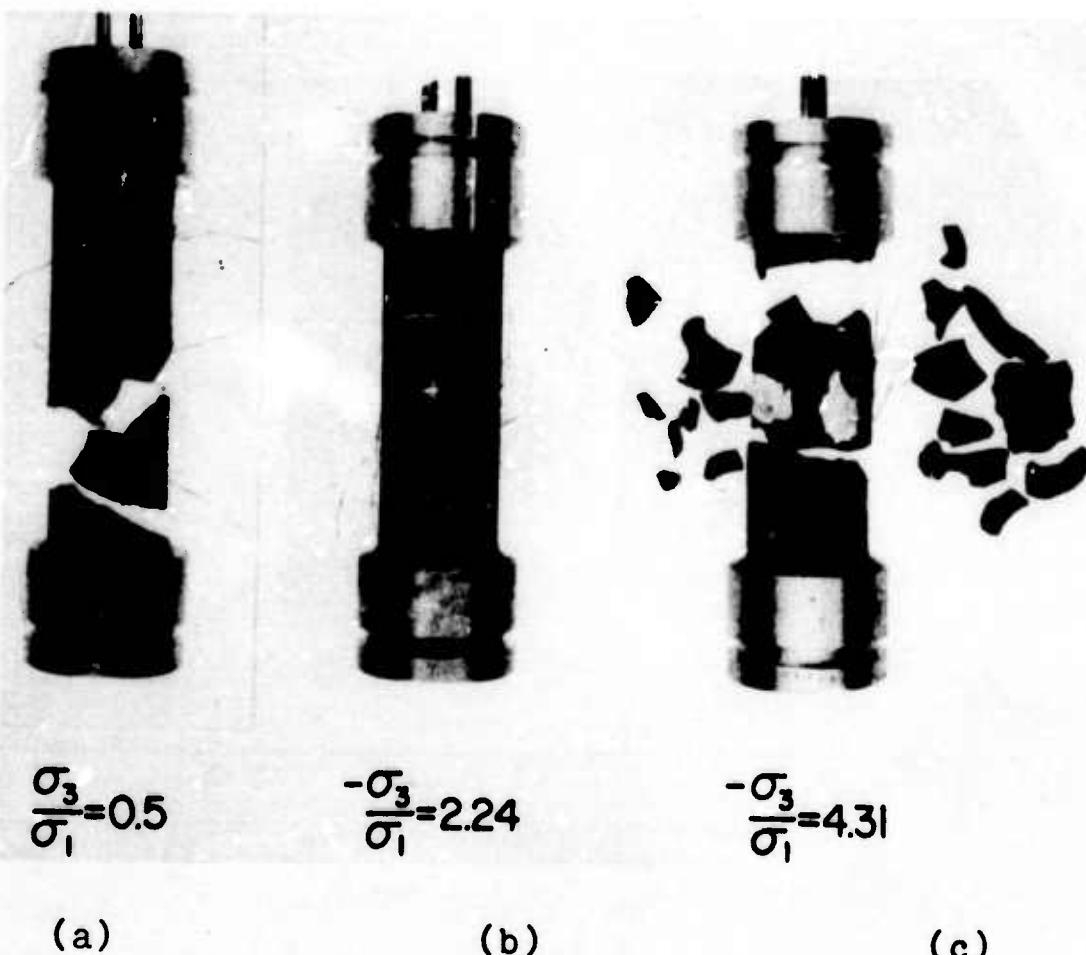
Figure 37.   Specimens Fractured Under Combined Stresses.

N-20612

     b.   Factors Affecting Stresses. The degree of aniso-
tropy in stress-strain properties varies with the orientation
of graphite particles and the quantity of the metallic additives.
The properties of the graphite particle itself are highly aniso-
tropic, whereas the properties of the metallic additives, ZrB_2
and Si, are relatively isotropic. Thus, the degree of anisotropy
of the JT-series composites varies from the moderately anisotropic
characteristics of graphite materials (no metallic additives)
to the fairly isotropic characteristics of the ZrB_2 and Si phases
(all metallic additives).

Tensile strength of the graphite particles in the direction of the symmetry axis is very weak because of the low bonding forces between basal planes. This anisotropic behavior of the graphite particles and the internal stress concentrations caused by the notch effect of pores are responsible for the fact that tensile strengths are considerably lower than compressive strengths for the JT-series composites. If stresses are concentrated around the pores, fracture in those graphite particles which are oriented with their symmetry axes parallel to the direction of loading can be initiated under a relatively low tensile stress. The anisotropy in the strengths in the graphite particles, together with the preferred orientation of the particles, are largely responsible for the fact that the against-grain tensile strength of the JT-series composites is lower than the with-grain tensile strength. The compressive strength of the graphite particles in the direction parallel to the basal planes is weaker than that in the direction normal to the basal planes, probably because a condition of the low bonding forces between the basal planes leads to premature failure due to separation and buckling of the basal planes when a compressive load is applied along the basal planes. When the metallic additives are added to a graphite matrix, the compressive strength increases because the metallic additives can carry more load and also act as interlocking agents which prevent the basal planes of the graphite particles from separating and buckling prematurely. Therefore, the compressive strength in the with-grain direction of the JT-series composites increases more rapidly than that in the against-grain direction as the percent of metallic additives increases.

SYMBOLS AND UNITS

Symbol	Unit	Description
$1/s_{11}$	10^6 psi	Young's modulus (with-grain direction)
$1/s_{33}$	10^6 psi	Young's modulus (against-grain direction)
$1/s_{44}$	10^6 psi	Shear modulus
σ_{t_1}	10^3 psi	Tensile strength (with-grain direction)
σ_{t_3}	10^3 psi	Tensile strength (against-grain direction)
σ_{c_1}	10^3 psi	Compressive strength (with-grain direction)
σ_{c_3}	10^3 psi	Compressive strength (against-grain direction)
σ_{f_1}	10^3 psi	Flexural strength (with-grain direction)
σ_{f_3}	10^3 psi	Flexural strength (against-grain direction)
σ_1	psi	Stress (with-grain direction)
σ_3	psi	Stress (against-grain direction)
ε_1	percent	Strain (with-grain direction)
ε_3	percent	Strain (against-grain direction)
α_1	$10^{-6}/°C$	Coefficient thermal expansion (with-grain direction)
α_3	$10^{-6}/°C$	Coefficient thermal expansion (against-grain direction)
K_1	cal/sec cm-deg	Thermal conductivity (with-grain direction)
K_3	cal/sec cm deg	Thermal conductivity (against-direction)
κ_1	cm^2/sec	Thermal diffusivity (with-grain direction)
κ_3	cm^2/sec	Thermal diffusivity (against-grain direction)
C_p	cal/g°C	Specific heat

REFERENCES

1. Union Carbide Corporation, National Carbon Company, <u>Research and Development on Advanced Graphite Materials - Oxidation Resistant Graphite Base Composites</u>, by K. J. Zeitsch and J. M. Criscione, WADD TR61-72, Vol. XXX, (April 1964), (AF 33(615)-6915).

2. Union Carbide Corporation, Carbon Products Division, <u>Improved Graphite Materials for High Temperature Aerospace Use - Development of Graphite - Refractory Composites</u>, by R. M. Bushong, et al, <u>ML-TDR-64-125, Vol. II</u> (Oct. 1964) (AF33(657)-11171).

3. IITRI, Properties of JTA Graphite, by Seymour A. Bortz, <u>AFML-TR-68-178</u> (July 1968) (AF 33(615)-3028).

4. Bell Aerosystems Company, <u>Selection Techniques for Brittle Materials--The Evaluation of JTA Graphite Composites as a Structural Refractory Body</u>, by Frank M. Anthony, et al, <u>AFML-TR-67-78</u> (May 1967) (AF33(615)-2376).

5. Union Carbide Corporation, Carbon Products Division, <u>JTA Graphite Composite Manufacturing Methods</u>, by Robert A. Reuter, <u>AFML-TR-69-57</u> (March 1969) (F33615-67-C-1498).

6. Union Carbide Corporation, Carbon Products Division, in Association with Case Western Reserve University and Bell Aerosystems Company, a Textron Company, <u>Integrated Research on Carbon Composite Materials</u>, AFML-TR-66-310 Part I (October 1966) (AF 33(615)-3110, Air Force Materials Laboratory, Wright-Patterson Air Force Base, Ohio).

7. Union Carbide Corporation, Carbon Products Division, in Association with Case Western Reserve University and Bell Aerosystems Company, a Textron Company, <u>Integrated Research on Carbon Composite Materials</u>, AFML-TR-66-310, Part II (December 1967) (AF33(615)-3110, Air Force Materials Laboratory, Wright-Patterson Air Force Base, Ohio).

8. Union Carbide Corporation, Carbon Products Division, in Association with Case Western Reserve University and Bell Aerosystems Company, a Textron Company, <u>Integrated Research on Carbon Composite Materials</u>, AFML-TR-66-310 Part III (January 1969) (AF 33(615)-3110, Air Force Materials Laboratory, Wright-Patterson Air Force Base, Ohio).

9. Union Carbide Corporation, Carbon Products Division, in Association with Case Western Reserve University and Bell Aerosystems Company, a Textron Company, <u>Integrated Research on Carbon Composite Materials</u>, AFML-TR-66-310 Part IV Volume I (September 1969) (AF 33(615)-3110, Air Force Materials Laboratory, Wright-Patterson Air Force Base, Ohio).

REFERENCES (Cont'd.)

10. Union Carbide Corporation, Carbon Products Division, in Association with Case Western Reserve University and Bell Aerosystems Company, a Textron Company, Integrated Research on Carbon Composite Materials, AFML-TR-66-310 Part IV Volume II (October 1969) (AF 33(615)-3110, Air Force Materials Laboratory, Wright-Patterson Air Force Base, Ohio).

11. Union Carbide Corporation, Carbon Products Division, in Association with Case Western Reserve University and Bell Aerosystems Company, a Textron Company, Integrated Research on Carbon Composite Materials, AFML-TR-66-310 Part IV Volume III (April 1970)(AF 33(615)-3110, Air Force Materials Laboratory, Wright-Patterson Air Force Base, Ohio).

12. A. Naidai, Theory of Flow and Fracture of Solids, Vol. I, (McGraw-Hill Book Company, New York, 1950), pp. 353-359.

13. W. J. Parker, R. J. Jenkins, C. P. Butler, and G. L. Abbott, "Flash Method of Determining Thermal Diffusivity, Heat Capacity, and Thermal Conductivity," J. Appl. Phys. 32, 1979-1984 (1961).

14. Union Carbide Corporation, National Carbon Company, Research and Development on Advanced Graphite Materials - Survey and Analytical Representation of the Measurements of the Specific Heat of Graphite, by G. B. Spence, WADD TR 61-72, Vol. XLI, (November 1963), (AF33(615)-6915).

15. Battelle Memorial Institute (Columbus), Refractory Ceramics of Interest in Aerospace Structural Applications--A Materials Selection Handbook, by J. R. Hague, J. F. Lynch, A Rudnick, F. C. Holden, and W. H. Duckworth, RTD-TDR-63-4102 (1963), p. 55, (AF33(657)-8326).

16. A. Goldsmith, T. E. Waterman, and H. J. Hirschhorn, Handbook of Thermophysical Properties of Solid Materials, Vol. III: Ceramics, (MacMillan Company, New York, 1961), p. 925.

17. Loc. cit., Reference 12, pp. 347-352.

18. H. W. Swift, "Length Changes in Metals Under Torsional Overstrain," Engineering, 163, 253-257 (1947).

19. R. Hill, The Mathematical Theory of Plasticity, (Oxford University Press, London, 1950) pp. 325-328.

REFERENCES (Cont'd.)

20. R. C. Grassi and I. Cornet, "Fracture of Gray-Cast-Iron Tubes Under Biaxial Stresses," J. of Appl. Mech. 16, Trans. ASME 71, 178-182 (1949).

21. H. W. Babel, "Biaxial-Fracture Strength of Brittle Materials," Technical Report AFML-TR-66-51, March 1966.

22. Joseph Marin, "Theories of Strength for Combined Stresses and Nonisotropic Materials," Journal of Aeronautical Sciences, Vol. 24, No. 4, April 1957, pp. 265-269.

23. F. Stassi-D'Alia, "Limiting Conditions of Yielding of Thick Walled-Cylinders and Spherical Shells," U. S. Army European Research Office (9851DU), Frankfort, Final Status Report Contract DA-91-591 EVC-1351 01-4263-61, November 24, 1959.

24. K. V. Zakharov, "Strength Criteria for Laminates," Plastmassy, Izd-vo Khimiya No. 8, 1961, pp. 59-62.

25. John E. Griffith and William M. Baldwin, "Failure Theories for Generally Orthotropic Materials," Development in Theoretical and Applied Mechanics, Vol. I, Proc. of the First Southeastern Conference on Theoretical and Applied Mechanics, Plenum Press, New York, 1963.

26. I. I. Gol'denblat and V. A. Kopnov, "Strength Criteria of Anisotropic Materials," Izv. Akad, Nank SSSR, Mekhanika No. 6, 1965, pp. 77-83.

27. Oscar Hoffman, "The Brittle Strength of Orthotropic Materials, Journal of Composite Materials, Vol. I, No. 2, April 1967, pp. 200-205.

28. L. Fisher, "Optimization of Orthotropic Laminates," Journal of Engineering for Industry, Trans. ASME, Vol. 89, Ser. B, No. 3, August 1967, pp. 399-402.

29. Charles Brazer Norris, "Strength of Orthotropic Materials Subjected to Combined Stresses," FPL Report No. 1816, 3rd ed., Madison, Wisconsin, U. S. Forest Products Laboratory, 1962.

30. R. Hill, The Mathematical Theory of Plasticity, Oxford University Press, London, England, 1950, pp. 315-321.

31. L. R. Jackson, K. F. Smith, and W. T. Lankford, "Plastic Flow in Anisotropic Sheet Metal," Metals Technology, T. P. 2440, August 1948.

REFERENCES,(Cont'd.)

32. J. E. Dorn, "Stress-Strain Relations for Anisotropic Plastic Flow," _Journal of Applied Physics_, Vol. 20, January 1949, pp. 15-20.

33. J. C. Fisher, "Anisotropic Plastic Flow," _Trans. ASME_, Vol. 71, 1949, pp. 349-356.

34. T. C. Hsu, "A Theory of the Yield Locus and Flow Rule of Anisotropic Materials," _Journal of Strain Analysis_, Vol. 1, No. 3, 1966.

35. L. W. Hu, "Studies on Plastic Flow of Anisotropic Metals," _Journal of Applied Mechanics_, Vol. 23, ASME Paper No. 55-A-79, September 1956, pp. 444-450.

DOCUMENT CONTROL DATA - R & D

(Security classification of title, body of abstract and indexing annotation must be entered when the overall report is classified)

1. ORIGINATING ACTIVITY (Corporate author)	2a. REPORT SECURITY CLASSIFICATION
Union Carbide Corporation Carbon Products Division	Unclassified
	2b. GROUP ---

3. REPORT TITLE

STRUCTURAL AND PHYSICAL PROPERTIES OF GRAPHITE-ZIRCONIUM DIBORIDE-SILICON CARBON COMPOSITES

4. DESCRIPTIVE NOTES (Type of report and inclusive dates)

Topical Report

5. AUTHOR(S) (First name, middle initial, last name)

Herbert F. Volk (Editor)

6. REPORT DATE	7a. TOTAL NO. OF PAGES	7b. NO. OF REFS
May 1970	66	35

8a. CONTRACT OR GRANT NO.	9a. ORIGINATOR'S REPORT NUMBER(S)
AF 33(615)-3110	
b. PROJECT NO.	
c. ARPA Order No. 719	9b. OTHER REPORT NO(S) (Any other numbers that may be assigned this report)
Program Code 6D10	
d.	AFML-TR-70-50

10. DISTRIBUTION STATEMENT

This document is subject to special export controls and each transmittal to foreign Governments or foreign Nationals may be made only with prior approval of Nonmetallic Materials Division, MAN, Air Force Materials Laboratory, Wright-Patterson Air Force Base, Ohio 45433.

11. SUPPLEMENTARY NOTES	12. SPONSORING MILITARY ACTIVITY
	Air Force Materials Laboratory Wright-Patterson AFB, Ohio

13. ABSTRACT

Three series of graphite based, refractory composites compositionally related to commercial Grade JTA, but containing 30, 50, and 70 weight percent additives (ZrB_2 and Si_2) were prepared. Within each series, the porosity was varied from approximately 2 to 17 percent. Property measurements were carried out as a function of composition and porosity and along the two principal symmetry axes, i.e., normal and parallel to the molding direction. Property measurements carried out at room temperature consisted of tension, compression, flexural, torsion, ultrasonic, and resonant bar tests. The specific heat, thermal conductivity, coefficient of thermal expansion, and effect of high temperature annealing were also determined. Stress-strain relations and fracture strength under multiaxial stress were determined for the material with 50 percent additive. A generalized stress-strain relation for a transversely isotropic, nonlinear material has been obtained without assuming volume constancy. Various theories of fracture for anisotropic materials were compared with the fracture strength of JT materials. The comprehensive property data compilations in this report should provide designers with sufficient information for structural applications of JT materials.

This abstract is subject to special export controls and each transmittal to foreign Governments or foreign Nationals may be made only with prior approval of Nonmetallic Materials Division, MAN, Air Force Materials Laboratory, Wright-Patterson Air Force Base, Ohio 45433.

DD FORM 1473 (PAGE 1)
S/N 0101-807-6811

14. KEY WORDS	LINK A		LINK B		LINK C	
	ROLE	WT	ROLE	WT	ROLE	WT
Graphite						
Composites						
Ceramics						
Physical Properties						
Stress-Strain Relations						
Anisotropic Material						

DD FORM 1473 (BACK)
S/N 0101-807-6821